Controlled Three-Phase Drives

Prof. Dr.-Ing. Joachim Böcker

Lecture Notes

Last Update 2016-01-26

Paderborn University

Power Electronics and
Electrical Drives

Preface

The course "Controlled Three-Phase Drives" is dedicated to the electric drive system. The electric *drive* does not only consist of the electric machine, but according to modern understanding also of power electronics, sensors and multi-level controls units.

After an overview and definitions, access to this issue is given by an analysis of the electrical machine. The permanent magnet synchronous motor is chosen as an entry into this topic. Due to its high torque and power density this motor type has gained great popularity and represents the state-of-the-art motor in a vast abundance of applications nowadays. However, in this context the machine analysis shall not and cannot be as profound as in a course focused only on electrical machines and their respective characteristics. Moreover, the important *flux-oriented control* scheme can be easily and clearly explained on the basis of this motor. Later it will be applied and extended also to the induction machine. Apart from the control principles, the power electronics, the pulse width modulation and the digital control implementation will be discussed, in consequence.

Even though this course is limited to the examples of the permanent magnet synchronous motor and the induction motor, the course participants shall be enabled to transfer the depicted principles to other drive systems, such as the separately excited synchronous motor, which cannot be dealt with in this course due to the limited amount of time.

I like to thank Mr. Dipl.-Ing. Tobias Huber who has done the translation of the German lecture notes to English language.

Paderborn, March 2013

Joachim Böcker

Contents

1   The Electrical Drive

measuring transducers
(current, voltage)

mech. sensor
(position, velocity)

electrical
power supply

u_n, i_n

motor

ω_{me}, T

mechanical
load

reference
values

low-level
control

measured
values

high-level
process control

state feedback

Fig. 1-1: Basic structure of electrical drive system

The modern electric drive consists of the following *basic components*:

- Motor as electromechanical energy transducer.
- Inverter (power electronics) for converting the electrical energy, the inverter is the actuator of the control loop.
- multi-level control unit (consisting of e.g. low-level current control & high level operating point selection unit)
- Transducers and sensors.

System boundaries:

The mentioned components represent the core of the electrical drive system. Depending on the assigned task and system boundaries the following items can be allocated to the drive system:

- Electric power supply, e.g. electric filters, transformers, if necessary, stationary or dynamic behavior of the power supply unit (battery, power grid) can also be included.
- Mechanical drive train, such as gear box, consideration of inertia, stiffness, accurate behavior of the driven mechanical load
- High-level / process control units for the realization of complex electrical drive tasks

External drive interfaces

- Within the power flow:
- to the electrical power supply (DC, AC, 3-phase voltage)
- to the mechanical load

- Within the information flow:
- Reference values and, if necessary, information from the superior high-level / process control or from the user.
- Feedback of internal states or measured values to high-level control

The electric drive can be described as a *controllable* electromechanical energy converter. Moreover, it can be characterized as a mechatronic system by its functional integration of power and information flow.

Power flow:
Many drive applications rely only on a unidirectional power flow (from the power supply to the load). However, if for example braking power shall be recuperated (operating mode: conversion of mechanical into electrical energy) a bidirectional power flow needs to be realized.

The structures for such kind of modern ways of electrical energy generation often do not vary from the basic structure of an electrical drive system. In contrast, generators for electrical energy supply purposes, as e.g. employed in conventional water- and thermal power plants, are connected directly to the grid without an intermediate electrical conversion stage. The necessary system control is not realized in an electrical way, but by controlling the applied mechanical power (impeller position of the turbine, throttle valve, etc.).

Examples:
- unidirectional electrical → mechanical: pumps, fans
- unidirectional mechanical → electrical: generators (wind power, water power, steam turbine)
- bidirectional electrical ↔ mechanical: traction drives for railways, drives in rolling lines, paper making machines

Fundamental drive tasks:
- Torque control
- Velocity control
- Position control

Mostly, those tasks are realized by using cascaded control structures: The position control relies on a subordinate velocity control, which in turn relies on a subordinate torque control.

Apart from these three fundamental tasks, there are numerous complex drive related tasks, which cannot be exactly allocated to one of the fundamental tasks, but rather represent combinations of these tasks, as for example in an elevator: positions control when stopping, velocity control during normal operation.

2 Structure and Modeling of Permanent Magnet Synchronous Motors (PMSM)

2.1 Modeling of a simplified motor with orthogonal windings
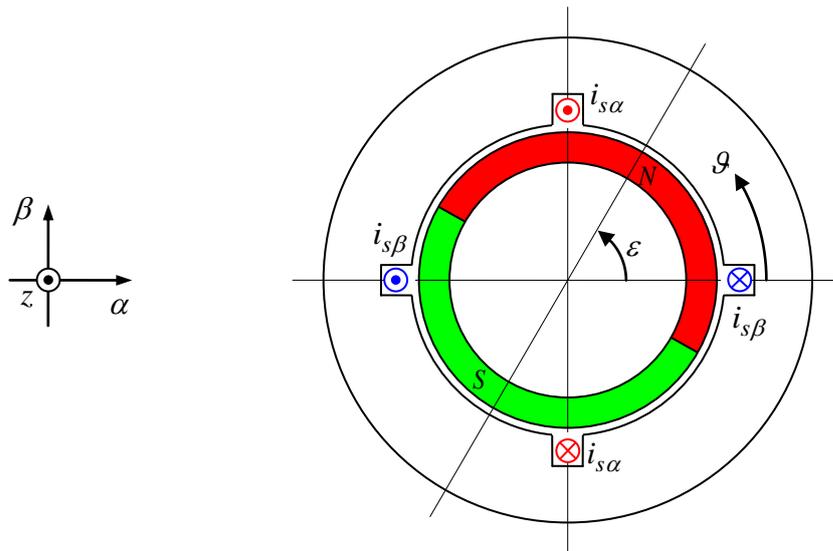
Fig. 2-1: Ideal permanent magnet motor with two orthogonal windings

ε : Angle of rotation of rotor against stator
ϑ : Circumference angle in stator fixed coordinates

Assumption: The normal component of the magnetic flux density caused by the permanent magnet is assumed to be sinusoidally distributed along the rotor circumference. The displacement of the sine curve depends on the rotor angle ε .

$$b_p(\vartheta) = \hat{b}_p \cos(\vartheta - \varepsilon) \tag{2.1}$$
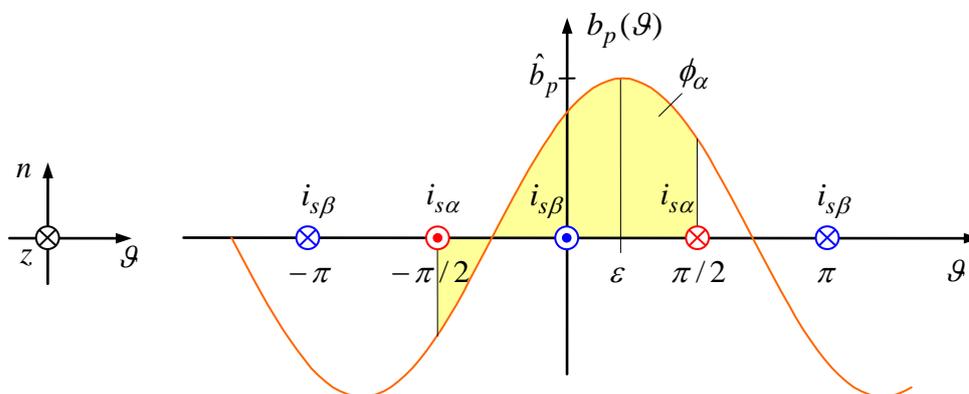
Fig. 2-2: Distribution of magnetic flux density vs. stator coordinate ϑ depending on the rotor angle ε

Remark on the direction of counting in the unwinded motor representation (motor cut open and made flat for better understanding): If the ϑ-axis is oriented to the right and the normal axis n is oriented upwards, then the z-axis, representing the longitudinal axis of the motor, has to be counted positively when going into the figure's sectional plane (i.e. into the paper). As a result, the directions of counting of the depicted currents are obtained. Geometrically speaking, this procedure corresponds to a view from the back onto the figure's sectional plane. In consequence, the directions of counting appear to be mirrored.

The flux through the stator winding α is now given by

$$\phi_{p\alpha} = rl \int_{-\pi/2}^{\pi/2} b_p(\vartheta)\, \mathrm{d}\vartheta \tag{2.2}$$

The included parameters are:

r effective radius
l magnetically effective motor length

It follows

$$\phi_{p\alpha} = rl\hat{b}_p \int_{-\pi/2}^{\pi/2} \cos(\vartheta - \varepsilon)\, \mathrm{d}\vartheta = 2rl\hat{b}_p \sin\left(\frac{\pi}{2} - \varepsilon\right) = 2rl\hat{b}_p \cos\varepsilon = \phi_p \cos\varepsilon \tag{2.3}$$

whereas

$$\phi_p = 2rl\hat{b}_p \tag{2.4}$$

Similarly, the flux through the stator winding β can be written as

$$\phi_{p\beta} = rl\hat{b}_p \int_{0}^{\pi} \cos(\vartheta - \varepsilon)\, \mathrm{d}\vartheta = 2rl\hat{b}_p \sin\varepsilon = \phi_p \sin\varepsilon \tag{2.5}$$

Taking into account the number of turns N for each stator winding, linkage fluxes result:

$$\psi_{p\alpha} = N\phi_{p\alpha} = \psi_p \cos\varepsilon \tag{2.6}$$

$$\psi_{p\beta} = N\phi_{p\beta} = \psi_p \sin\varepsilon \tag{2.7}$$

whereas

$$\psi_p = N\phi_p = 2Nrl\hat{b}_p \tag{2.8}$$

According to Faraday's law of induction, the induced voltages are:

$$e_\alpha = \dot{\psi}_{s\alpha} \tag{2.9}$$

$$e_\beta = \dot{\psi}_{s\beta} \tag{2.10}$$

where the fluxes $\psi_{s\alpha}, \psi_{s\beta}$ penetrate the conductor windings. The fluxes are composed of two portions, one generated by the permanent magnets, the other one by the conductor currents via the self inductance.

$$\psi_{s\alpha} = L_s i_{s\alpha} + \psi_{p\alpha} = L_s i_{s\alpha} + \psi_p \cos\varepsilon \tag{2.11}$$

$$\psi_{s\beta} = L_s i_{s\beta} + \psi_{p\beta} = L_s i_{s\beta} + \psi_p \sin\varepsilon \tag{2.12}$$
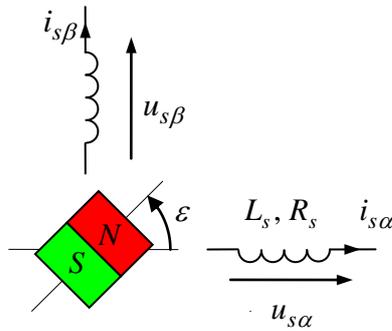
Furthermore, we shall as well consider the internal resistance of the windings, which leads to the following voltage equations

$$u_{s\alpha} = R_s i_{s\alpha} + \dot{\psi}_{s\alpha} \tag{2.13}$$

$$u_{s\beta} = R_s i_{s\beta} + \dot{\psi}_{s\beta} \tag{2.14}$$

$$u_{s\alpha} = R_s i_{s\alpha} + L_s \dot{i}_{s\alpha} + u_{i\alpha} = R_s i_{s\alpha} + L_s \dot{i}_{s\alpha} - \psi_p \omega \sin\varepsilon \tag{2.15}$$

$$u_{s\beta} = R_s i_{s\beta} + L_s \dot{i}_{s\beta} + u_{i\beta} = R_s i_{s\beta} + L_s \dot{i}_{s\beta} + \psi_p \omega \cos\varepsilon \tag{2.16}$$

$$\omega = \dot{\varepsilon} \tag{2.17}$$
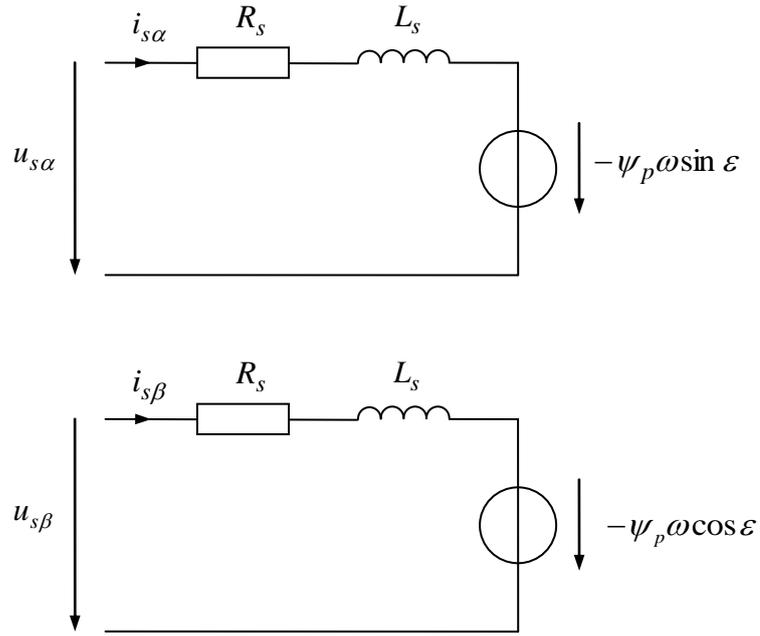
Fig. 2-3: Equivalent circuit diagram of a permanent magnet synchronous motor

Now, we can determine the torque from the power balance, i.e. by multiplying the above voltage equations with the currents:

$$u_{s\alpha}i_{s\alpha} = R_s i_{s\alpha}^2 + L_s \dot{i}_{s\alpha}i_{s\alpha} - i_{s\alpha}\psi_p\omega\sin\varepsilon \qquad (2.18)$$

$$u_{s\beta}i_{s\beta} = R_s i_{s\beta}^2 + L_s \dot{i}_{s\beta}i_{s\beta} + i_{s\beta}\psi_p\omega\cos\varepsilon \qquad (2.19)$$

The electrical power is given by

$$P_{el} = P_V + \dot{E}_{mag} + P_{me} \qquad (2.20)$$

whereas,

$$P_{el} = u_{s\alpha}i_{s\alpha} + u_{s\beta}i_{s\beta} \qquad (2.21)$$

$$P_V = R_s i_{s\alpha}^2 + R_s i_{s\beta}^2 \qquad (2.22)$$

$$P_{me} = \omega T = -i_{s\alpha}\psi_p\omega\sin\varepsilon + i_{s\beta}\psi_p\omega\cos\varepsilon \qquad (2.23)$$

In the equivalent circuit diagram, we can interpret the mechanical power as the power generated directly at the equivalent voltage sources.

The output torque can now be derived from the mechanical power as

$$T = -i_{s\alpha}\psi_p \sin\varepsilon + i_{s\beta}\psi_p \cos\varepsilon \qquad (2.24)$$

Introduction of vector notation:

$$\mathbf{i}_s = \begin{bmatrix} i_{s\alpha} \\ i_{s\beta} \end{bmatrix}, \quad \boldsymbol{\psi}_p = \begin{bmatrix} \psi_{p\alpha} \\ \psi_{p\beta} \end{bmatrix} = \begin{bmatrix} \psi_p \cos\varepsilon \\ \psi_p \sin\varepsilon \end{bmatrix} = \psi_p \begin{bmatrix} \cos\varepsilon \\ \sin\varepsilon \end{bmatrix}$$

Thus, the torque follows as

$$T = \psi_{p\alpha} i_{s\beta} - \psi_{p\beta} i_{s\alpha} = \begin{bmatrix} \boldsymbol{\psi}_p, \mathbf{i}_s \end{bmatrix} = \boldsymbol{\psi}_p \times \mathbf{i}_s \qquad (2.25)$$

The bracket [,] or cross × in the above equation represents the outer or vector/cross product of two vectors in a plane. The cross product now corresponds to the area covered by the parallelogram spanned by the two vectors, as shown in the figure below.
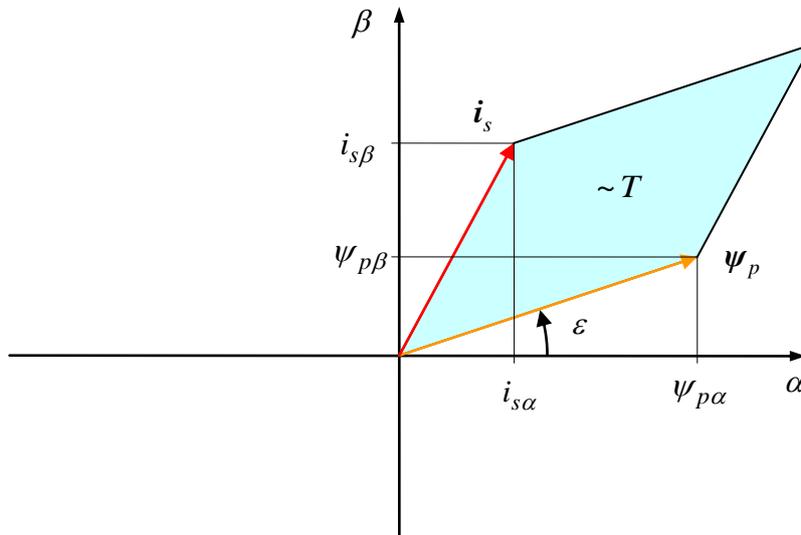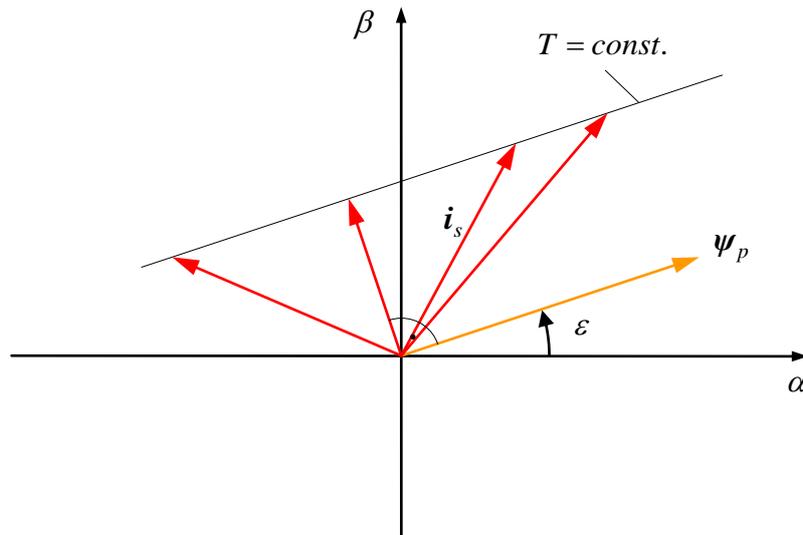
For a given vector of the permanent magnet flux, all current vectors lying on the shear line (*T=const.*) of the parallelogram generate the same output torque. However, only the current vector which is perpendicular to the magnetic flux produces torque with a minimum current magnitude and thus with minimum heat/ohmic losses.

2.2 The rotating rotor-fixed d/q coordinate system:
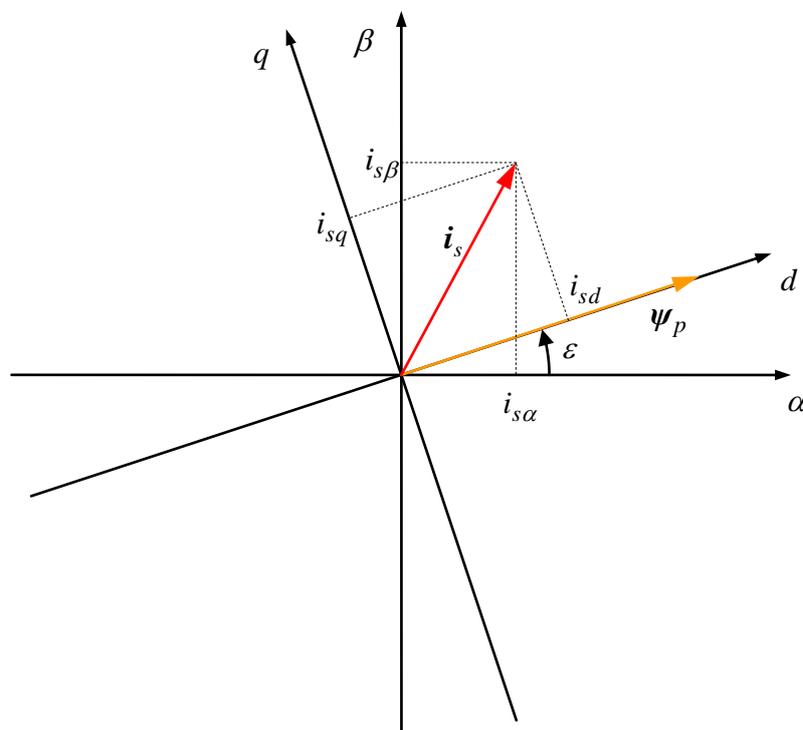
Fig. 2-4: Introduction of a rotor-fixed coordinate system aligned in the direction of the permanent magnet flux

In the *d/q* -rotating frame, the equation for the torque can be simply expressed by

$$T = \psi_p i_{sq} \tag{2.26}$$

The i_{sd} component does not affect the torque, as it is aligned to the *d*-axis. Given a desired torque *T*, the necessary current component i_{sq} can be calculated by

$$i_{sq} = \frac{T}{\psi_p} \tag{2.27}$$

In order to set a torque with minimum current magnitude, the current component i_{sd} should be set to its minimal value, i.e.

$$i_{sd} = 0 \tag{2.28}$$

The *d/q*- coordinate system is named after its two axes, the *direct* and *quadrature* axis. The *direct* axis is hereby aligned with the permanent magnet flux vector, while the *quadrature* axis is perpendicular to the *d*-axis.

The transformation of a general vector *x* between stator-fixed coordinates *α/β* and rotor-fixed coordinates *d/q* is given the expression

$$\begin{bmatrix} x_\alpha \\ x_\beta \end{bmatrix} = \boldsymbol{Q}(\varepsilon) \begin{bmatrix} x_d \\ x_q \end{bmatrix}$$

where $\boldsymbol{Q}$ represents the rotational transformation matrix, given by

$$\boldsymbol{Q}(\varepsilon) = \begin{bmatrix} \cos\varepsilon & -\sin\varepsilon \\ \sin\varepsilon & \cos\varepsilon \end{bmatrix}$$

In the field of electrical machines this transformation is also commonly known as the *Park-Transformation*. For an inverse transformation can thus be written as

$$\begin{bmatrix} x_d \\ x_q \end{bmatrix} = \boldsymbol{Q}(-\varepsilon) \begin{bmatrix} x_\alpha \\ x_\beta \end{bmatrix} = \boldsymbol{Q}^{-1}(\varepsilon) \begin{bmatrix} x_\alpha \\ x_\beta \end{bmatrix}$$

Later, we also need the time derivative of the rotation matrix, which can be expressed as

$$\dot{\boldsymbol{Q}}(\varepsilon) = \dot{\varepsilon} \frac{d}{d\varepsilon} \boldsymbol{Q}(\varepsilon) = \omega \begin{bmatrix} -\sin\varepsilon & -\cos\varepsilon \\ \cos\varepsilon & -\sin\varepsilon \end{bmatrix} = \omega \boldsymbol{J} \boldsymbol{Q}(\varepsilon) = \omega \boldsymbol{Q}(\varepsilon) \boldsymbol{J}$$

whereas

$$J = \begin{bmatrix} 0 & -1 \\ 1 & 0 \end{bmatrix}$$

Transforming the voltage equations results in

$$Q(-\varepsilon)\begin{bmatrix} u_{s\alpha} \\ u_{s\beta} \end{bmatrix} = R_s\, Q(-\varepsilon)\begin{bmatrix} i_{s\alpha} \\ i_{s\beta} \end{bmatrix} + Q(-\varepsilon)\frac{d}{dt}\begin{bmatrix} \psi_{s\alpha} \\ \psi_{s\beta} \end{bmatrix}$$

$$\begin{aligned}
\begin{bmatrix} u_{sd} \\ u_{sq} \end{bmatrix} &= R_s\begin{bmatrix} i_{sd} \\ i_{sq} \end{bmatrix} + Q(-\varepsilon)\frac{d}{dt}\left(Q(\varepsilon)\begin{bmatrix} \psi_{sd} \\ \psi_{sq} \end{bmatrix} \right) \\
&= R_s\begin{bmatrix} i_{sd} \\ i_{sq} \end{bmatrix} + Q(-\varepsilon)Q(\varepsilon)\frac{d}{dt}\begin{bmatrix} \psi_{sd} \\ \psi_{sq} \end{bmatrix} + Q(-\varepsilon)\dot{Q}(\varepsilon)\begin{bmatrix} \psi_{sd} \\ \psi_{sq} \end{bmatrix} \\
&= R_s\begin{bmatrix} i_{sd} \\ i_{sq} \end{bmatrix} + \frac{d}{dt}\begin{bmatrix} \psi_{sd} \\ \psi_{sq} \end{bmatrix} + \omega J\begin{bmatrix} \psi_{sd} \\ \psi_{sq} \end{bmatrix} \\
&= R_s\begin{bmatrix} i_{sd} \\ i_{sq} \end{bmatrix} + \frac{d}{dt}\begin{bmatrix} \psi_{sd} \\ \psi_{sq} \end{bmatrix} + \omega\begin{bmatrix} -\psi_{sq} \\ \psi_{sd} \end{bmatrix} \\
&= R_s\begin{bmatrix} i_{sd} \\ i_{sq} \end{bmatrix} + L_s\frac{d}{dt}\begin{bmatrix} i_{sd} \\ i_{sq} \end{bmatrix} + \omega L_s\begin{bmatrix} -i_{sq} \\ i_{sd} \end{bmatrix} + \omega\begin{bmatrix} 0 \\ \psi_p \end{bmatrix}
\end{aligned} \qquad (2.29)$$

Representing the voltages in component notation leads to

$$u_{sq} = R_s\, i_{sq} + \dot{\psi}_{sq} + \omega\psi_{sd} \qquad (2.30)$$

$$u_{sd} = R_s\, i_{sd} + \dot{\psi}_{sd} - \omega\psi_{sq} \qquad (2.31)$$

Now, transforming the flux equations results in

$$Q(-\varepsilon)\begin{bmatrix} \psi_{s\alpha} \\ \psi_{s\beta} \end{bmatrix} = L_s Q(-\varepsilon)\begin{bmatrix} i_{s\alpha} \\ i_{s\beta} \end{bmatrix} + \psi_p Q(-\varepsilon)\begin{bmatrix} \cos\varepsilon \\ \sin\varepsilon \end{bmatrix}$$

$$\begin{bmatrix} \psi_{sd} \\ \psi_{sq} \end{bmatrix} = L_s\begin{bmatrix} i_{sd} \\ i_{sq} \end{bmatrix} + \psi_p\begin{bmatrix} 1 \\ 0 \end{bmatrix} \qquad (2.32)$$

Applying component notation again leads to

$$\psi_{sq} = L_s i_{sq} \qquad (2.33)$$

$$\psi_{sd} = L_s i_{sd} + \psi_p \qquad (2.34)$$

When substituting the flux derivatives by the current derivatives in the above voltage equations, it follows

$$u_{sd} = R_s\, i_{sd} + L_s\dot{i}_{sd} - \omega L_s i_{sq} \tag{2.35}$$

$$u_{sq} = R_s\, i_{sq} + L_s\dot{i}_{sq} + \omega L_s i_{sd} + \omega \psi_p \tag{2.36}$$
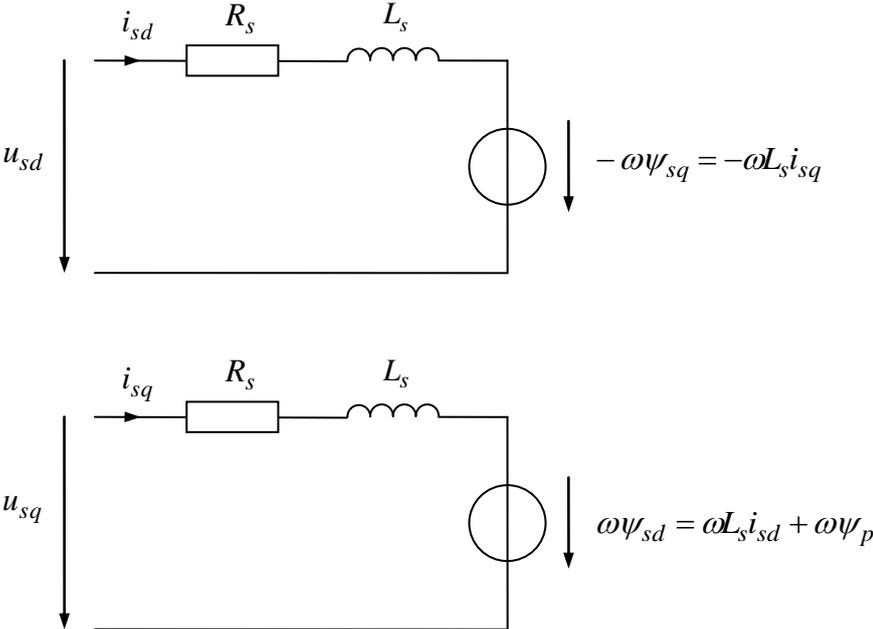
Fig. 2-5: Equivalent circuit diagram of the PMSM motor in *d/q*-coordinates

2.3 The Three-Phase Motor
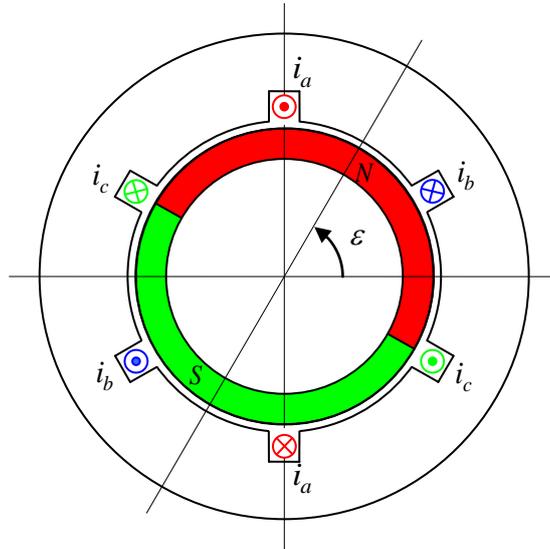
Fig. 2-6: Three phase motor with windings fixed at 120° to each other on the stator
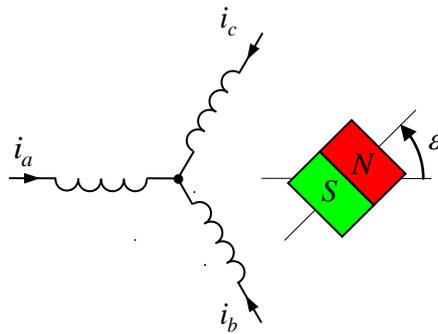
Fig. 2-7: Schematic diagram of the three-phase motor

The sinusoidal flux density produced by the permanent magnets is distributed among the *a, b, c* stator windings similar as in the two-phase orthogonal motor case.

$$\psi_{pa} = \psi_p \cos\varepsilon \tag{2.37}$$

$$\psi_{pb} = \psi_p \cos\left(\varepsilon - \frac{2\pi}{3}\right) \tag{2.38}$$

$$\psi_{pc} = \psi_p \cos\left(\varepsilon + \frac{2\pi}{3}\right) \tag{2.39}$$

The voltage equations are given by

$$u_a = R^w i_a + \dot{\psi}_a \tag{2.40}$$

$$u_b = R^w i_b + \dot{\psi}_b \tag{2.41}$$

$$u_c = R^w i_c + \dot{\psi}_c \tag{2.42}$$

Due to symmetry reasons, there is no coupling between the orthogonal windings in the two-phase motor case. The mutual inductance between these two windings is zero in consequence. In the three-phase motor case, each of the 120° shifted windings has a self inductance L^w. Moreover, always two of these windings, respectively, are linked with each other through a flux. These couplings are expressed by the mutual inductance L_h^w. Due to motor symmetry, all pair wise couplings have to be of the same magnitude. Due to the introduced directions for the currents the couplings have a negative sign, indicated by prefixing the positive mutual inductance with a negative sign, as well.

$$\psi_a = L^w i_a - L_h^w (i_b + i_c) + \psi_{pa} \tag{2.43}$$

$$\psi_b = L^w i_b - L_h^w (i_c + i_a) + \psi_{pb} \tag{2.44}$$

$$\psi_c = L^w i_c - L_h^w (i_a + i_b) + \psi_{pc} \tag{2.45}$$

If the motor is constructed in that way that that the return path of the flux ψ_a is split half by half through the windings b and c, the relation between self and mutual inductance results directly as

$$L_h^w = \frac{1}{2} L^w \tag{2.46}$$

In the general case, there will exist usually also return paths which are not linked with the neighbored coils b and c so that a smaller mutual results. However, at least an upper bound can be concluded like

$$L_h^w \leq \frac{1}{2} L^w \tag{2.47}$$
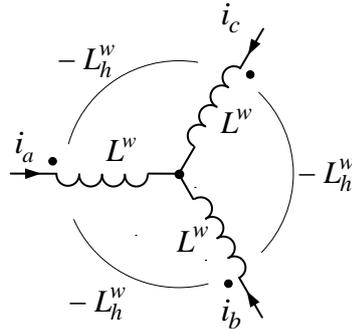
Fig. 2-8: Self and mutual inductances of a 3-phase motor

2.4 Transformation of three-phase components into orthogonal components

The transformation of the three vector components x_a, x_b, x_c to orthogonal components is given by

$$\begin{bmatrix} x_\alpha \\ x_\beta \\ x_0 \end{bmatrix} = \begin{bmatrix} \frac{2}{3} & -\frac{1}{3} & -\frac{1}{3} \\ 0 & \frac{1}{\sqrt{3}} & -\frac{1}{\sqrt{3}} \\ \frac{\sqrt{2}}{3} & \frac{\sqrt{2}}{3} & \frac{\sqrt{2}}{3} \end{bmatrix} \begin{bmatrix} x_a \\ x_b \\ x_c \end{bmatrix} = T \begin{bmatrix} x_a \\ x_b \\ x_c \end{bmatrix} \tag{2.48}$$

The transformation results in two orthogonal components x_α, x_β and a zero component x_0. A commonly known alternative definition of the zero component is

$$x_0 = \tfrac{1}{3}(x_a + x_b + x_c) \tag{2.49}$$

In this case, the zero component represents the arithmetic mean value of the three phase components x_a, x_b, x_c and differs from the above expression in the transformation matrix only by the factor $\sqrt{2}$. However, as far as the representation of power terms is concerned, the first definition of the zero component has turned to be advantageous (see below).

The inverse transformation can be performed as shown below

$$\begin{bmatrix} x_a \\ x_b \\ x_c \end{bmatrix} = \begin{bmatrix} 1 & 0 & \frac{1}{\sqrt{2}} \\ -\frac{1}{2} & \frac{\sqrt{3}}{2} & \frac{1}{\sqrt{2}} \\ -\frac{1}{2} & -\frac{\sqrt{3}}{2} & \frac{1}{\sqrt{2}} \end{bmatrix} \begin{bmatrix} x_\alpha \\ x_\beta \\ x_0 \end{bmatrix} = T^{-1} \begin{bmatrix} x_\alpha \\ x_\beta \\ x_0 \end{bmatrix} .$$

Scalar/inner products, as they commonly occur in power terms, can be written as follows

$$\begin{bmatrix} x_a \\ x_b \\ x_c \end{bmatrix}^{\mathrm{T}} \begin{bmatrix} y_a \\ y_b \\ y_c \end{bmatrix} = \begin{bmatrix} x_\alpha \\ x_\beta \\ x_0 \end{bmatrix}^{\mathrm{T}} \boldsymbol{T}^{-\mathrm{T}} \boldsymbol{T}^{-1} \begin{bmatrix} y_\alpha \\ y_\beta \\ y_0 \end{bmatrix}$$

$$x_a y_a + x_b y_b + x_c y_c = \frac{3}{2}\left(x_\alpha y_\alpha + x_\beta y_\beta + x_0 y_0\right) \tag{2.50}$$

$\boldsymbol{T}^{-\mathrm{T}}$ represents the transposed inverse matrix. Aside from this,

$$\boldsymbol{T}^{-1} = \frac{3}{2}\boldsymbol{T}^{\mathrm{T}}, \quad \boldsymbol{T}^{\mathrm{T}}\boldsymbol{T} = \boldsymbol{T}\boldsymbol{T}^{\mathrm{T}} = \frac{2}{3}\boldsymbol{I}_3 \tag{2.51}$$

Note: The transformation could also be defined as

$$\widetilde{\boldsymbol{T}} = \sqrt{\frac{3}{2}}\boldsymbol{T} \tag{2.52}$$

As compared to $\boldsymbol{T}$, $\widetilde{\boldsymbol{T}}$ is *orthogonal*, and therefore has the property

$$\widetilde{\boldsymbol{T}}^{-1} = \widetilde{\boldsymbol{T}}^{\mathrm{T}} \quad \text{and} \quad \widetilde{\boldsymbol{T}}^{\mathrm{T}}\widetilde{\boldsymbol{T}} = \widetilde{\boldsymbol{T}}\widetilde{\boldsymbol{T}}^{\mathrm{T}} = \boldsymbol{I}_3 \tag{2.53}$$

The modified Transformation $\widetilde{\boldsymbol{T}}$ is called *power-invariant*, due to the fact that the 3/2 scaling factor disappears during the transformation of the inner products. The major drawback of this transformation is, however, that the projections of the vectors onto the corresponding axes can no longer be directly interpreted as phase components (see below). Therefore, the here presented transformation $\boldsymbol{T}$ has been generally accepted.

If the absence of a zero component can be assumed, the above equations can be simplified as follows.

$$\begin{bmatrix} x_\alpha \\ x_\beta \end{bmatrix} = \boldsymbol{T}_{23} \begin{bmatrix} x_a \\ x_b \\ x_c \end{bmatrix}$$

$$\boldsymbol{T}_{23} = \begin{bmatrix} \frac{2}{3} & -\frac{1}{3} & -\frac{1}{3} \\ 0 & \frac{1}{\sqrt{3}} & -\frac{1}{\sqrt{3}} \end{bmatrix} = \frac{2}{3}\begin{bmatrix} 1 & -\frac{1}{2} & -\frac{1}{2} \\ 0 & \frac{\sqrt{3}}{2} & -\frac{\sqrt{3}}{2} \end{bmatrix} \tag{2.54}$$

and

$$\begin{bmatrix} x_a \\ x_b \\ x_c \end{bmatrix} = \boldsymbol{T}_{32} \begin{bmatrix} x_\alpha \\ x_\beta \end{bmatrix} \tag{2.55}$$

$$\boldsymbol{T}_{32} = \begin{bmatrix} 1 & 0 \\ -\frac{1}{2} & \frac{\sqrt{3}}{2} \\ -\frac{1}{2} & -\frac{\sqrt{3}}{2} \end{bmatrix} = \frac{3}{2} \boldsymbol{T}_{23}^{\mathrm{T}} \tag{2.56}$$

For the reduced transformation matrices the following properties apply.

$$\boldsymbol{T}_{23}\boldsymbol{T}_{32} = \boldsymbol{I}_2 = \begin{bmatrix} 1 & 0 \\ 0 & 1 \end{bmatrix} \tag{2.57}$$

but,

$$\boldsymbol{T}_{32}\boldsymbol{T}_{23} = \begin{bmatrix} \frac{2}{3} & -\frac{1}{3} & -\frac{1}{3} \\ -\frac{1}{3} & \frac{2}{3} & -\frac{1}{3} \\ -\frac{1}{3} & -\frac{1}{3} & \frac{2}{3} \end{bmatrix} = \boldsymbol{I}_3 - \frac{1}{3}\begin{bmatrix} 1 & 1 & 1 \\ 1 & 1 & 1 \\ 1 & 1 & 1 \end{bmatrix} \tag{2.58}$$

The relationships between the differences of the phase components (also known as linked or phase-to-phase components)

$$\begin{aligned} x_{ab} &= x_a - x_b \\ x_{bc} &= x_b - x_c \end{aligned} \tag{2.59}$$

and the orthogonal components

$$\begin{bmatrix} x_\alpha \\ x_\beta \end{bmatrix} = \begin{bmatrix} \frac{2}{3} & \frac{1}{3} \\ 0 & \frac{1}{\sqrt{3}} \end{bmatrix} \begin{bmatrix} x_{ab} \\ x_{bc} \end{bmatrix} \tag{2.60}$$

$$\begin{bmatrix} x_{ab} \\ x_{bc} \end{bmatrix} = \begin{bmatrix} \frac{3}{2} & -\frac{\sqrt{3}}{2} \\ 0 & \sqrt{3} \end{bmatrix} \begin{bmatrix} x_\alpha \\ x_\beta \end{bmatrix} \tag{2.61}$$

are also useful.
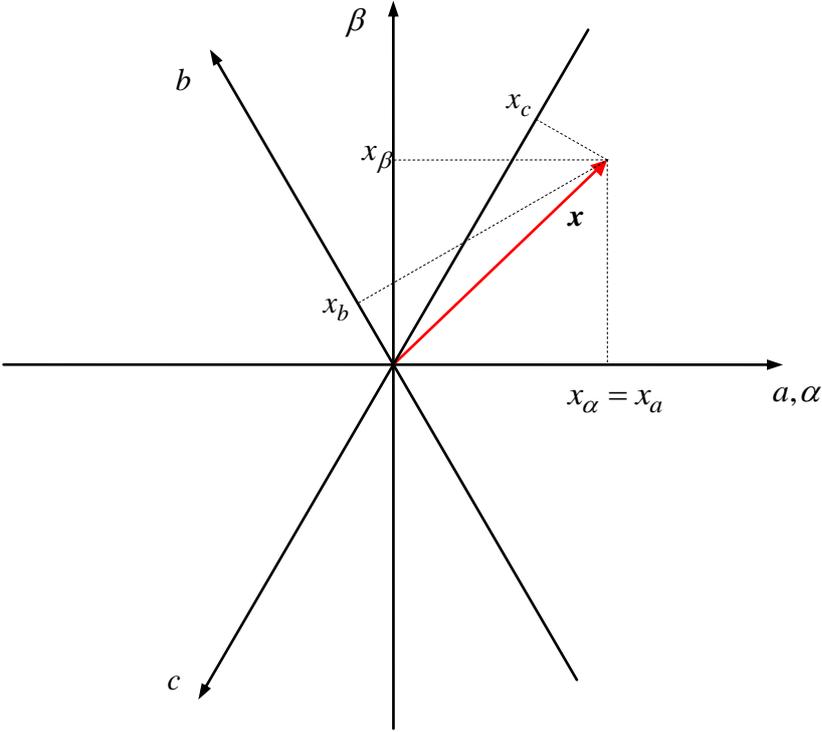
Fig. 2-9: Geometrical interpretation of the transformation with no zero components
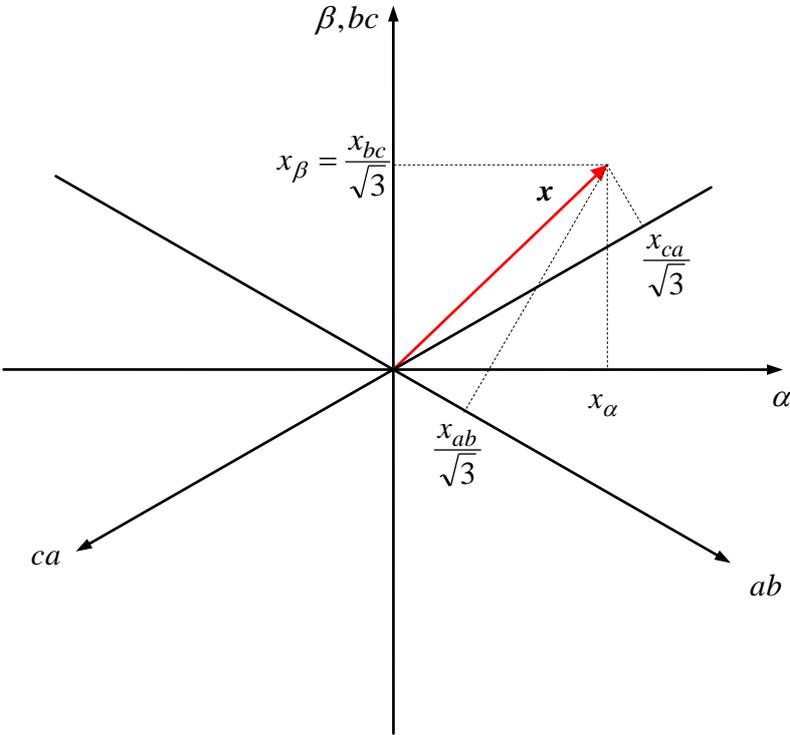
Fig. 2-10: Geometrical interpretation of the linked components

2.5　Mapping the Three-Phase Model on the Orthogonal Two-Phase Model

With the law of induction, the equations of the three-phase motor in vector notation are given:

$$\begin{bmatrix} u_a \\ u_b \\ u_c \end{bmatrix} = R^w \begin{bmatrix} i_a \\ i_b \\ i_c \end{bmatrix} + \frac{d}{dt} \begin{bmatrix} \psi_a \\ \psi_b \\ \psi_c \end{bmatrix} \tag{2.62}$$

Flux linkage equations:

$$\begin{aligned} \begin{bmatrix} \psi_a \\ \psi_b \\ \psi_c \end{bmatrix} &= \boldsymbol{L}^w \begin{bmatrix} i_a \\ i_b \\ i_c \end{bmatrix} + \begin{bmatrix} \psi_{pa} \\ \psi_{pb} \\ \psi_{pc} \end{bmatrix} \\ &= \boldsymbol{L}^w \begin{bmatrix} i_a \\ i_b \\ i_c \end{bmatrix} + \psi_p \begin{bmatrix} \cos\varepsilon \\ \cos(\varepsilon - 2\pi/3) \\ \cos(\varepsilon + 2\pi/3) \end{bmatrix} \end{aligned} \tag{2.63}$$

with the inductance matrix

$$\boldsymbol{L}^w = \begin{bmatrix} L^w & -L_h^w & -L_h^w \\ -L_h^w & L^w & -L_h^w \\ -L_h^w & -L_h^w & L^w \end{bmatrix} = \left(L^w + L_h^w\right)\begin{bmatrix} 1 & 0 & 0 \\ 0 & 1 & 0 \\ 0 & 0 & 1 \end{bmatrix} - L_h^w \begin{bmatrix} 1 & 1 & 1 \\ 1 & 1 & 1 \\ 1 & 1 & 1 \end{bmatrix} \tag{2.64}$$

Assumption: Motor windings are connected in star configuration

$$i_a + i_b + i_c = 0 \tag{2.65}$$

i.e. current components are free from a zero component:

$$i_0 = 0$$

We quickly see that also the following equations apply:

$$u_0 = 0$$

$$\psi_0 = 0$$

Note, that when taking saturation or structural asymmetries of the motor into account, the zero component of the flux and thus the voltage cannot be neglected anymore. In the following, however, all quantities shall be considered as free of zero components, allowing a two-dimensional vector representation, respectively.

Exercise: Under which conditions do the zero components disappear when the motor windings are connected in delta configuration?

Applying the transformation matrix $\boldsymbol{T}_{23}$ to the voltage equations leads to

$$\boldsymbol{T}_{23}\begin{bmatrix} u_a \\ u_b \\ u_c \end{bmatrix} = R^w \boldsymbol{T}_{23}\begin{bmatrix} i_a \\ i_b \\ i_c \end{bmatrix} + \boldsymbol{T}_{23}\frac{d}{dt}\begin{bmatrix} \psi_a \\ \psi_b \\ \psi_c \end{bmatrix} \quad \Rightarrow \quad \begin{bmatrix} u_{s\alpha} \\ u_{s\beta} \end{bmatrix} = R^w \begin{bmatrix} i_{s\alpha} \\ i_{s\beta} \end{bmatrix} + \frac{d}{dt}\begin{bmatrix} \psi_{s\alpha} \\ \psi_{s\beta} \end{bmatrix} \tag{2.66}$$

That means that the winding resistance value of the orthogonal motor model corresponds to the one of the three-phase motor model:

$$R_s = R^w$$

Flux linkage equations:

$$\boldsymbol{T}_{23}\begin{bmatrix} \psi_a \\ \psi_b \\ \psi_c \end{bmatrix} = \boldsymbol{T}_{23}\boldsymbol{L}^w \begin{bmatrix} i_a \\ i_b \\ i_c \end{bmatrix} + \psi_p \boldsymbol{T}_{23}\begin{bmatrix} \cos\varepsilon \\ \cos(\varepsilon - 2\pi/3) \\ \cos(\varepsilon + 2\pi/3) \end{bmatrix}$$

$$\begin{bmatrix} \psi_{s\alpha} \\ \psi_{s\beta} \end{bmatrix} = \boldsymbol{T}_{23}\boldsymbol{L}^w \boldsymbol{T}_{32}\begin{bmatrix} i_{s\alpha} \\ i_{s\beta} \end{bmatrix} + \psi_p \begin{bmatrix} \cos\varepsilon \\ \sin\varepsilon \end{bmatrix}$$

$$\begin{bmatrix} \psi_{s\alpha} \\ \psi_{s\beta} \end{bmatrix} = \boldsymbol{T}_{23}\boldsymbol{L}^w \boldsymbol{T}_{32}\begin{bmatrix} \psi_{s\alpha} \\ \psi_{s\beta} \end{bmatrix} + \psi_p \begin{bmatrix} \cos\varepsilon \\ \sin\varepsilon \end{bmatrix} \tag{2.67}$$

Now evaluating the transformation of the inductance matrix results in

$$\boldsymbol{T}_{23}\boldsymbol{L}^w \boldsymbol{T}_{32} = \left(L^w + L_h^w\right)\boldsymbol{T}_{23}\boldsymbol{I}_3 \boldsymbol{T}_{32} - L_h^w \begin{bmatrix} \frac{2}{3} & -\frac{1}{3} & -\frac{1}{3} \\ 0 & \frac{1}{\sqrt{3}} & -\frac{1}{\sqrt{3}} \end{bmatrix}\begin{bmatrix} 1 & 1 & 1 \\ 1 & 1 & 1 \\ 1 & 1 & 1 \end{bmatrix}\begin{bmatrix} 1 & 0 \\ -\frac{1}{2} & \frac{\sqrt{3}}{2} \\ -\frac{1}{2} & -\frac{\sqrt{3}}{2} \end{bmatrix} \tag{2.68}$$

$$= \left(L^w + L_h^w\right)\boldsymbol{I}_2$$

Based on this equation, the equivalent inductance of the orthogonal model

$$L_s = L^w + L_h^w \approx \frac{3}{2}L^w \tag{2.69}$$

is determined.

So far, the torque of the three-phase motor model has not been identified. However, based on the introduced transformation matrix notation, the torque can again be easily derived through a consideration of the power terms. According to section 2.4, when expressing the power of a three-phase system through the product of the corresponding orthogonal components, the scaling factor 3/2 has to be taken into account. The torque of the three-phase motor can now be written as

$$T = \frac{3}{2}\left(\psi_{p\alpha}i_{s\beta} - \psi_{p\beta}i_{s\alpha}\right) = \frac{3}{2}\psi_{p}i_{sq}. \tag{2.70}$$

Memorizing rule: The factor 3/2 can be understood from scaling up the power and the torque of a two-phase motor model to three phases.

2.6 Determining Stator Resistance and Stator Inductance Using Measuring Techniques

The parameters of R_s and L_s can be determined by measuring a single winding between a terminal and the star/neutral point, as shown in the previous paragraph. As the neutral point is often not accessible, measurements have to be made between two phases. Assuming that the third terminal remains open, the resistance between the two terminals a and b results to

$$R_{ab} = 2R^w = 2R_s$$

Moreover, while regarding $i_a = -i_b$, the phase-to-phase inductance results to

$$L_{ab} = 2L^w + 2L_h^w = 2L_s.$$

2.7 Multi-Pole Motors

In case the arrangement of mutually magnetized magnets repeats over the rotor circumference, we speak of multi-pole motors. As no monopoles of magnetic fields exist, the *pole pair* number p is used as the characteristic quantity in this context, instead of the pole number. Note, that the stator windings in multi-pole motors need to be rearranged, as well.

Along the motor circumference, the magnetic field as well as the winding arrangement have an angular periodicity of $2\pi / p$. In order to continue to be able to work with quantities with a periodicity of 2π, the angle variable

$$\varepsilon = p\varepsilon_{me} \tag{2.71}$$

is introduced. The variable ε refers to the electrical system and is therefore denoted as *electrical* (rotation) angle.
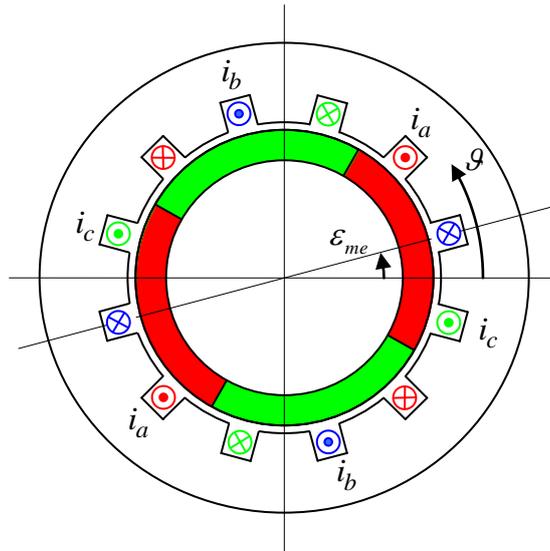
Fig. 2-11: Motor with pole pair number $p = 2$
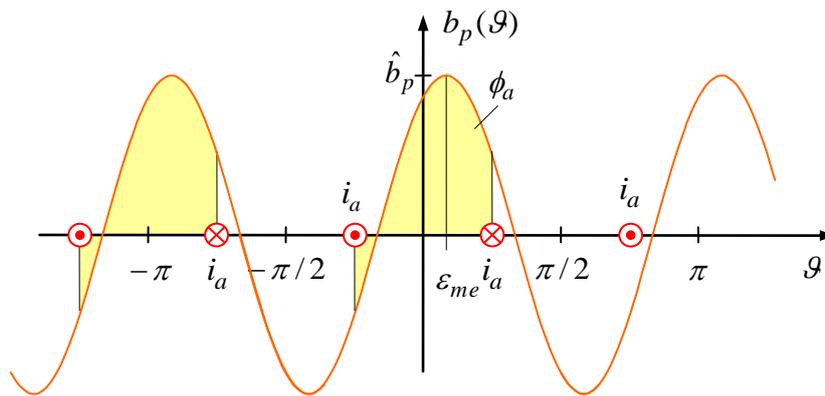
Fig. 2-12: Flux distribution in a motor with two pole pairs and flux through a conductor loop

The relationships between the geometrical field quantities and the equivalent electromagnetic quantities slightly change: The permanent magnetic flux through a single conductor loop is now expressed by

$$\phi = \phi_p \cos p(\varepsilon_{me} - \vartheta_0) = \phi_p \cos(\varepsilon - p\vartheta_0) \tag{2.72}$$

whereas ϑ_0 indicates the geometrical angular location of the considered loop. For example, as for the two loops (phase a) presented in the above figure, $\vartheta_0 = 0$ and $\vartheta_0 = \pi$, respectively. The peak or crest value of the flux through *one* of these loops reduces to

$$\phi_p = 2\frac{r}{p}l\hat{b}_p \tag{2.73}$$

due to the fact, that in multi-pole motors a single winding only spans over the mechanical angle π / p instead of π. Adding up all conductor loops of one stator winding corresponds to a multiplication of the flux with the number of turns N. In this context, it should be noted, that all conductor loops of a winding, no matter over which magnetic pole the corresponding winding is located, always provide the same flux contribution. The flux linkage of the windings can now be written as follows:

$$\psi_{pa} = \psi_p \cos\varepsilon \tag{2.74}$$

$$\psi_{pb} = \psi_p \cos\left(\varepsilon - \frac{2\pi}{3}\right) \tag{2.75}$$

$$\psi_{pc} = \psi_p \cos\left(\varepsilon + \frac{2\pi}{3}\right) \tag{2.76}$$

with

$$\psi_p = N\phi_p = \frac{2Nrl\hat{b}_p}{p} \tag{2.77}$$

As N represents the total number of turns per winding, N / p turns can thus be allocated to a single pole pair. When using the electrical angle ε, the relationships get the same appearance as in the case of the motor with pole pair number $p = 1$.

As far as the transition from three phases to orthogonal coordinates and transformation into the rotating d/q-system is concerned, the general procedure does not change, except for the torque. The torque can be derived from the power balance again, whereas now it has to be distinguished between the mechanical angular frequency ω_{me} and the electrical angular frequency ω :

$$P_{me} = \omega_{me}T = \frac{\omega}{p}T = \frac{3}{2}\omega\psi_p i_{sq} \tag{2.78}$$

Thus,

$$T = \frac{3}{2} p\psi_p i_{sq} \; . \tag{2.79}$$

2.8　Winding Configuration

So far we have assumed that the conductors of a winding are located at the geometrically ideal positions inside the stator. In fact, the conductors of a winding are usually distributed along the circumference of the stator. The copper wires are embedded inside *slots,* as shown below. In case round copper wire is wound inside the slots, we commonly speak of *random-wound* machines. However, as for machines with high power ratings and high degrees of utilization usually *shaped wires* or *shaped bars* are employed, which fit perfectly inside the stator slots. In this case, we speak of *form-wound* machines. As for the random-wound machines, *fill factors* between 0.3 - 0.5 can be achieved, for form-wound machines fill factors between 0.8 - 0.9 are even possible.
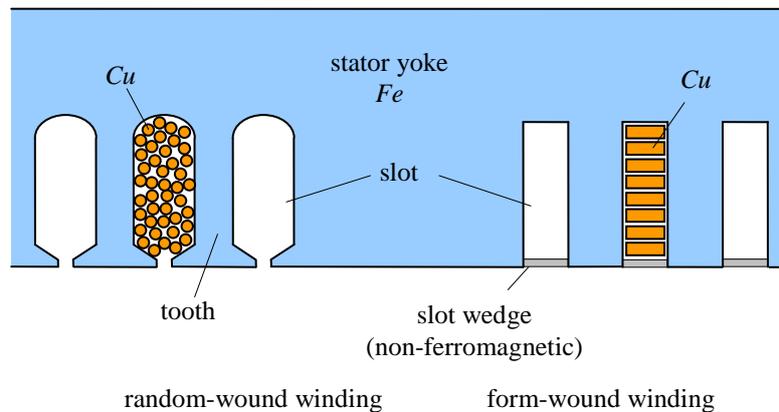
Fig. 2-13: Stator structure (linear representation)
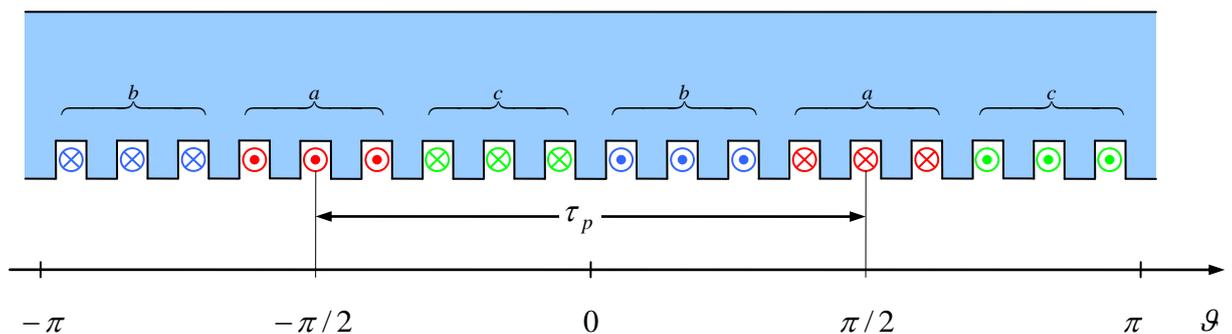
Scheme of a distributed winding with $Q = 18$, $p = 1$, $q = 3$
(Usually, the teeth bottoms are shoe-shape-like widened,
this is not shown in this schematic diagram)

Definitions:

Q	Number of slots
m	Number of phases (only three-phase machines shall be assumed here, i.e. $m = 3$)
p	Number of pole pairs

$$\tau_p = \frac{2\pi}{2p} \quad \text{pole pitch}$$

$$q = \frac{Q}{2pm} \quad \text{Number of notches (Number of slots per phase and pole)}$$

If q is an integer, we speak of *integral-slot winding*, otherwise of *fractional-slot winding*.
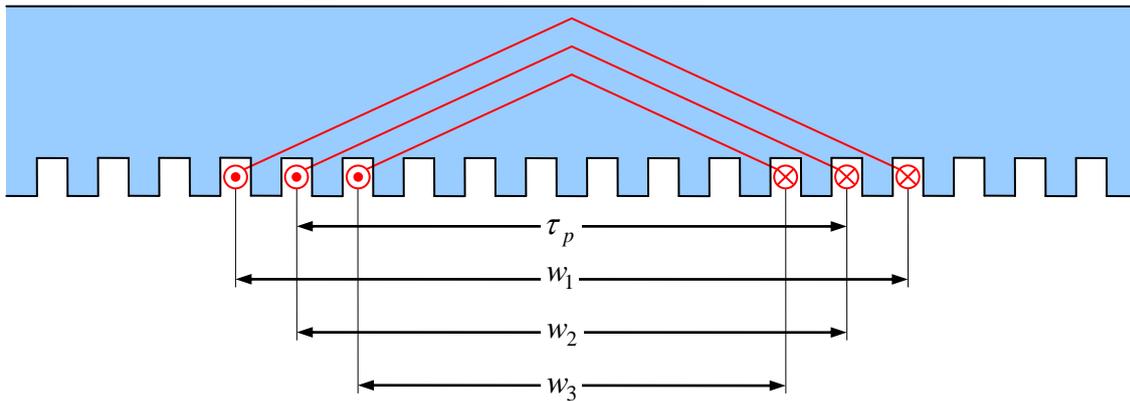
Fig. 2-14: Realization of the distributed winding a through concentric windings with varying widths
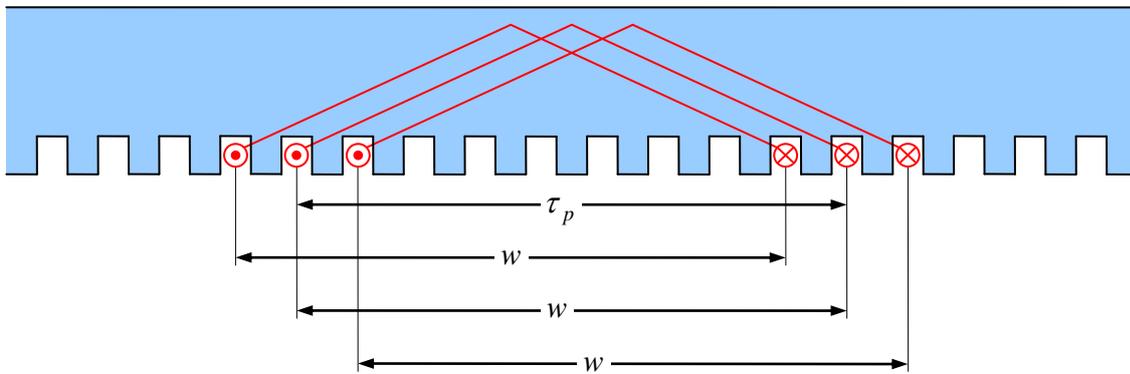
Fig. 2-15: Realization of the distributed winding a through windings with the same width $w = \tau_p$

Flux linkage of distributed windings: The windings can be configured differently for the same distribution onto the slots. As these different configurations concern only the end windings, however, conductor loops of the same width w can be assumed. The flux of a single conductor loop (see above) can be expressed by

$$\phi = \phi_p \cos(\varepsilon - p\theta_0) \tag{2.80}$$

Now the conductors are no longer concentrated in one location, but distributed over the zone width ζ. In case the conductors are uniformly distributed on the m phases (relative to the electrical angle)

$$\zeta = \frac{2\pi}{2m} \tag{2.81}$$

can be applied. The flux linkage, however, cannot be calculated as the flux of a single conductor loop multiplied by the number of turns, anymore. Instead, it is given by the sum of fluxes of the all windings with their different corresponding angular orientations. For simplicity, it can be abstracted from the concrete number of slots by approximating the sum of fluxes via averaging over the zone width. As an example, the following calculation holds for winding a:

$$
\begin{aligned}
\psi_{pa} &= N\phi_p \frac{1}{\zeta/p} \int_{-\zeta/2p}^{\zeta/2p} \cos p(\varepsilon_{me} - \vartheta_0)\,d\vartheta_0 \\
&= N\phi_p \frac{1}{\zeta} \int_{-\zeta/2}^{\zeta/2} \cos(\varepsilon - \varepsilon_0)\,d\varepsilon_0 \quad \text{with} \quad \varepsilon_0 = p\theta_0, \varepsilon = p\varepsilon_{me} \\
&= N\phi_p \frac{1}{\zeta} \left[-\sin(\varepsilon - \varepsilon_0)\right]_{\varepsilon_0=-\zeta/2}^{\zeta/2} \\
&= N\phi_p \frac{1}{\zeta} \left[-\sin(\varepsilon - \zeta/2) + \sin(\varepsilon + \zeta/2)\right] \\
&= N\phi_p \frac{2}{\zeta} \sin\frac{\zeta}{2} \cos\varepsilon
\end{aligned}
\tag{2.82}
$$

The term

$$\xi_z = \frac{2}{\zeta}\sin\frac{\zeta}{2} \tag{2.83}$$

is called *winding factor*. It indicates which portion of the flux of an idealized winding of maximum span can be achieved through the actual winding arrangement. In the case of uniformly distributed three-phase windings, the following value results:

$$\xi_z = \frac{6}{\pi}\sin\frac{\pi}{6} = \frac{6}{\pi}\frac{1}{2} = \frac{3}{\pi} = 0.955$$

This calculation is based on the assumption, that the number of slots is large enough, that a simplified continuous current distribution can be assumed. The calculation of winding factors with discrete slots is discussed below.
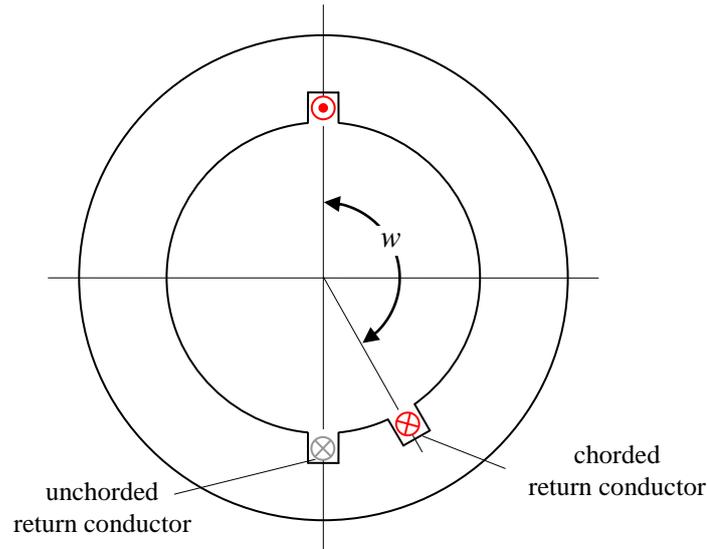
Fig. 2-16: The concept of chording shown here for $p = 1$

In case the winding width is smaller than the pole pitch we speak of *chording* or *fractional pitch winding*. The chording / pitch factor can be defined as follows:

$$s = \frac{w}{\tau_p} \tag{2.84}$$

To calculate the winding factor, it is useful to use the more compact complex notation. The actual flux distribution is then represented by the real part of the complex value. The geometrical angular positions of the conductors are given by

$$\vartheta_{1,2} = \mp \frac{\pi}{p} \frac{w}{2\tau_p} \tag{2.85}$$

whereas the number of pole pairs p is also considered. The resulting flux linkage with a conductor turn is given by

$$\phi_p = rl\hat{b}_p \operatorname{Re} \int_{\vartheta_1}^{\vartheta_2} e^{jp(\vartheta - \varepsilon)} d\vartheta = rl\hat{b}_p \operatorname{Re} e^{-jp\varepsilon} \int_{\vartheta_1}^{\vartheta_2} e^{jp\vartheta} d\vartheta = \frac{rl\hat{b}_p}{p} \operatorname{Re} e^{-jp\varepsilon} \frac{e^{jp\vartheta_2} - e^{jp\vartheta_1}}{j} .$$

On the other hand, the ideal flux linkage in case of full unchorded winding widths results in

$$\phi_{p0} = rl\hat{b}_p \operatorname{Re} \int_{-\frac{\pi}{2p}}^{\frac{\pi}{2p}} e^{jp(\vartheta - \varepsilon)} d\vartheta = rl\hat{b}_p \operatorname{Re} e^{-jp\varepsilon} \int_{-\frac{\pi}{2p}}^{\frac{\pi}{2p}} e^{jp\vartheta} d\vartheta = \frac{rl\hat{b}_p}{p} \operatorname{Re} e^{-jp\varepsilon} \cdot 2 ,$$

Thus, the winding factor is

$$\xi_s = \frac{\phi_p}{\phi_{p0}} = \frac{e^{jp\vartheta_2} - e^{jp\vartheta_1}}{2j} = \sin p\vartheta_2 = \sin\left(\frac{\pi}{2}\frac{w}{\tau_p}\right) = \sin\left(\frac{\pi}{2}s\right) \tag{2.86}$$
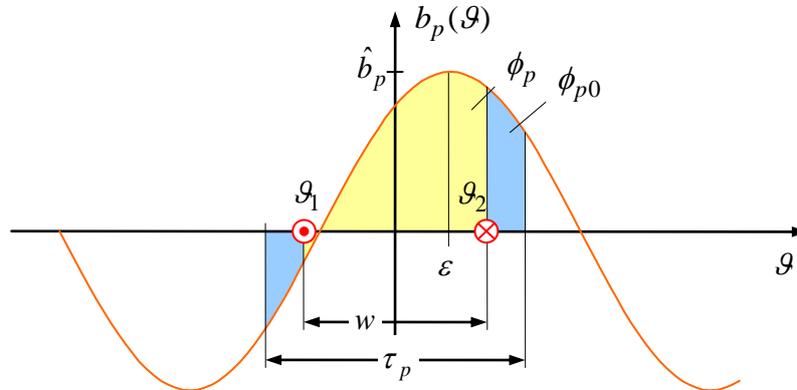
Fig. 2-17: Flux linkage of a chorded winding

Summing up, the two effects zone winding and chording yield a total winding factor[1] of

$$\xi = \xi_z\xi_s = \frac{\sin\zeta/2}{\zeta/2}\sin\left(\frac{w}{\tau_p}\frac{\pi}{2}\right) \tag{2.87}$$

Chording is e.g. employed in multi-layer windings, although two-layer windings are usually preferred. In other words, one slot can comprise conductors from two different phases. One benefit of such an elaborate winding scheme is to approximate a sine-shaped winding distribution. That way, harmonics in the field distribution can be successfully suppressed (below, harmonic winding factors are introduced; compare their values in the table at the end of this section for zone windings with and without chording).

---

[1] Although neglected in these lectures notes, it shall be noted that the process of *skewing* also has an impact on the winding factor.
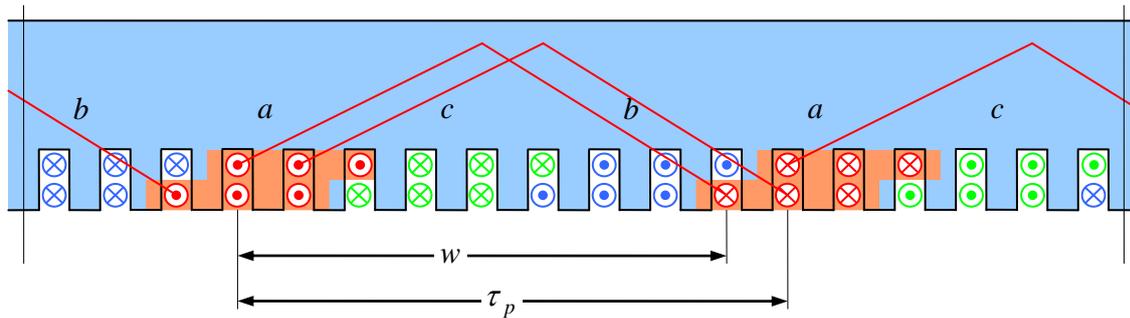
Fig. 2-18: Example of a two-layer winding with chording factor $s = 8/9$

Getting closer to the rotor, the teeth usually widen in a shoe-like shape (unlike the simplified representation of the previous pictures suggest). That way, a preferably uniform field distribution along the circumference shall be achieved. However, just in between two adjacent pole shoes a slot gap always remains. That way, a preferably large magnetic resistance along the tangential direction of the inner stator surface shall be maintained, preventing the magnetic field from short-circuiting along the inner stator surface instead of generating the desired flux linkage between rotor and stator.

Another winding type, which is often employed in machines with large pole numbers are the so-called *concentrated windings*, each wound around only one tooth (*tooth windings*[2]), i.e. incoming wire and return wire are allocated in neighboring slots.
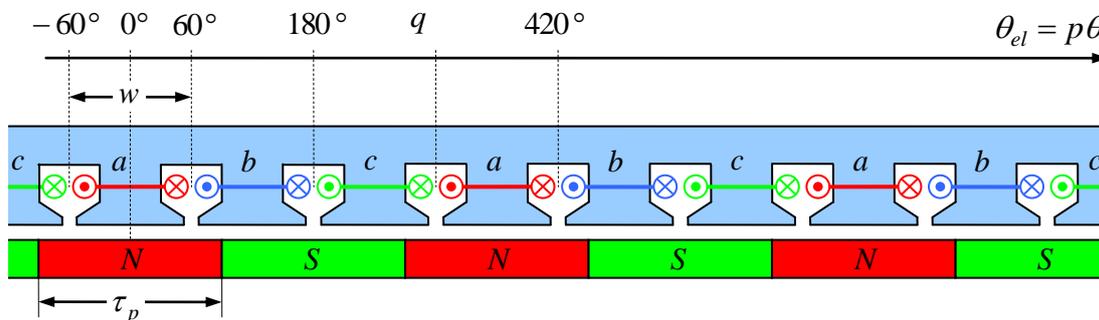
Fig. 2-19: Winding scheme with concentrated windings,
$Q/2p = 3/2$, $q = 1/2$, $s = 2/3$, $\xi = 0.866$

In this winding scheme, only three slots are allocated to one pole pair. In principle, we are dealing with a two-layer winding since each slot comprises conductors of two different phases. However, the conductors are here arranged side by side instead of on top of each other. The number of notches q, i.e. the number of slots per phase and pole, therefore results to

---

[2] Sometimes the term "pole winding" is (incorrectly) applied when speaking of tooth windings. Although the numbers of poles and teeth are of similar dimensions in this winding scheme, however, one pole is not represented by one tooth.

$$q = \frac{Q}{2pm} = \frac{1}{2}. \tag{2.88}$$

Consequently, we speak of a fractional-slot winding in this context. The chording factor of the winding equals to

$$s = \frac{2}{3} \tag{2.89}$$

The winding is not distributed across a zone, the conductors are concentrated in only one slot. The total winding factor is given by

$$\xi = \sin \frac{s\pi}{2} = \sin \frac{\pi}{3} = \frac{\sqrt{3}}{2} = 0.866.$$

Thus, the chording causes a significant reduction of the theoretically achievable flux linkage. Nevertheless, the advantages compensate for this disadvantage: The windings can be wound on winding machines and in a prefabricated stage simply pushed over the teeth. A crucial and further important advantage of concentrated windings lies in the reduction of the end winding[3] to a minimum.
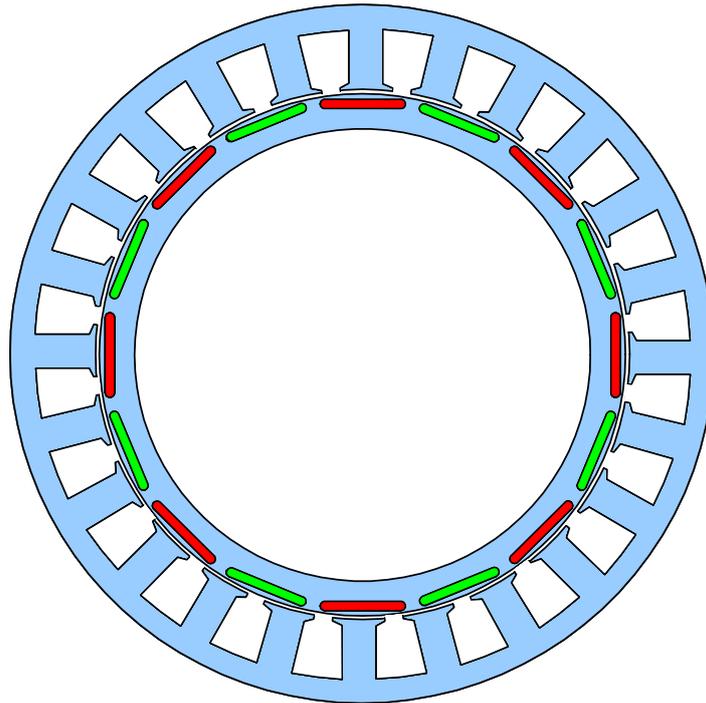
Fig. 2-20: Cross-sectional view of a PMSM with magnets embedded in the rotor and concentrated windings (not shown in this figure)
$$p = 8, Q = 24, q = 1/2, s = 2/3, \xi = 0.866$$

---

[3] The part of the wire that connects the incoming and return conductors is called *end winding*. Though this electrical connection is of course mandatory, it does not contribute to the generation of torque. End windings, however, contribute to the stator resistance and the stator self inductance and require considerable construction space within the motor.

In the previously considered schemes, the winding arrangement is repeated periodically over one magnetic pole pair. However, this is not strictly mandatory. The following figure shows a winding scheme in which the winding arrangement is repeated only after 5 pole pairs. The same scheme, but in a linear representation is shown again further below.
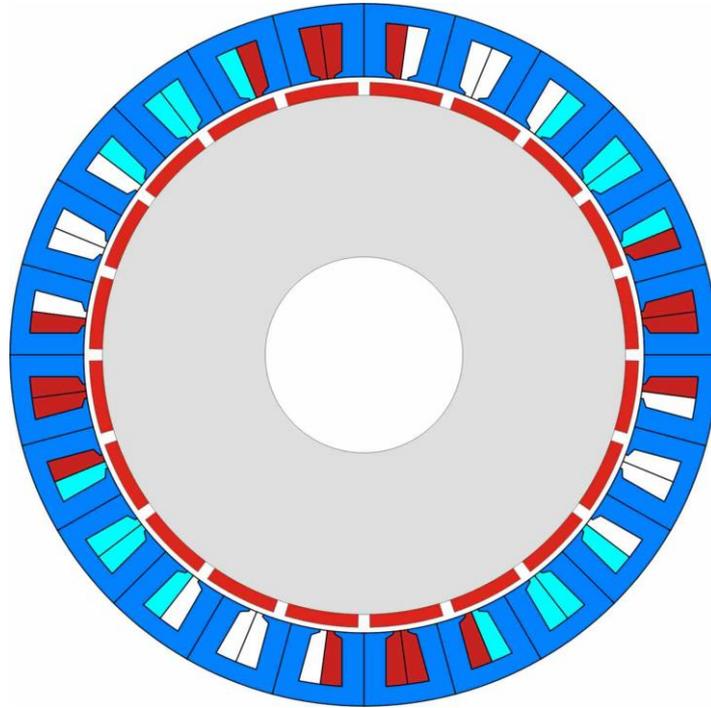
Fig. 2-21: Winding scheme, which is only repeated periodically after five pole pair pitches (the three phases are represented by different colors, the winding direction cannot be seen in this figure, refer to the following linear representation in this context)

To determine the winding factor of such arrangements the flux linkage with all the conductors of a winding needs be determined first. Just as we determined the chording factor earlier, we again resort to the compact complex notation. As a generalization of these earlier results the expression

$$\underline{\xi}_a = \frac{1}{2jN_a} \sum_{i=1}^{Q} N_{ai} e^{jp\theta_i} \tag{2.90}$$

can be obtained. Here, it is added up over all slots i, whereas the angle θ_i indicates the mechanical angular position of the slots in the stator. Although the slots are typically distributed equidistant along the circumference, the formula $\theta_i = 2\pi i / Q$ is also applicable for special cases with non-equidistant slots. N_{ai} is the number of conductors in a given phase a in the respective slot, whereas the orientation of the conductor is taken into account by the sign of N_{ai}. In case no phase a conductors are available in the i-th slot, this is expressed through $N_{ai} = 0$.

The total number of conductors leads to the total number of turns N_a of phase a. Hereby, one has to be aware that one turn is composed of exactly one outgoing conductor and one incoming conductor, thus

$$N_a = \frac{1}{2} \sum_{i=1}^{Q} |N_{ai}| \tag{2.91}$$

Contrary to the previous procedure, here the winding factor is regarded as a complex number, whereas the angle of the complex winding factor gives information about the phase shift.

In the same way, the winding factors $\underline{\xi}_b$, $\underline{\xi}_c$ for the other phases can be determined. These factors must be equal in magnitude and have a defined phase shift of 120° to each other, ensuring a symmetrical three-phase system:

$$\xi = \left|\underline{\xi}_a\right| = \left|\underline{\xi}_b\right| = \left|\underline{\xi}_c\right| \quad \text{i.e.} \quad \underline{\xi}_a = e^{j\frac{2\pi}{3}} \underline{\xi}_b = e^{-j\frac{2\pi}{3}} \underline{\xi}_c \, .$$

That way, it can be tested whether a symmetrical three-phase system occurs, even for winding arrangements in which the geometry of the scheme is not symmetric with reference to the three phases. Also, errors regarding winding direction or phase sequence can be detected in virtually symmetrical schemes by testing the above equations.

In a similar manner, winding factors of the not yet considered harmonics waves[4] can be determined, where k represents the order of the corresponding harmonic wave:

$$\underline{\xi}_{ak} = \frac{1}{2 j N_a} \sum_{i=1}^{Q} N_{ai} \, e^{jkp\theta_i} \tag{2.92}$$

An objective in the selection of an appropriate winding scheme could also be to eliminate certain undesired harmonic waves or at least to minimize them (see table at the end of this section).

The figure below shows the linear representation of the already introduced winding scheme, whose winding arrangement is not repeated after one, but only after 5 pole pair pitches (in the figure, only slightly more than half of this period is shown). The slots to poles ratio is 6 / 5, resulting in a notch number of $q = 0,4$. In this scheme, as well, concentrated windings (tooth windings) are employed. The corresponding advantages of this winding type were discussed earlier. The winding factor can be calculated according to above formula:

---

[4] *Waves* represent *periodics in space*, while *oscillations* are *periodic in time*. Therefore, it has to be distinguished between harmonic waves and harmonic oscillations. Here, the focus is put on deviations of the spatial field distribution from the sine shape, i.e. harmonic waves. One the other hand, the impact of harmonic waves on the temporal processes at the motor terminals due to magnetic induction are harmonic oscillations.

$$\xi = \left|\underline{\xi}_a\right| = \frac{1}{8}\left|-e^{-j150°} + 2e^{j0°} - e^{j150°} + e^{j750°} - 2e^{j900°} + e^{j1050°}\right| = 0.933 \; .$$

The resulting winding factor of this scheme is even slightly better than the one of the simple winding scheme with concentrated windings (0.866). Moreover, the 5th and 7th harmonic waves are suppressed more effectively (see table below).
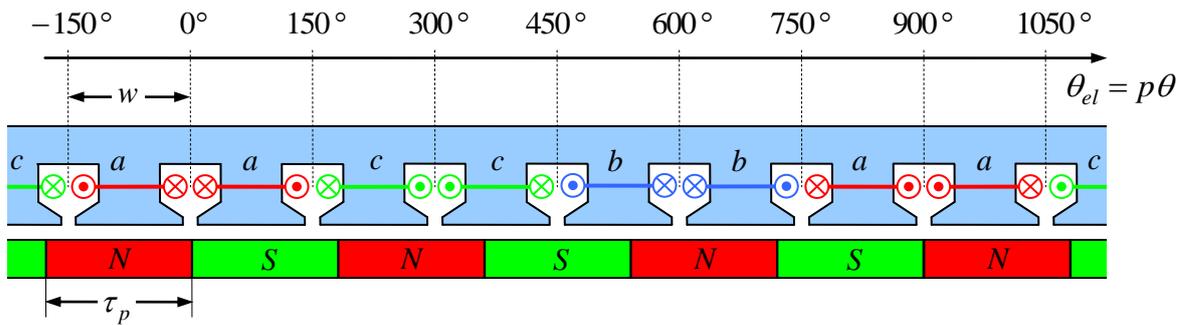
Fig. 2-22: Winding scheme with concentrated windings
$Q/2p = 12/10$, $q = 0.4$, $\xi = 0.933$

The following table summarizes the results for different winding schemes and also shows the winding factors for the harmonic waves. Here, also the data for the zone windings were not determined as above by approximation of a continuous current coverage, but by taking into account the individual slot numbers.

Nr.	winding scheme	p	Q	q	ξ_1	ξ_5	ξ_7	ξ_{11}	ξ_{13}
1	Zone winding	1	6	1	1	1	1	1	1
2	Zone winding	1	12	2	0.966	0.259	0.259	0.966	0.966
3	Zone winding	1	18	3	0.960	0.218	0.177	0.177	0.218
4	Zone winding with chording factor 8/9	1	18	3	0.945	0.140	0.061	0.061	0.140
5	Zone winding with chording factor 7/9	1	18	3	0.902	0.038	0.136	0.136	0.038
6	Concentrated winding	1	3	0.5	0.866	0.866	0.866	0.866	0.866
7	Concentrated winding	5	12	0.4	0.933	0.067	0.067	0.933	0.933
8	Concentrated winding	4	9	0.375	0.945	0.140	0.061	0.061	0.140

The results apply equally well to multiples of the specified pole pairs and slot numbers. The winding factors for even orders are not listed. Due to reasons of symmetry, in most winding schemes $\xi_{2k} = 0$ holds anyways, however, not in the schemes No. 6 and 8 for example. As usually the field distribution can be assumed as symmetrical, harmonic waves of even orders $2k$ do not exist so that even-order winding factors, even if non-zero, are irrelevant. However, harmonic waves of orders $3k$ do occur with winding factors being unequal to zero. Nevertheless, due to the electrical connection of the windings in star or delta configuration no harmonic oscillations of orders $3k$ occur in the terminal quantities. Therefore, these winding factors, as well, are irrelevant and therefore not listed. In consequence, only the order numbers 1, 5, 7, 11, 13, 17, 19 etc. are of interest.

2.9 Relation Between Motor Geometry and Torque Output

The equation for the torque is given as

$$T = \frac{3}{2} p \psi_p i_{sq} \tag{2.93}$$

The torque equation suggests that motors with high pole pair numbers are more suitable for the generation of high torques. This shall be examined more carefully in the following. According to the previous chapter

$$\psi_p = N\phi_p = \frac{2N\xi\, r\, l\, \hat{b}_p}{p} \tag{2.94}$$

and thus

$$T = 3\xi\, r\, l\, \hat{b}_p N\, i_{sq} \tag{2.95}$$

holds. Under the assumption $i_{sd} = 0$, i_{sq} represents the amplitude of the phase currents i_a, i_b, i_c, exclusively:

$$\hat{i}_a = \hat{i}_b = \hat{i}_c = i_{sq} \tag{2.96}$$

The root mean square (RMS) values for the three phases result to

$$I_a = I_b = I_c = \frac{1}{\sqrt{2}} i_{sq} \tag{2.97}$$

Let us assume that for each phase a, b, c, the outgoing and incoming conductor, respectively, cover 1/6 of the circumference length $2\pi r$. With respect to zone windings, this applies exactly. As far as the problem of heat dissipation is concerned, this assumption may, however, also be applied to other types of windings schemes. Thus, the effective current density results to

$$A = \frac{NI_a}{2\pi r/6} = \frac{6N}{\sqrt{2}\, 2\pi r} i_{sq} = \frac{3N}{\sqrt{2}\,\pi r} i_{sq}. \tag{2.98}$$

The maximum effective current density depends on the design of the motor and the method of cooling, in particular. This characteristic quantity can be regarded as approximately constant for motors of different ratings, but same design. Typical values lie in the range of

$$A_{\max} \approx 40...80\, \frac{\text{kA}}{\text{m}}$$

With this quantity, the maximum possible torque can be calculated as follows:

$$T_{\max} = \frac{3}{2} p \psi_p i_{sq\max} = \frac{3}{2} p \frac{2N\xi \, r l \hat{b}_p}{p} \frac{\sqrt{2} \, \pi \, r}{3N} A_{\max}$$
$$= \sqrt{2} \, \xi \hat{b}_p \pi \, r^2 l \, A_{\max} = \sqrt{2} \, \xi \hat{b}_p A_{\max} V_{\text{rotor}} \tag{2.99}$$

whereas

$$V_{\text{rotor}} = \pi \, r^2 l \tag{2.100}$$

represents the volume of the magnetic active portion of the rotor.

The same result can be reached by considering the average shear stress $\bar{\sigma}$, experienced by a surface element of the rotor due to the Lorentz force. The average shear stress can be calculated directly as the product of the RMS values of current and flux densities, whereas the winding factor ξ accounts for geometrically non-ideal arrangements.

$$\bar{\sigma} = \xi \frac{\hat{b}_p}{\sqrt{2}} A \tag{2.101}$$

The integration of the shear stress over the rotor surface $2\pi \, r \, l$ and multiplication by the lever arm r leads to the already introduced formula for the maximum achievable torque output

$$T_{\max} = \sqrt{2} \, \pi \, r \, l \, r \, \xi \hat{b}_p A = \sqrt{2} \, \xi \hat{b}_p V_{\text{rotor}} A_{\max} \cdot \tag{2.102}$$

One can see, that apart from the motor design and material specific constants $A_{\max}$, $\hat{b}_p$, ξ the torque output of a motor also depends on the rotor volume V_{rotor}. For $\hat{b}_p \approx 1\,\text{T}$ and $\xi \approx 0.9$, typical torque densities result to

$$\frac{T_{\max}}{V_{\text{rotor}}} = \sqrt{2} \, \xi \hat{b}_p \, A_{\max} = 2\bar{\sigma}_{\max} \approx 50...100 \frac{\text{kNm}}{\text{m}^3}$$

It becomes obvious, that this result does *not* depend on the number of pole pairs.

However, the number of pole pairs has an impact on the resulting motor size: The magnetic flux generated by a pole pair can be calculated according to the above relations via

$$\phi_p = \frac{2\xi r l \hat{b}_p}{p} \tag{2.103}$$

This flux must be fed back through the stator yoke of one magnetic pole to the next with opposite magnetization. The higher the number of pole pairs, the smaller the flux contribution of a single pole pair. Consequently, the stator yoke can be of thinner design. According to this, the number of pole pairs has a quite considerable impact and on the thickness of the stator and thus on the outer diameter of the motor. Additionally, a thinner yoke improves the

heat dissipation characteristics of the motor, potentially allowing higher current densities in return.

Moreover, the pole-pair number has an influence on the end windings: The higher the number of poles pairs, the shorter the connection paths between outgoing and incoming conductors of a winding. With a high number of pole pairs, the end windings can be made small and thus reduce the overall length of motor.

2.10 Steady-State Operational Behavior

Steady state voltage equations are:

$$u_{sd} = R_s \, i_{sd} - \omega\psi_{sq} = R_s \, i_{sd} - \omega L_s i_{sq} \tag{2.104}$$

$$u_{sq} = R_s \, i_{sq} + \omega\psi_{sd} = R_s \, i_{sq} + \omega L_s i_{sd} + \omega\psi_p \tag{2.105}$$
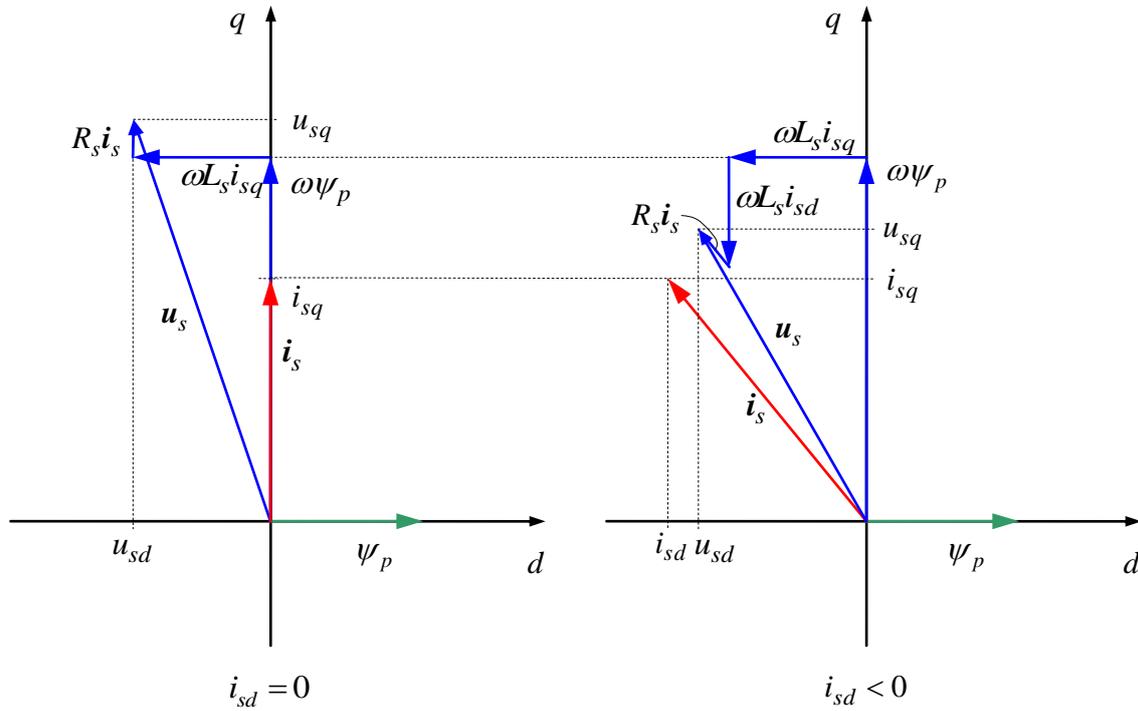
Fig. 2-23: Steady-state phasor diagrams for same motor torque and speed, respectively, left without negative *d*-axis current, right with negative *d*-axis current.
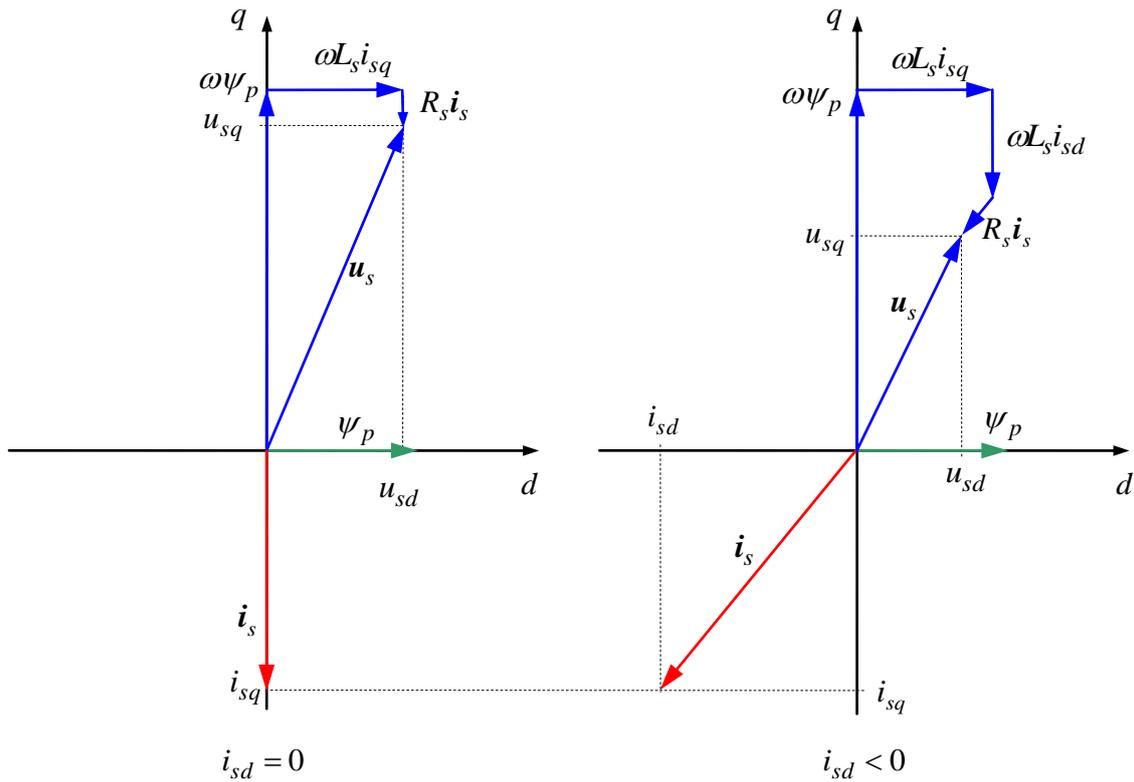
Fig. 2-24: Steady-state phasor diagrams for same generator torque and speed, respectively, left without negative d-axis current, right with negative d-axis current.

In case of no constraints in selecting the two current components i_{sd}, i_{sq}, the desired torque T^* can be set with minimal losses (i.e. with minimum current phasor amplitude) according to

$$i_{sq} = \frac{2}{3p\psi_p}T^*, \quad i_{sd} = 0.$$ (2.106)

The same torque output can also be achieved by applying a negative i_{sd} current leading to a reduction of the resulting stator voltage. Although, this is of course at the expense of the losses this operation mode is of great significance when operating the motor at voltage limits. Since the flux in d-direction can be expressed by

$$\psi_{sd} = L_s i_{sd} + \psi_p$$ (2.107)

a negative d-component current weakens the flux portion provided by the permanent magnets. In consequence, this operation mode is also called *flux-weakening mode*. Moreover, you can see from the above figure that the permanent magnet synchronous motor exhibits both inductive behavior (voltage phasor leads the current phasor) and capacitive behavior (current phasor leads the voltage phasor). By suitable choice of i_{sd} operation with power factor 1 is also possible.

Operation at current and voltage limits

The inverter supplying the power to the motor, but also the motor itself, are exposed to current handling capacity limits as well as voltage limits:

$$i_s^2 = i_{sd}^2 + i_{sq}^2 \leq i_{max}^2 \tag{2.108}$$

$$u_s^2 = u_{sd}^2 + u_{sq}^2 \leq u_{max}^2 \tag{2.109}$$

Accordingly, the voltage is small at low speeds; here, the voltage limits do not play any role. The corresponding region of operation is known as *voltage control range* or in terms of the DC-Motor *armature control range*. If the motor is operated with $i_{sd} = 0$ then the current limit restricts the available torque to

$$|T| \leq T_{max\,0} = \frac{3}{2} p \psi_p i_{max} \,. \tag{2.110}$$

In the armature control range, the maximum achievable torque is independent of the speed.

Increasing the motor speed leads to higher voltages that will eventually reach the voltage limit. Substituting the steady-state voltage equations into the voltage limits expressions while neglecting ohmic voltage drops leads to
.

$$u_s^2 = u_{sd}^2 + u_{sq}^2 = \omega^2 \left((L_s i_{sd} + \psi_p)^2 + L_s^2 i_{sq}^2 \right) \leq u_{max}^2 \tag{2.111}$$

The assumption of neglecting the ohmic voltage portions is only reasonable for machines with high power ratings, i.e. several 10 kW or higher. As for small motors which operate at only a few Watts, the ohmic voltage drops can be of similar order as the back-EMF and armature reaction even at high speeds. Also, would have EMF and armature reaction of same magnitude. In this case, the following calculations may only be considered as rough approximations.

The voltage limit can be transformed into a condition for acceptable currents:

$$(L_s i_{sd} + \psi_p)^2 + L_s^2 i_{sq}^2 \leq \frac{u_{max}^2}{\omega^2} \tag{2.112}$$

Geometrically, this can be interpreted as a circle in the i_d, i_q - plane with center point at

$$i_{d0} = -\frac{\psi_p}{L_s}, \; i_{q0} = 0 \tag{2.113}$$

and a radius of

$$i_U = \frac{u_{max}}{L_s |\omega|} \, . \tag{2.114}$$

By the way, the magnitude

$$i_0 = -i_{d0} = \frac{\psi_p}{L_s} \tag{2.115}$$

represents the flux weakening current necessary compensate the permanent magnet flux ψ_p completely. Furthermore, when neglecting the ohmic resistance the current i_0 is equal to the short-circuit current of motor, as discussed in section 7.

For the following, the design parameter

$$k = \frac{i_0}{i_{max}} = \frac{\psi_p}{L_s i_{max}} \tag{2.116}$$

and the reference frequency

$$\omega_0 = \frac{u_{max}}{\psi_p} \tag{2.117}$$

are introduced. The frequency ω_0 refers to the no-load operation speed at which the voltage limit is reached. Above this frequency, flux-weakening current is always required independent of the desired torque output, i.e. also at no-load operation.
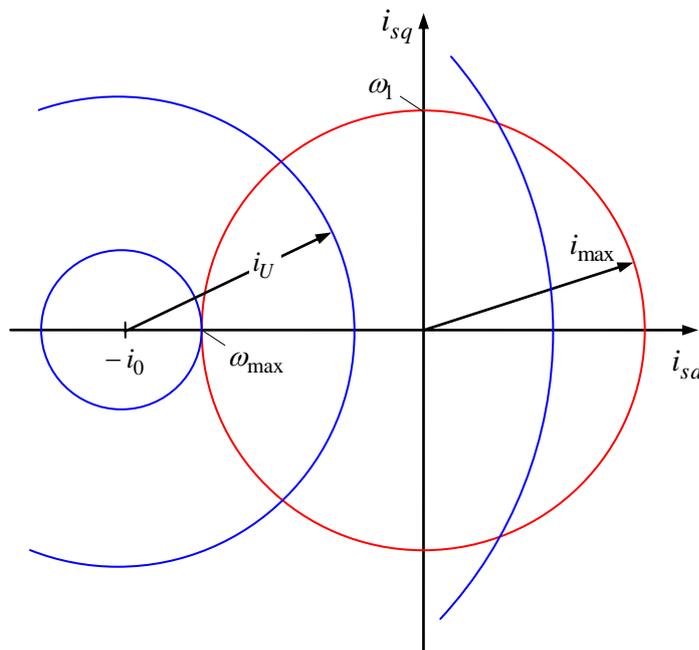
Fig. 2-25: Current and voltage limits for $i_0 > i_{max}$

The above figure depicts in the i_d, i_q-plane the limiting circles resulting from the corresponding current- and voltage limits. At low speeds, the radius i_U is large and does not play a role. Therefore, the current only needs to be kept below the maximum current limit i_{max}. As the rotational speed increases the radius $i_U = u_{max}/\omega$ reduces requesting negative i_d current in consequence.

In the following, the maximum achievable torque during flux-weakening mode shall be determined. In other words, the current limit as well as the voltage limit are reached. From the voltage limit, it follows

$$\frac{u_{max}^2}{L_s^2\omega^2} = (i_{d\,max} + i_0)^2 + i_{q\,max}^2$$

$$i_0^2\frac{\omega_0^2}{\omega^2} = i_{d\,max}^2 + 2i_{d\,max}i_0 + i_0^2 + i_{q\,max}^2 = i_{max}^2 + i_0^2 + 2i_{d\,max}i_0$$

$$0 = i_{max}^2 + i_0^2\left(1 - \frac{1}{\Omega^2}\right) + 2i_{d\,max}i_0$$

whereas

$$\Omega = \frac{\omega}{\omega_0} \tag{2.118}$$

represents the normalized speed. Solving this equation for the flux-weakening current leads to:

$$i_{d\,max} = -\frac{i_0}{2}\left(1 - \frac{1}{\Omega^2}\right) - \frac{i_{max}^2}{2i_0} = -\frac{1}{2}i_{max}\left(\frac{1}{k} + k\left(1 - \frac{1}{\Omega^2}\right)\right) \tag{2.119}$$

The starting point at which flux-weakening comes into effect, i.e. the point of maximum current or torque at which a flux-weakening current is required for the first time, can be determined by

$$\omega_1 = \frac{u_{max}}{L_s\sqrt{i_{max}^2 + i_0^2}} = \frac{\omega_0}{\sqrt{\frac{1}{k^2} + 1}} \tag{2.120}$$

or alternatively,

$$\Omega_1 = \frac{\omega_1}{\omega_0} = \frac{k}{\sqrt{k^2 + 1}} \tag{2.121}$$

Using the above flux-weakening current, we now find the *torque-generating* current to be

$$i_{q\,max} = \sqrt{i_{max}^2 - i_{d\,max}^2} = I_{max}\sqrt{1 - \frac{1}{4}\left(\frac{1}{k} + k\left(1 - \frac{1}{\Omega^2}\right)\right)^2}.$$

(2.122)

The corresponding torque results to

$$T_{max} = \frac{3}{2}p\psi_p I_{max}\sqrt{1 - \frac{1}{4}\left(\frac{1}{k} + k\left(1 - \frac{1}{\Omega^2}\right)\right)^2}$$

(2.123)

or (normalized) to

$$\frac{T_{max}}{T_{max\,0}} = \sqrt{1 - \frac{1}{4}\left(\frac{1}{k} + k\left(1 - \frac{1}{\Omega^2}\right)\right)^2}.$$

(2.124)

For the following considerations of the flux-weakening range two cases shall be distinguished. They are characterized by the short-circuit current i_0 being either smaller or larger than the maximum current i_{max}, i.e. whether $k < 1$ or $k > 1$ applies.

Case 1: Limited speed, $i_0 > i_{max}$ **or** $k > 1$

In this case, the center point of the circle i_U lies outside the current limiting circle. Above a certain speed the intersection of the two circles is empty. The maximum speed results directly from electrical limitations and is reached when the circle i_U barely touches the current limiting circle i_{max}. Then, the following equations hold:

$$i_0 = i_U + i_{max} = \frac{u_{max}}{\omega_{max}L_s} + i_{max}$$

(2.125)

$$\omega_{max} = \frac{u_{max}}{L_s}\frac{1}{i_{max} - i_0}$$

(2.126)

or

$$\Omega_{max} = \frac{\omega_{max}}{\omega_0} = \frac{i_0}{i_{max} - i_0} = \frac{k}{k-1}$$

(2.127)

The above formula derived for the maximum available torque

$$\frac{T_{max}}{T_{max\,0}} = \sqrt{1 - \frac{1}{4}\left(\frac{1}{k} + k\left(1 - \frac{1}{\Omega^2}\right)\right)^2}$$

(2.128)

can thus be applied for the (normalized) speed range

$$\Omega_1 \leq \Omega \leq \Omega_{max} .$$

Now, what is the maximum power available for different speeds? In the voltage control range $\Omega < \Omega_1$, the maximum power results to

$$P_{max} = \omega_{me} T_{max\,0} = \frac{1}{p} \omega T_{max\,0} . \tag{2.129}$$

Thus, the power increases linearly with the speed. In the following, the performance will be referred to the maximum available apparent power of the converter, given by

$$S_{max} = \frac{3}{2} u_{max} i_{max} . \tag{2.130}$$

Defining the normalized power leads to

$$\lambda = \frac{P_{max}}{S_{max}} . \tag{2.131}$$

Generally speaking, this value does not represent the power factor, as the *current* real power is not referred to the *current* apparent power, but to the *maximum* apparent power of the inverter. The maximum apparent power is utilized to its full extent only when operating at the current *and* voltage limits. In this case, λ is equal to the power factor. In general, the value λ can be considered as a measure for the utilization of the installed converter power, also known as *inverter utilization degree*.

For the voltage control range $\Omega < \Omega_1$, the normalized maximum power or inverter utilization degree follows to

$$\lambda = \frac{\omega \psi_p}{u_{max}} = \Omega \tag{2.132}$$

On the other hand, for the flux-weakening range $\Omega_1 \leq \Omega \leq \Omega_{max}$, it holds

$$\lambda = \frac{P_{max}}{S_{max}} = \Omega \sqrt{1 - \frac{1}{4} \left(\frac{1}{k} + k \left(1 - \frac{1}{\Omega^2} \right) \right)^2} \tag{2.133}$$

The speed at which maximum possible power is provided can be derived through a several calculation steps and results to

$$\Omega_{P_{\max}} = \frac{k}{\sqrt{k^2 - 1}} \tag{2.134}$$

In this case, $\lambda = 1$ and $P_{\max} = S_{\max}$.

Drives with $k > 1$ do not have a constant power range. For pump sets and fans, whose performance increases with increasing speed, anyways, a constant power range is not necessary. However, if the drive shall exhibit a constant power range $k < 1$ has to be selected.

Case 2: Unlimited speed, $i_0 < i_{\max}$ **or** $k < 1$
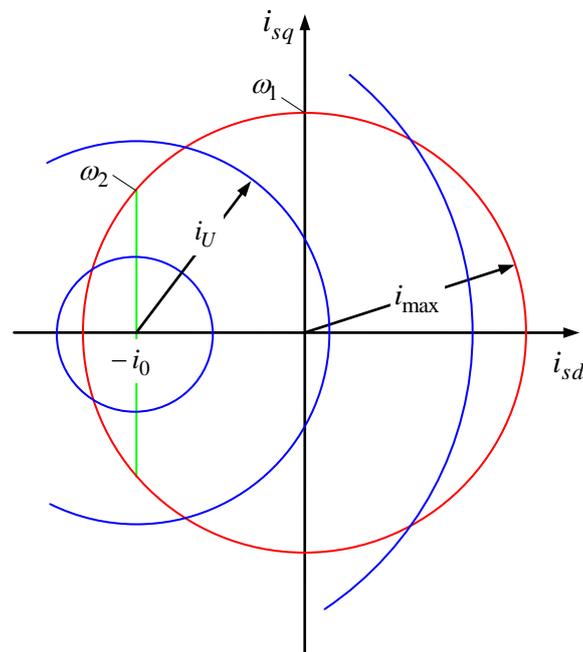
Fig. 2-26: Current and voltage limitations for $i_0 < i_{\max}$

In the voltage control range $\Omega < \Omega_1$ there is no fundamental difference to the previously discussed case. In spite of the similar behavior when entering the flux-weakening region, increasing speeds give rise to a qualitatively different behavior: Unlike in case 1, $i_0 < i_{\max}$ and $k < 1$ lead to non-empty intersections of the limiting circles for *any* given speed. Consequently, there exist valid operating points for any speed. The speed is *not* limited by the electrical behavior.

The flux-weakening region $\Omega > \Omega_1$ can be divided into two ranges. In the lower flux weakening region the motor is operated at current and voltage limits to achieve maximum torque. The torque is calculated just as before:

$$\frac{T_{\max}}{T_{\max 0}} = \sqrt{1 - \frac{1}{4}\left(\frac{1}{k} + k\left(1 - \frac{1}{\Omega^2}\right)\right)^2} \tag{2.135}$$

The maximum power is given by

$$\lambda = \frac{P_{\max}}{S_{\max}} = \Omega\sqrt{1 - \frac{1}{4}\left(\frac{1}{k} + k\left(1 - \frac{1}{\Omega^2}\right)\right)^2} \; . \tag{2.136}$$

This operation is, however, only reasonable until $\Omega < \Omega_2$. The limit Ω_2 is reached when the flux-weakening current i_d reaches the $-i_0$ value. This limit is determined by

$$\omega_2 = \frac{u_{\max}}{L_s\sqrt{i_{\max}^2 - i_0^2}} = \frac{\omega_0}{\sqrt{\frac{1}{k^2} - 1}} \tag{2.137}$$

or

$$\Omega_2 = \frac{\omega_2}{\omega_0} = \frac{1}{\sqrt{\frac{1}{k^2} - 1}} \; . \tag{2.138}$$

It does not make sense to decrease i_d below $-i_0$ while speed is further increasing, as the maximum torque utilization would be reduced. For speeds $\Omega > \Omega_2$ the maximum torque is always achievable with the following flux-weakening current and torque-generating current, resulting from voltage limits:

$$i_{d\,\max} = -i_0 = -ki_{\max} \tag{2.139}$$

$$i_{q\,\max} = \frac{u_{\max}}{L_s\omega_{rs}} = \frac{1}{\Omega}i_0 = \frac{k}{\Omega}i_{\max} \tag{2.140}$$

The torque and power can be expressed by

$$T_{\max} = \frac{3}{2}p\psi_p\frac{k}{\Omega}I_{\max} = \frac{k}{\Omega}T_{\max 0} \tag{2.141}$$

$$\lambda = \frac{P_{\max}}{S_{\max}} = k \tag{2.142}$$

The region, where the available power is constant is called the upper *flux weakening region*. The last equation shows that the inverter utilization degree can be at most equal to the design

parameter k. Accordingly, the inverter utilization is poor for small values of k. For a technically and economically optimized design of a drive with a constant-power range, as it is common in automotive applications, k values close to 1 are thus preferred. Quite often, values in the range of $k = 0.8...0.9$ can be found in this context.
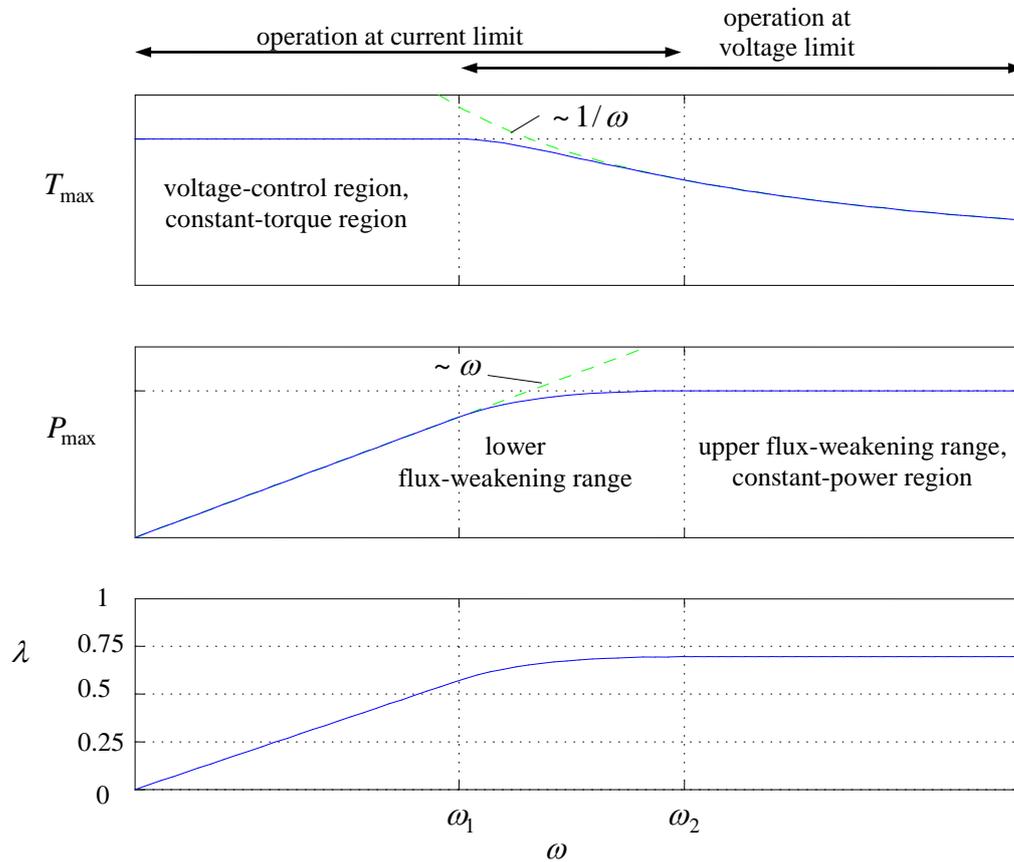
Fig. 2-27: Maximum torque, maximum power and normalized power
(inverter utilization degree λ) vs. motor speed with $k < 1$
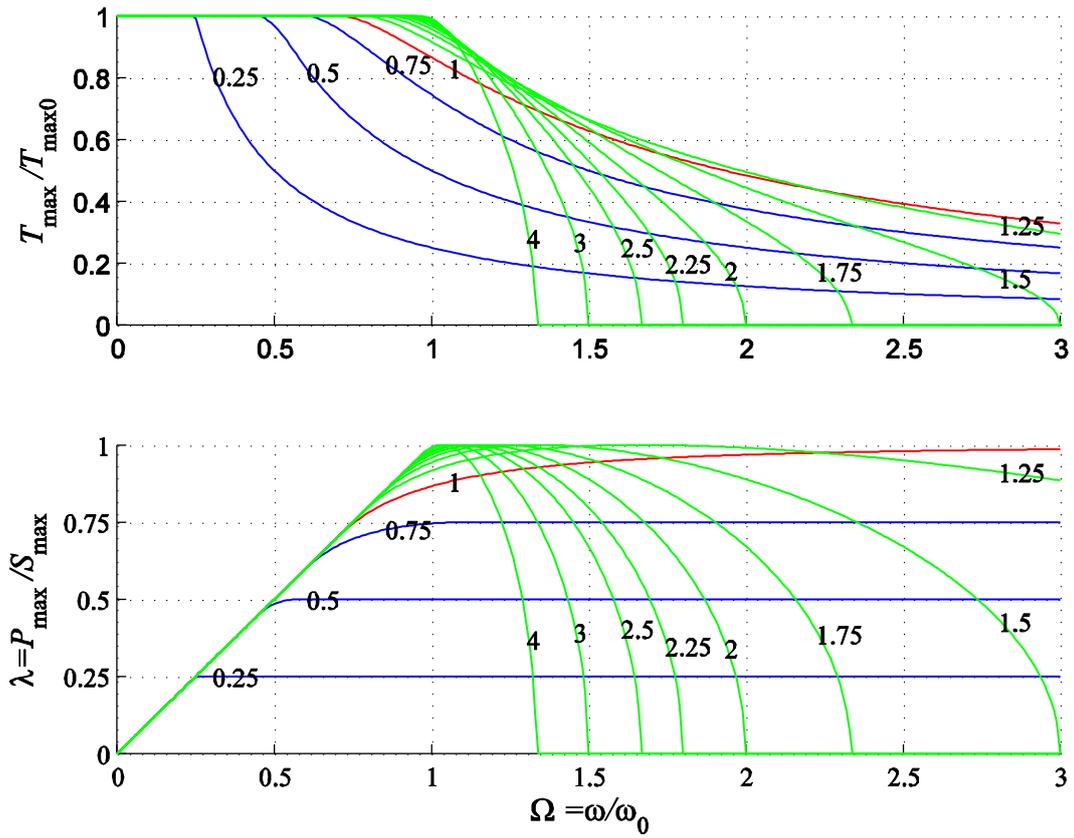
Fig. 2-28: Maximum torque and maximum power vs. speed in a normalized representation. Parameter of the array of curves is the design parameter $k = i_0 / i_{max}$

3 Inverter

Today's state-of-the-art technology relies on feeding AC- or three-phase-motors from a DC source, also known as *voltage source DC-link*, via a frequency- or voltage-source inverter (VSI).

For AC motors with very high power ratings up to 10 MW or above, inverters with *current source DC-link* (*I*-inverters, *current*-source inverter, CSI) or cyclo-converters or matrix inverters are also employed. In this lecture, we will focus on the DC-fed inverter, also known as pulse inverter, exclusively.

The inverter with DC-link is a three-phase bridge circuit (B6). The operating principle can be illustrated with ideal switches, as shown in the figure below.
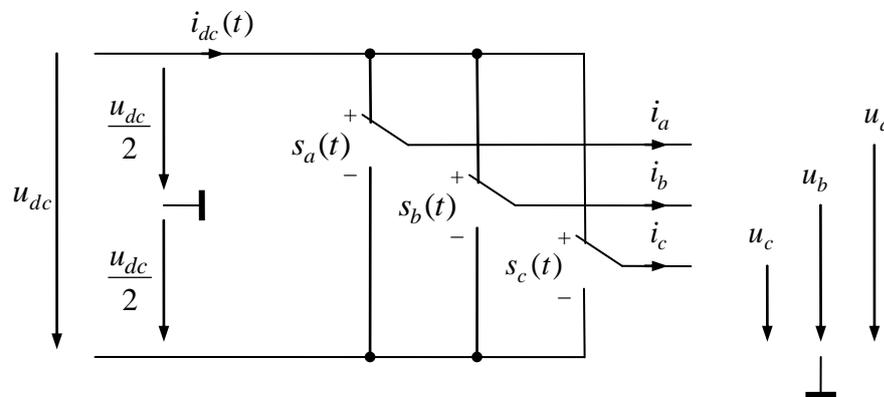
Fig. 3-1: Idealized inverter with DC power supply

Fig. 3-2: Common circuit symbols for inverter with DC power supply

The switch positions are described by the *switching functions* $s_a(t), s_b(t), s_c(t)$. Whereas switching state $s_{a,b,c} = +1$ is assigned to the upper switch position, $s_{a,b,c} = -1$ represents the lower position. At the input (DC side) of the inverter a DC voltage is applied and at the output (AC side, motor) currents are fed into a connected inductive load. Depending on the switch positions, the output voltages as well as the input current can be determined with the help of the switching functions as follows:

$$u_{a,b,c}(t) = \frac{1}{2} s_{a,b,c}(t)\, u_{dc}(t) \qquad (3.1)$$

$$i_{dc}(t) = \frac{1}{2} \sum_{a,b,c} s_k(t)\, i_k(t) \qquad (3.2)$$

For simplification, the reference potential for the output voltages is set to the midpoint of the DC input voltage, as shown in the figure. In terms of actual circuitry this point does not exist, however. Moreover, there is no current balancing via this potential. The motor is connected in star or delta configuration, so that the following condition for the currents,

$$\sum_{a,b,c} i_k(t) = 0\,.$$

holds.
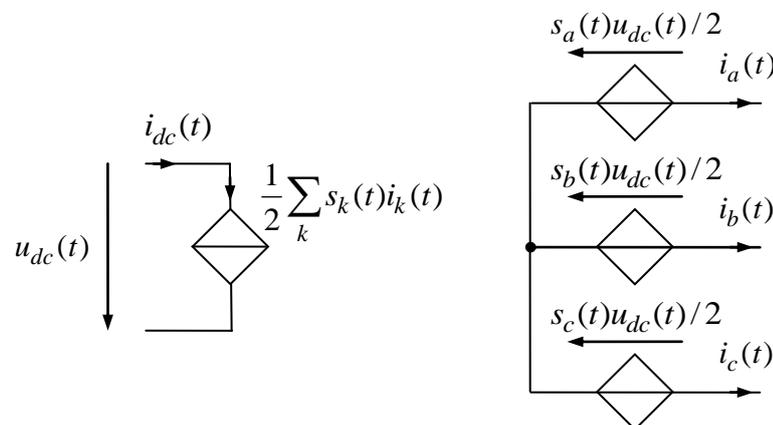
Fig. 3-3: Equivalent circuit diagram of the inverter with controlled current- and voltage sources

The actual design of the inverter using transistors is shown in the figure below. Depending on the power and voltage requirements the following power electronics devices are commonly employed as switches.

- MOSFET (Metal Oxide Field Effect Transistor)
- IGBT (Isolated Gate Bipolar Transistor)
- GTO-Thyristor (Gate Turn Off)
- IGCT (Integrated Gate-Commutated Thyristor)

Each of these three components is connected with an anti-parallel diode, thus forming a switching element which can carry current in both the directions (except for the MOSFET, which due to its body structure already includes a so-called body-diode making the usage of a separate diode redundant). However, the switching element only allows unidirectional voltages, which is sufficient, as the polarity of the supplying DC-link voltage usually does not change. On the DC-side close to the power semiconductors a capacitor is installed, preventing

the abruptly changing current i_{dc} during switching instants to be fed to the input voltage source via a potentially long inductive cable.

The target applications of the following power semiconductor devices is characterized in the table below:

	MOSFET	IGBT	GTO/IGCT
Voltages [3]	600 V [1] 1600 V [2]	600 V/1200 V [1] 6500 V [2]	6000 V
Currents	1 - 50 A [1] 690 A [2]	50 - 400 A [1] 2400 A [2]	4000 A
typical switching frequencies	10 - 1000 kHz	2 - 20 kHz	0.2 - 1 kHz

[1] Typical standard elements

[2] technological limits (2008)

[3] Here, the maximum blocking voltages are given. One should be aware, that the nominal operating voltage of an inverter utilizes only 65-80% of the blocking voltage of the power transistors. This is due to safety margins that need to be kept, enabling the device to handle transient voltage peaks which occur during commutations.
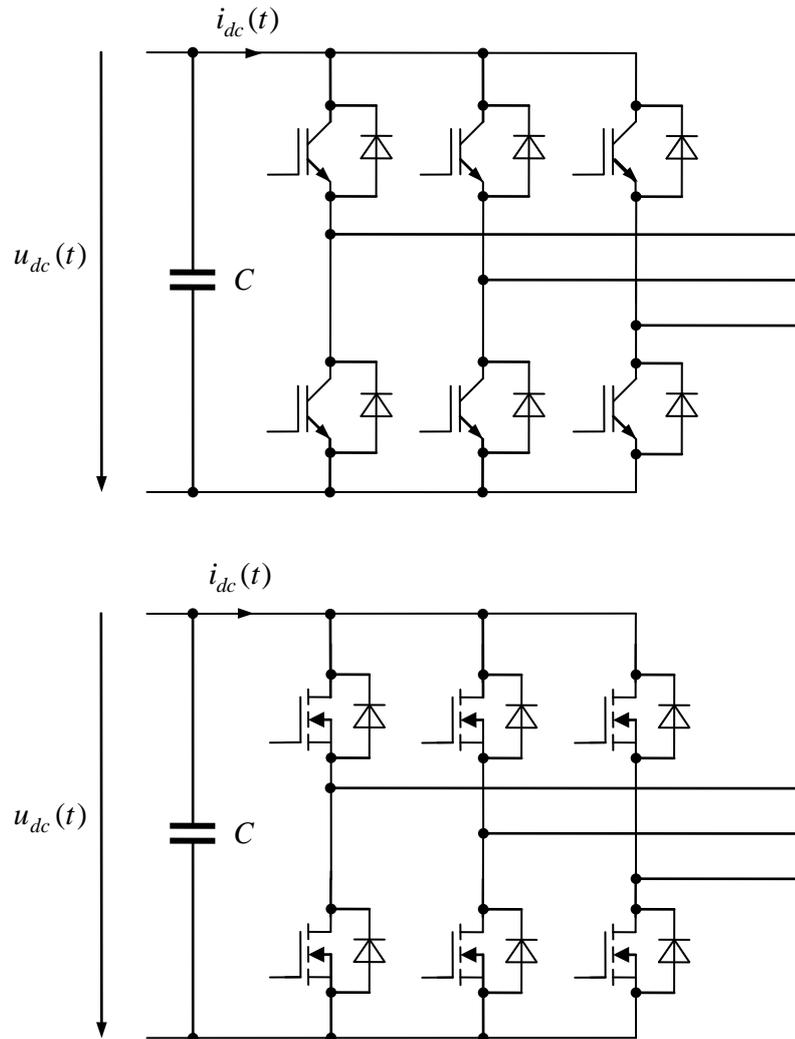
Fig. 3-4: Three-Phase inverter with IGBT (above) or MOSFET (below)

The DC supply feeding the inverter is referred to as intermediate circuit or DC-link, in case the DC voltage itself results from a conversion procedure, such as rectification of an AC- or three-phase voltage grid (see figure below). The rectifier can be composed of a simple bridge diode circuit. In case of more complex systems, especially when a regenerative feedback of electrical power into the grid is requested, the same inverter circuit as on the motor side (mirrored) can be used as rectifier between the grid and the DC-link.
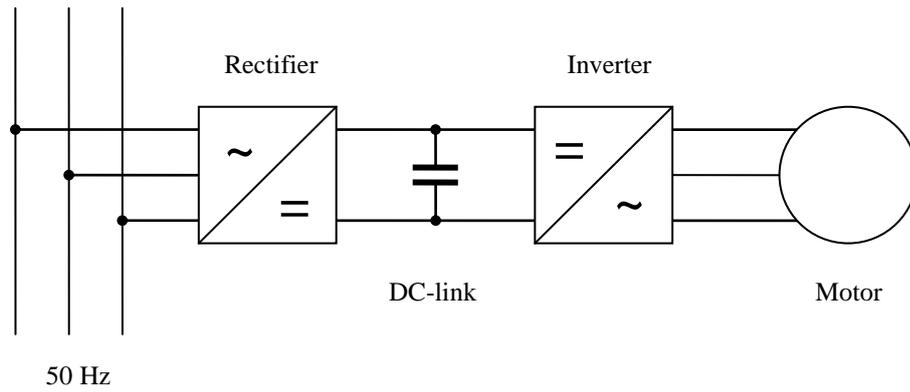
Fig. 3-5: Configuration with DC-link

The three-phase inverter can only adopt $2^3 = 8$ switching states. The resulting output voltages u_a, u_b, u_c can be mapped to two orthogonal components u_α, u_β and a zero component u_0 via the transformation matrix T. The zero component describes the common mode behavior of the inverter output voltages. Usually the motor windings, which are connected to the inverter are isolated. The zero component which shifts all three motor phase potentials in common mode, thus, has no impact and does not need to be considered in consequence.

When having a closer look, however, one realizes that the zero component is still of importance, as it is responsible for displacement currents through parasitic capacitances between the motor windings and the housing or shielding or GND. Nevertheless, the zero component will not be considered in this basic modeling approach.

The eight fundamental voltage vectors in orthogonal α / β coordinates generated by the eight switching states are denoted by v_i. With the help of the transformation

$$v_i = T_{23} \begin{bmatrix} u_{ai} \\ u_{bi} \\ u_{ci} \end{bmatrix} = \frac{u_{dc}}{2} T_{23} \begin{bmatrix} s_{ai} \\ s_{bi} \\ s_{ci} \end{bmatrix}$$

they can be calculated from the switching states $s_{a,b,c} = -1, +1$. For simplification, the normalized fundamental voltage vectors

$$\tilde{v}_i = \frac{v_i}{u_{dc}/2} = T_{23} \begin{bmatrix} s_{ai} \\ s_{ci} \\ s_{ci} \end{bmatrix} \tag{3.3}$$

shall be used in the following. With the help of the transformation matrix

$$T_{23} = \frac{2}{3}\begin{bmatrix} 1 & -\frac{1}{2} & -\frac{1}{2} \\ 0 & \frac{\sqrt{3}}{2} & -\frac{\sqrt{3}}{2} \end{bmatrix}$$

(3.4)

the following table can be obtained.

	s_a	s_b	s_c	$\tilde{v}_{i\alpha}$	$\tilde{v}_{i\beta}$
$\tilde{v}_0$	-1	-1	-1	0	0
$\tilde{v}_1$	$+1$	-1	-1	$+4/3$	0
$\tilde{v}_2$	$+1$	$+1$	-1	$+2/3$	$+2/\sqrt{3}$
$\tilde{v}_3$	-1	$+1$	-1	$-2/3$	$+2/\sqrt{3}$
$\tilde{v}_4$	-1	$+1$	$+1$	$-4/3$	0
$\tilde{v}_5$	-1	-1	$+1$	$-2/3$	$-2/\sqrt{3}$
$\tilde{v}_6$	$+1$	-1	$+1$	$+2/3$	$-2/\sqrt{3}$
$\tilde{v}_7$	$+1$	$+1$	$+1$	0	0

The zero voltage vectors can be realized by two different switching states i.e. $v_0 = v_7 = 0$. We can depict the fundamental vectors geometrically in the α / β plane, where they span a regular hexagon.
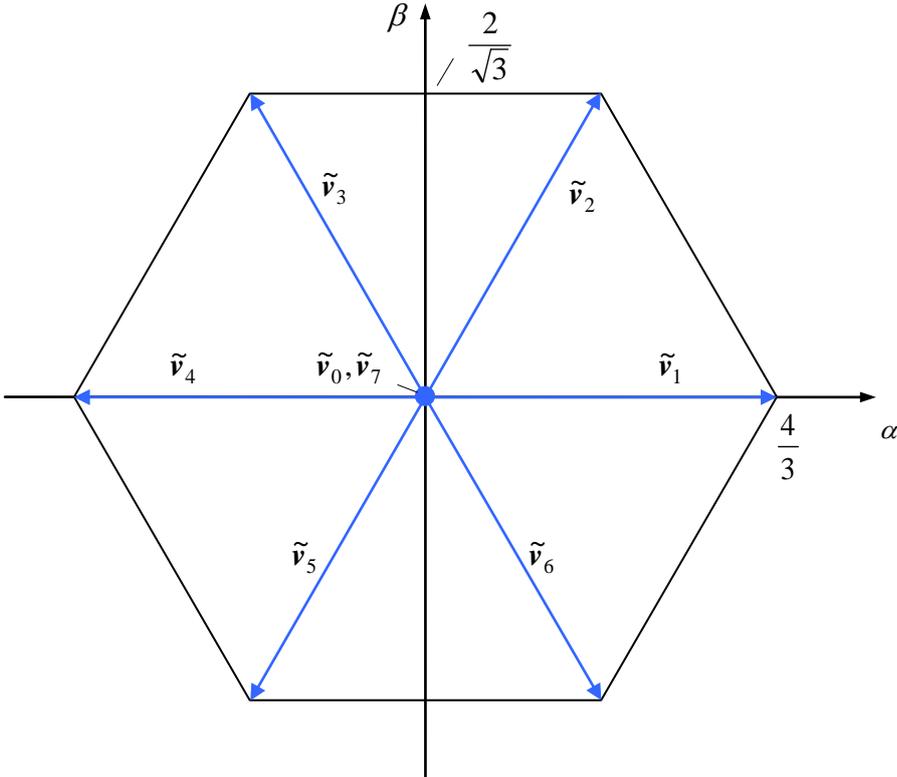
Fig. 3-6: Fundamental vectors in the orthogonal plane

4 Pulse Width Modulation

Since an inverter accepts only discrete switching states and thus can generate only 7 different output voltage levels, we therefore realize intermediated voltage values with the help of a Pulse Width Modulation (PWM). The principle will first be introduced through a single phase example which will later be extended to three phases.

4.1 Single-Phase Pulse Width Modulation

The normalized reference voltage

$$\widetilde{u}* = \frac{u*}{u_{dc}/2} \tag{4.1}$$

is the input variable, the reference switching function for the PWM is given by

$$s* = \widetilde{u}* \tag{4.2}$$

The switching function $s(t)$ is generated by comparing the normalized voltage value with a triangular modulation carrier. The output of the comparator can be directly referred to as the switching function. Through geometric interpretation of this procedure it becomes clear that the time average of the switching function corresponds to the reference, as long as the reference can be assumed constant or only slowly varying. (For a more detailed investigation of the temporal behavior, see also section 4.8, especially 4.8.2):

$$\overline{s(t)} = s^*$$
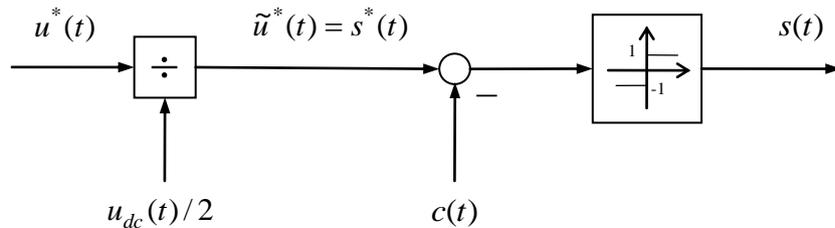
Fig. 4-1: Implementation of pulse width modulation through
triangular carrier modulator and comparator
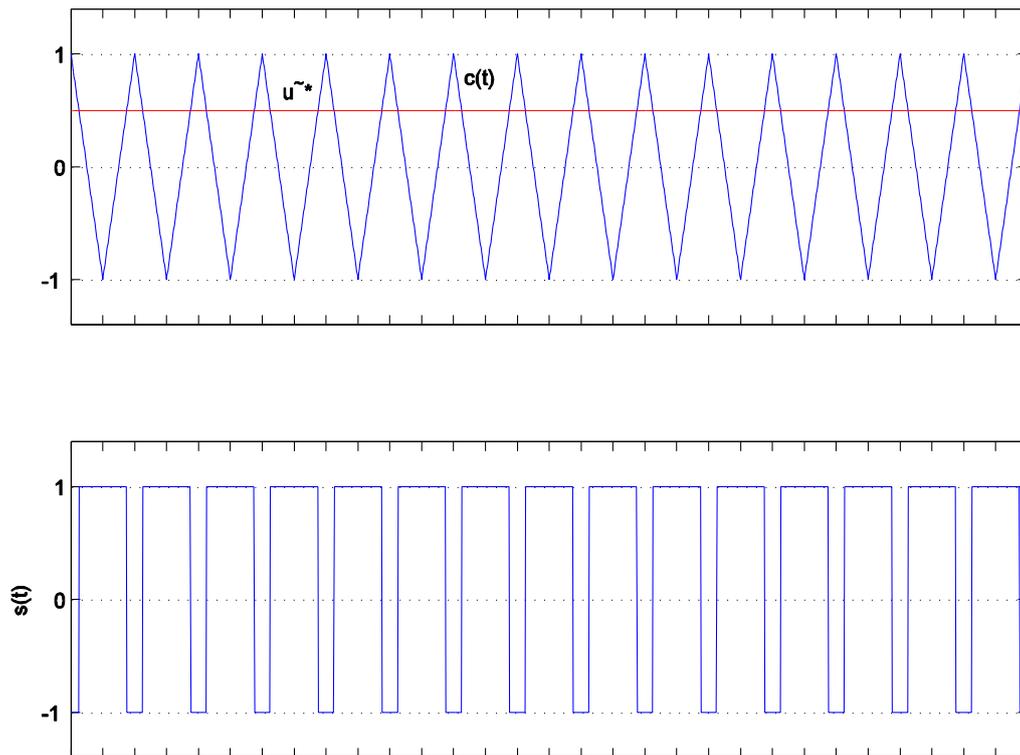
Fig. 4-2: Modulation of a constant reference value

The above procedure is called *Triangular Modulation* due of the shape of its carrier signal. Especially with regard to sinusoidal reference values (see below), the term *Sine-Triangular-Modulation* is also common. Unfortunately, the last term is a bit misleading as it implies that this method can only be used for the modulation of sinusoidal reference values. Although sinusoidal reference values are also considered in the below example, it should be noted that the PWM method can be used for any arbitrary transient reference signal.

Here, we always assume symmetrical triangular functions as modulation carrier. It is, however, also possible to use rising or falling saw-tooth functions instead.

The resulting switching frequency f_s of the PWM is directly determined through the frequency of triangular carrier signal $c(t)$. For many industrial devices a switching frequency standard of $f_s = 8...16\,\text{kHz}$ has evolved. Nevertheless, especially in certain high power industrial applications, switching frequencies of just few hundreds of hertz are usual. On the other hand, switching frequencies of several 10 kHz can be found in some special low power applications.
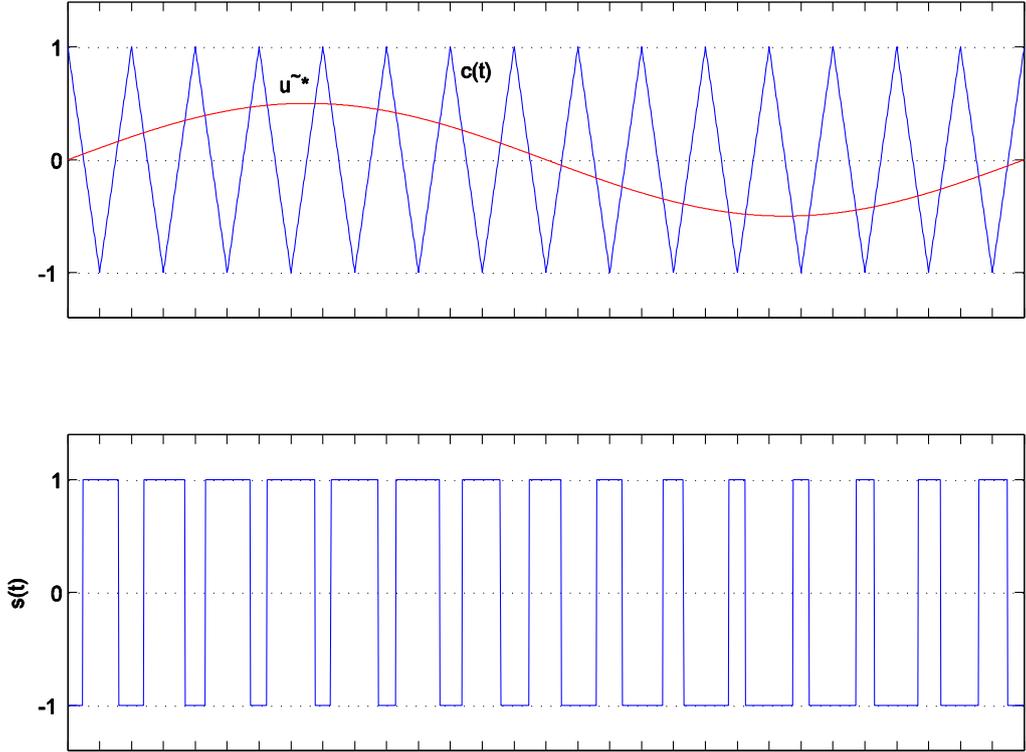
Fig. 4-3: Modulation of a sinusoidal reference value

The *modulation index* is given as the normalized peak voltage

$$A = \max\left|\frac{u^*(t)}{u_{dc}/2}\right| = \max\left|\tilde{u}^*(t)\right| \tag{4.3}$$

4.2 Three-Phase Pulse Width Modulation
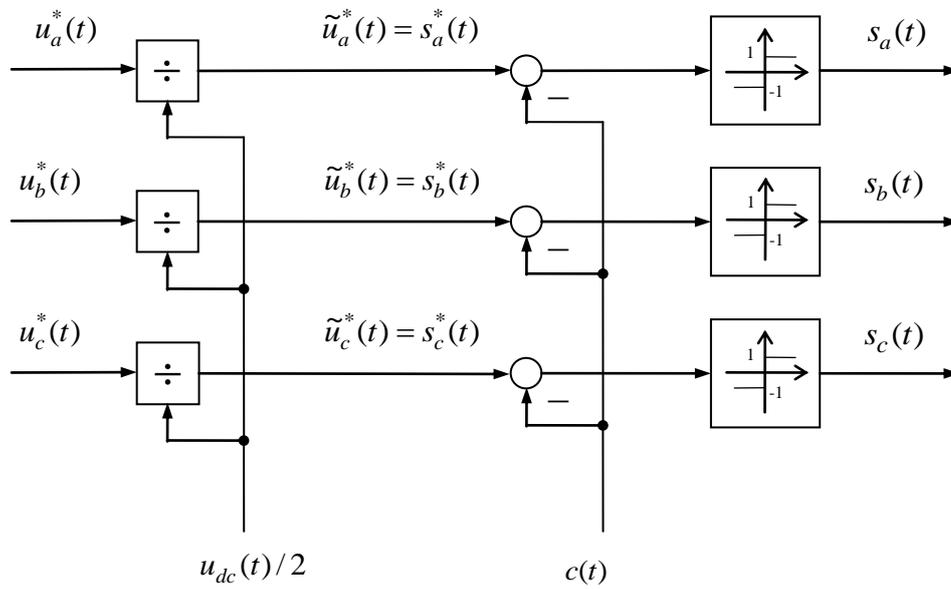
Fig. 4-4: Pulse width modulation with triangular carrier signal for three phase system
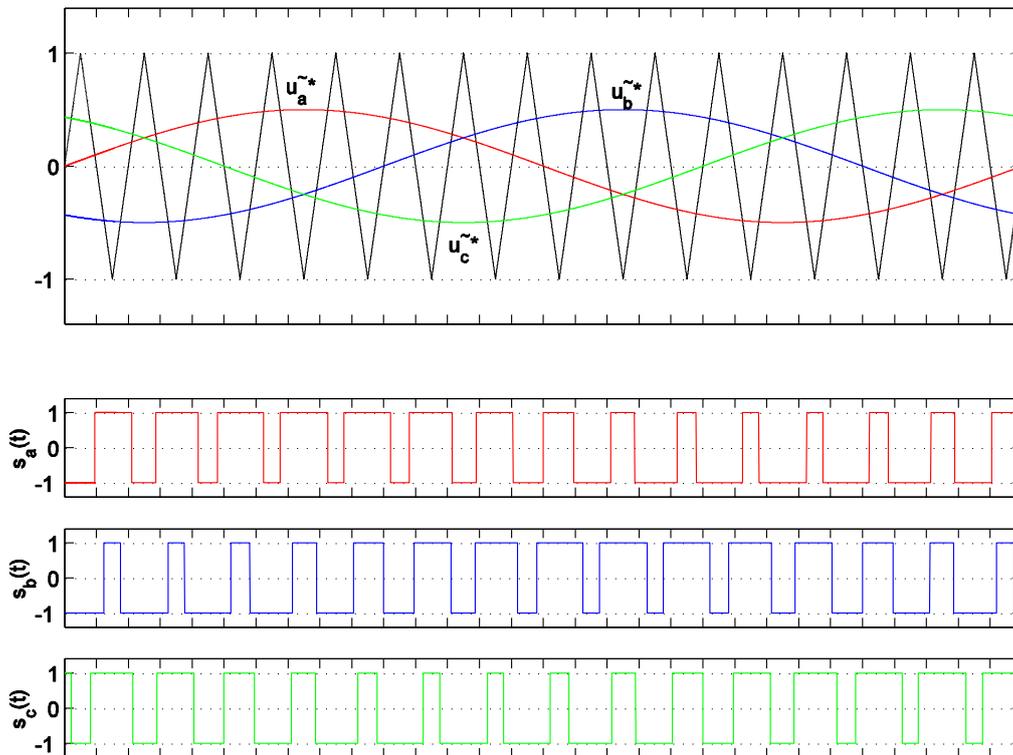
Fig. 4-5: PWM for sinusoidal three phase system
with modulation index $A = 0.5$
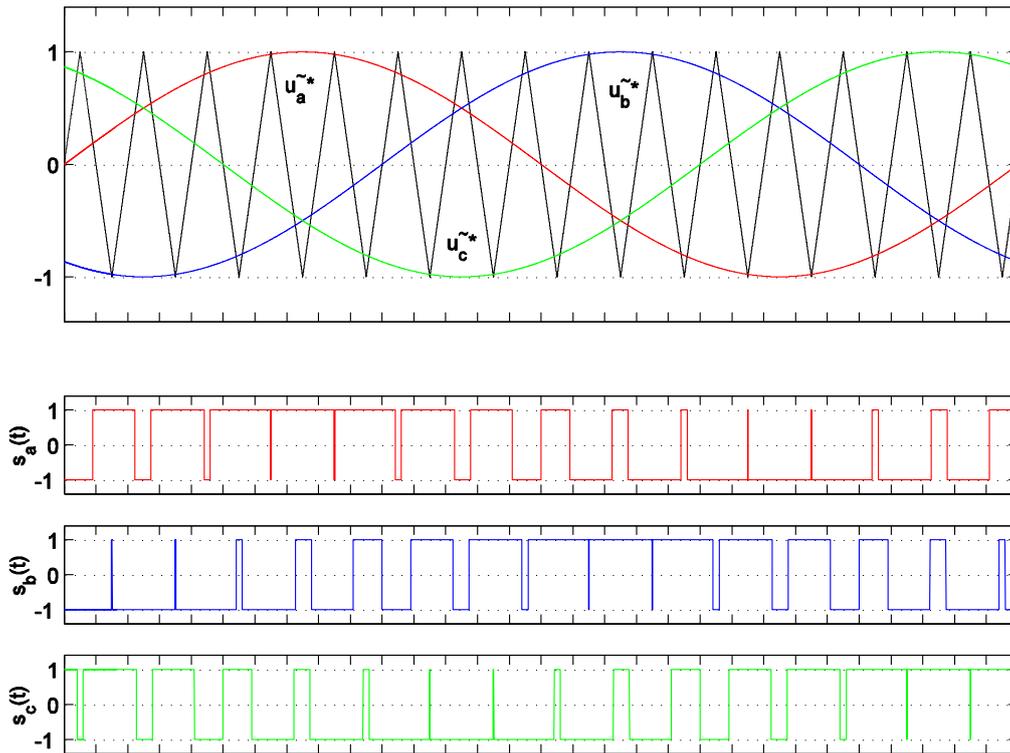
Fig. 4-6: PWM for sinusoidal three phase system
with modulation index $A = 1.0$

The modulation index range is given by

$$\left|\widetilde{u}_{a,b,c}(t)\right| \leq 1$$

In the figure below, this condition leads in the orthogonal α / β plane to stripes around the a, b or c axis, whose intersection forms the depicted inner hexagon. Each voltage vector $\widetilde{\boldsymbol{u}}^{*}$ of this hexagon can be realized through PWM. Considering only the magnitude of the voltage vector independent of its direction in the plane, in any case a vector following

$$A = \left|\widetilde{\boldsymbol{u}}^{*}\right| \leq A_{\max} = 1$$

can be implemented through this type of modulation.

The maximum line-to-line voltage, the inverter can apply to the motor, is represented by the input DC voltage u_{dc}. However, this potential is not being utilized by the current modulation method.
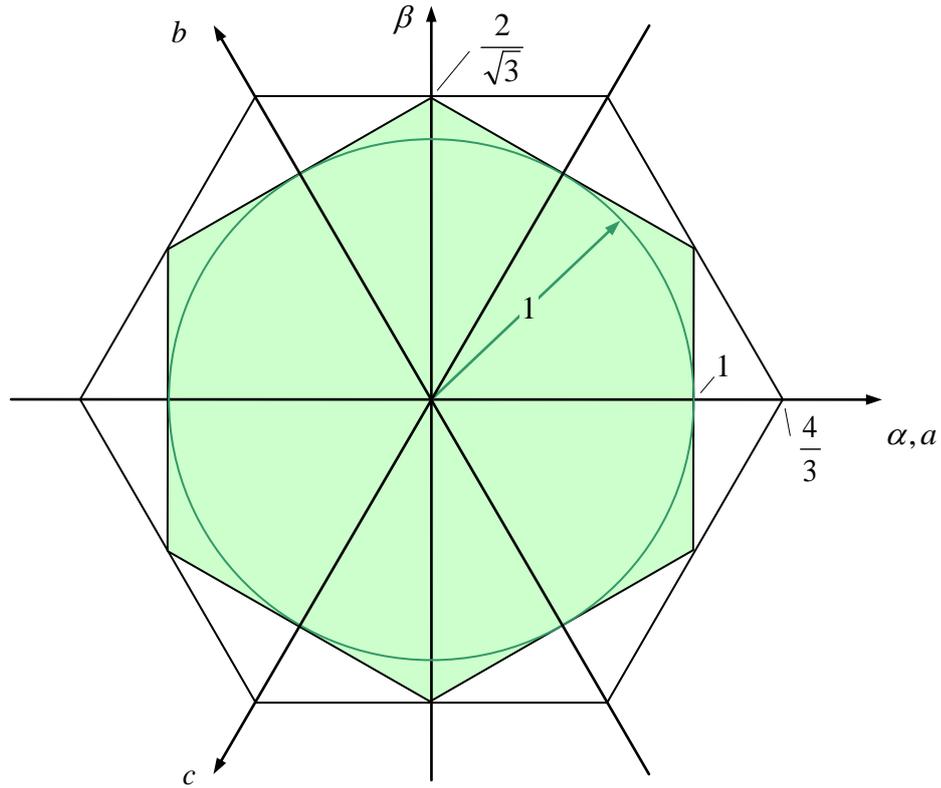
Fig. 4-7: Realization of voltage vectors through triangular modulation (PWM)

Shifting the reference potential (i.e. adding a zero component to the phase voltages) does not change the line-to-line voltages, but increases the dynamic modulation range.

$$u_0(t) = \frac{1}{2}\left[\max\left\{u_a^*(t), u_b^*(t), u_c^*(t)\right\} + \min\left\{u_a^*(t), u_b^*(t), u_c^*(t)\right\}\right] \tag{4.4}$$

$$u_a^{**}(t) = u_a^*(t) - u_0(t) \tag{4.5}$$

$$u_b^{**}(t) = u_b^*(t) - u_0(t) \tag{4.6}$$

$$u_c^{**}(t) = u_c^*(t) - u_0(t) \tag{4.7}$$
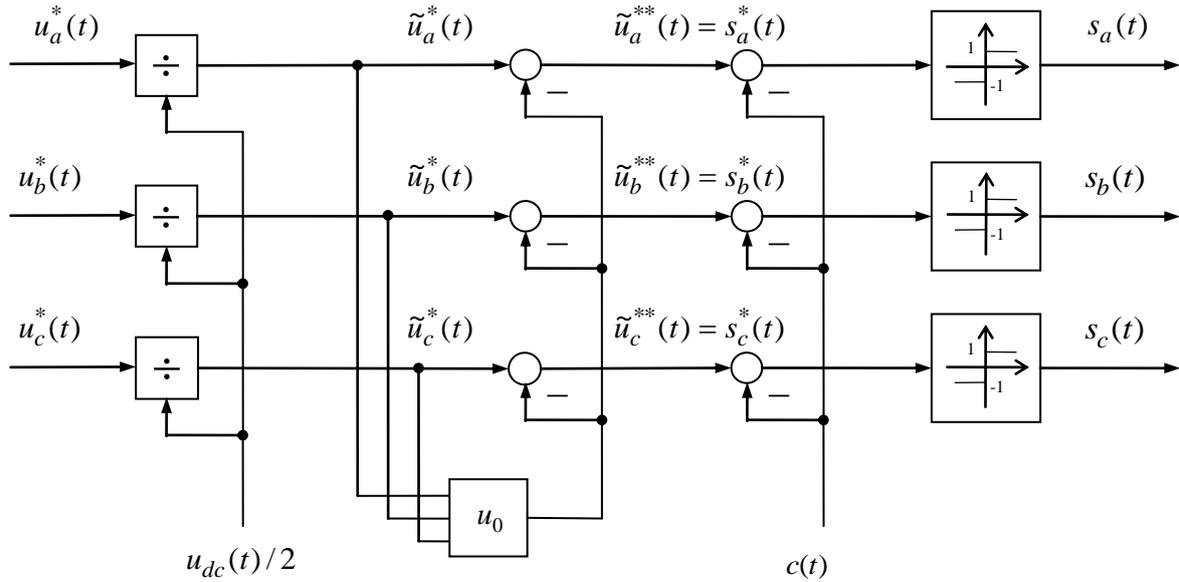
Triangular modulation (PWM) with zero point shift

With this zero point shift, the maximum possible dynamic modulation range of the line-to-line voltages is utilized as shown in the figure.

$$\frac{\left|u_{ab,bc,ca}(t)\right|}{u_{dc}} \leq 1 \quad \text{and} \quad \left|\tilde{u}_{ab,bc,ca}(t)\right| \leq 2$$

Regardless of the direction of the desired voltage vector in the orthogonal coordinates, each vector in the orthogonal system is realizable.

$$\tilde{\boldsymbol{u}}^* = \frac{\boldsymbol{u}^*}{u_{dc}/2}$$

$$A = \left|\tilde{\boldsymbol{u}}^*\right| \leq \frac{2}{\sqrt{3}} = 1{,}15 \tag{4.8}$$

Due to the zero point shift, the voltage utilization is thus increased by 15%. Although, the reference phase voltages lose their sinusoidal shape, the line-to-line voltages remain sinusoidal.
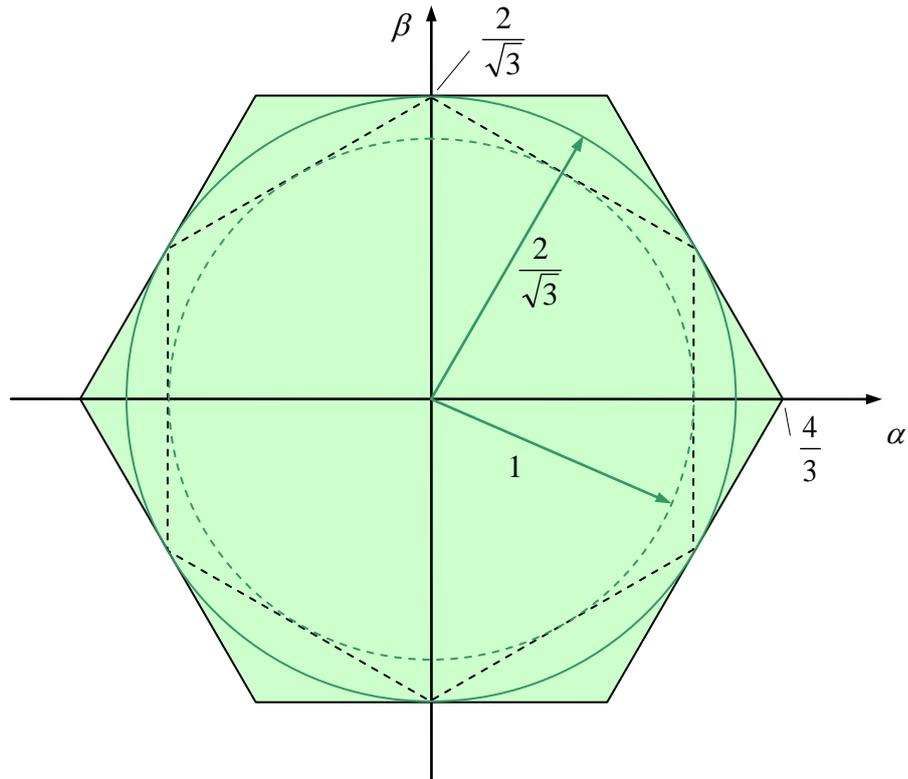
Fig. 4-8: Realizable voltage vectors with triangular modulation and zero point shift
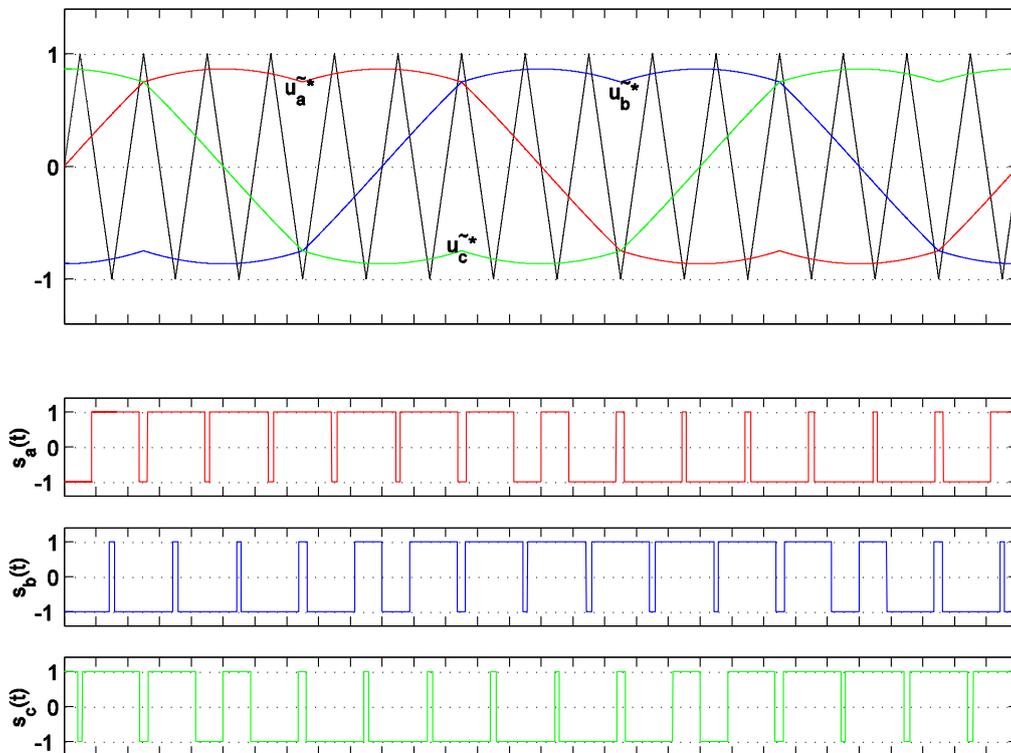
Fig. 4-9: Three phase triangular modulation with zero point shift,
$A = 1.0$
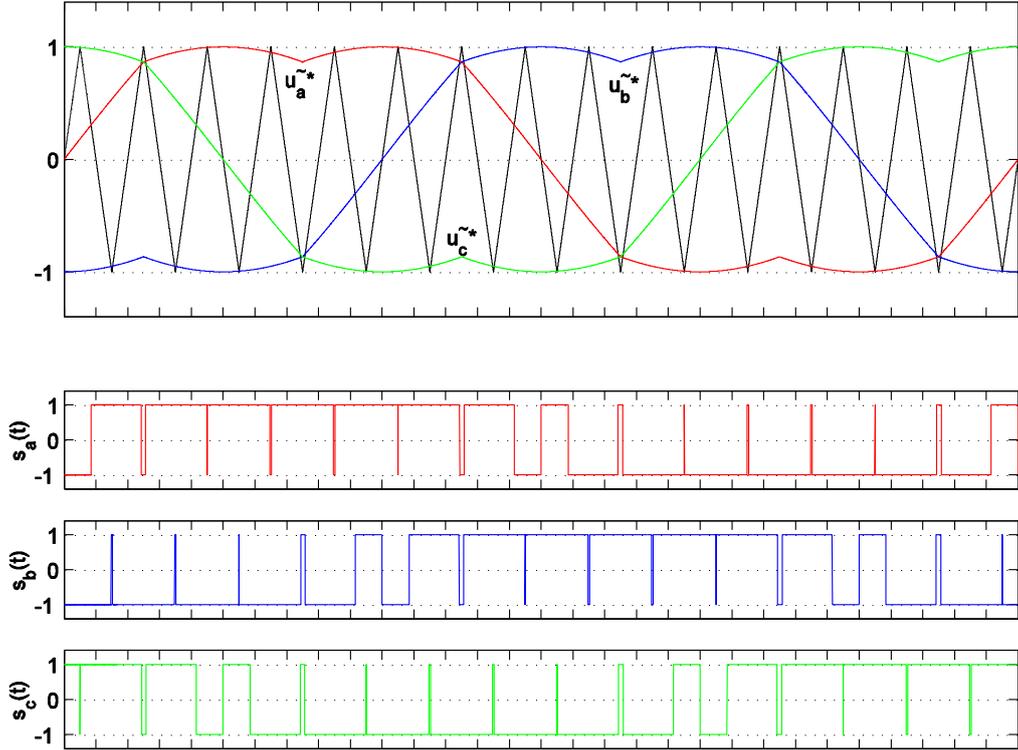
Fig. 4-10: Three phase triangular modulation with zero point shift,

$$A = 2/\sqrt{3} = 1.15$$

4.3 Space Vector Modulation

In contrast to PWM in which each of the three phases are modulated separately, *space vector modulation* is based on a reference vector $\boldsymbol{u}^*$ in orthogonal coordinates: Given a time interval of length T_a, also known as the sampling interval, the mean value of the inverter output voltage vector $\boldsymbol{u}(t)$, which can be realized via an appropriate sequence of fundamental voltage vectors $\boldsymbol{v}_k$, shall be equal to the desired voltage reference $\boldsymbol{u}^*(k)$ for this time interval:

$$\boldsymbol{u}^*(k) = \frac{1}{T_a} \int_{kT_a}^{(k+1)T_a} \boldsymbol{u}(t)\,dt = \frac{1}{T_a}\left(t_0\boldsymbol{v}_0 + t_1\boldsymbol{v}_1 + t_2\boldsymbol{v}_2 + t_3\boldsymbol{v}_3 + t_4\boldsymbol{v}_4 + t_5\boldsymbol{v}_5 + t_6\boldsymbol{v}_6 + t_7\boldsymbol{v}_7 \right)$$

$$= \tau_0\boldsymbol{v}_0 + \tau_1\boldsymbol{v}_1 + \tau_2\boldsymbol{v}_2 + \tau_3\boldsymbol{v}_3 + \tau_4\boldsymbol{v}_4 + \tau_5\boldsymbol{v}_5 + \tau_6\boldsymbol{v}_6 + \tau_7\boldsymbol{e}_7, \tag{4.9}$$

whereas

$$\tau_i = \frac{t_i}{T_a} \tag{4.10}$$

and considering the constraints

$$\sum_i \tau_i = 1 \quad \text{und} \quad \tau_i \geq 0.$$

In other words, the sum of all normalized times τ_i has to exactly correspond to the available sampling interval. The above equation can be also written with the normalized vectors

$$\tilde{\boldsymbol{u}}^*(k) = \frac{\boldsymbol{u}^*(k)}{u_{dc}/2} \;, \quad \tilde{\boldsymbol{v}}_i = \frac{\boldsymbol{v}_i}{u_{dc}/2} \tag{4.11}$$

leading to

$$\tilde{\boldsymbol{u}}^*(k) = \frac{1}{T_a} \int_{kT_a}^{(k+1)T_a} \tilde{\boldsymbol{u}}(t)\,dt = \tau_0\tilde{\boldsymbol{v}}_0 + \tau_1\tilde{\boldsymbol{v}}_1 + \tau_2\tilde{\boldsymbol{v}}_2 + \tau_3\tilde{\boldsymbol{v}}_3 + \tau_4\tilde{\boldsymbol{v}}_4 + \tau_5\tilde{\boldsymbol{v}}_5 + \tau_6\tilde{\boldsymbol{v}}_6 + \tau_7\tilde{\boldsymbol{v}}_7. \tag{4.12}$$

In order to do so, the factor $u_{dc}/2$ is taken outside of the integral under the assumption that the voltage $u_{dc}(t)$ is constant in time or at least varies slowly with respect to the sampling interval T_a. This assumption is true in many applications, but not always given. The DC voltage supply is usually stabilized by a capacitor. If the capacitor is dimensioned very small

then $u_{dc}(t)$ would vary quite rapidly, thus violating the prerequisite of an approximately constant voltage. This leads to errors in the desired motor voltage (see Section 4.5).

Depending on the location of the desired voltage vector $\boldsymbol{u}^*(k)$ maximum three out of the eight vectors are sufficient for vector modulation. In the case shown in the below figure, the reference vector lies in sector 1 of the hexagon. Therefore, vectors $\boldsymbol{v}_1, \boldsymbol{v}_2$ together with zero voltage vector $\boldsymbol{v}_0$ are sufficient for vector modulation.

$$\boldsymbol{u}^*(k) = \frac{1}{T_a} \int\limits_{kT_a}^{(k+1)T_a} \boldsymbol{u}(t)dt = \frac{1}{T_a}\left(t_0\boldsymbol{v}_0 + t_1\boldsymbol{v}_1 + t_2\boldsymbol{v}_2\right) = \tau_0\boldsymbol{v}_0 + \tau_1\boldsymbol{v}_1 + \tau_2\boldsymbol{v}_2 \tag{4.13}$$
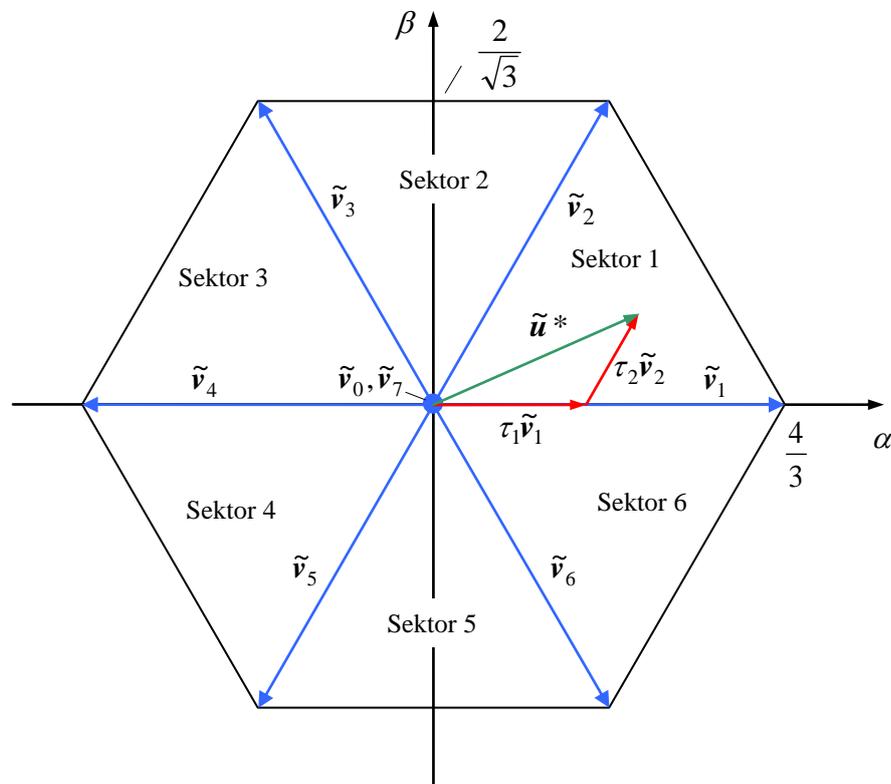
Fig. 4-11: Principles of space vector modulation

For a given vector $\boldsymbol{u}^*(k)$, this system of equations can be resolved algebraically for the times τ_i. From a geometric point of view, the times τ_i can be interpreted as *dual coordinates*, which can be read off axes, which are perpendicular to the fundamental vectors. By considering the projections of the reference vector on the dual τ_1- and τ_2-axes in the below figure, it directly follows:

$$\tau_1 = \frac{\tilde{u}_\alpha^*}{4/3} - \frac{1}{2}\frac{\tilde{u}_\beta^*}{2/\sqrt{3}} = \frac{3}{4}\tilde{u}_\alpha^* - \frac{\sqrt{3}}{4}\tilde{u}_\beta^* \tag{4.14}$$

$$\tau_2 = \frac{\tilde{u}_\beta^*}{2/\sqrt{3}} = \frac{\sqrt{3}}{2}\tilde{u}_\beta^* \tag{4.15}$$

Similarly, we find the corresponding relations for the other sectors, which are summed up in the table below.
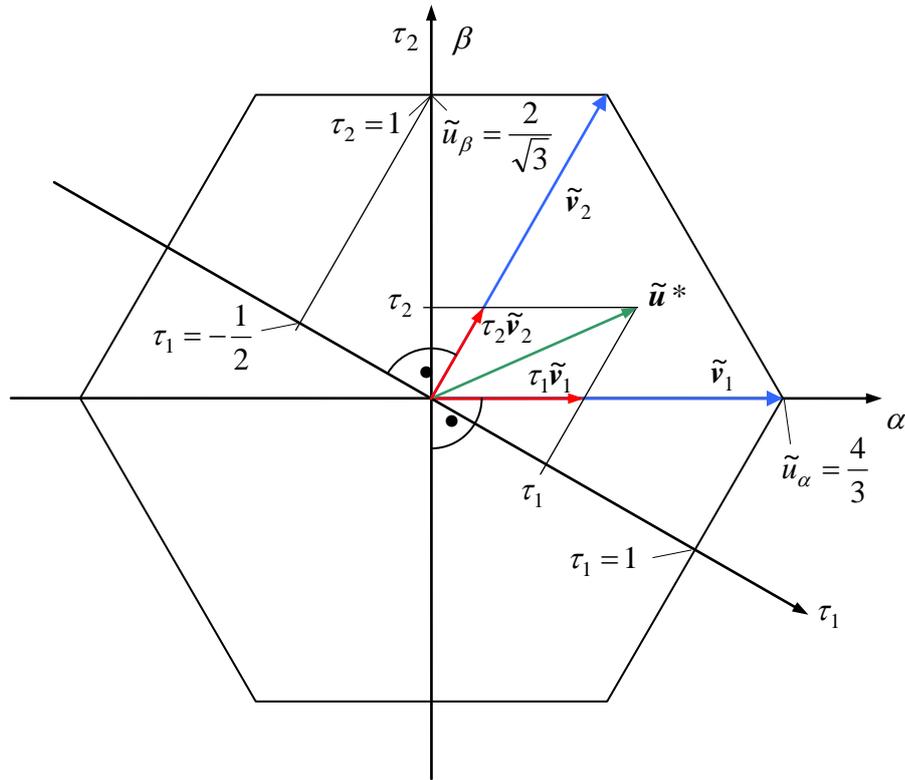
Fig. 4-12: Geometrical construction of times τ_k in dual coordinates

By suitable choice of the fundamental vectors, all reference vectors within the hexagon can be realized. Therefore, the dynamic modulation range of the space vector modulation covers the entire hexagon spanned by the fundamental vectors. It is identical to the three phase pulse width modulation, if zero point shift has been applied. Regardless of the direction each reference vector of the magnitude

$$\left|\tilde{u}^*\right| < \frac{2}{\sqrt{3}}$$

can be realized (see figure below).
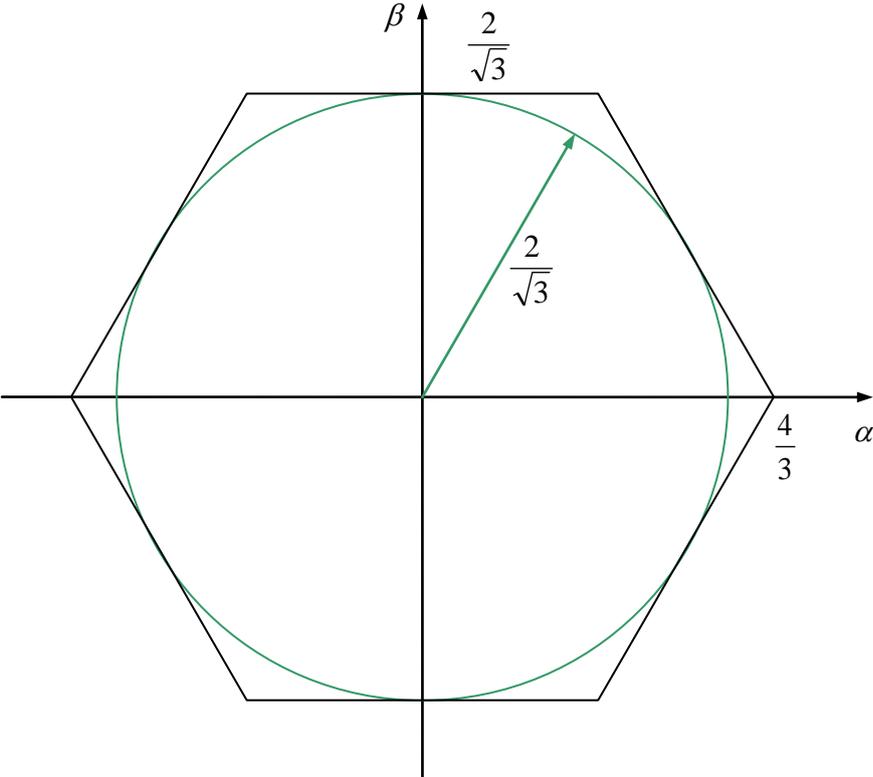
Fig. 4-13: Dynamic modulation range of space vector modulation

Depending on the sector the voltage reference vector is located in, the following pulse times follow (s. below table). The two pulse times refer to the active fundamental vectors, respectively, and are expressed as functions of the orthogonal components of the voltage reference. The times for the zero voltage vectors, i.e. τ_0 or τ_7, must complement the first two periods to a full (sampling) interval T_a.

Sector	Times for active vectors		Zero voltage vector
1	$\tau_1 = +\frac{3}{4}\tilde{u}_\alpha^* - \frac{\sqrt{3}}{4}\tilde{u}_\beta^*$	$\tau_2 = +\frac{\sqrt{3}}{2}\tilde{u}_\beta^*$	$\tau_0 + \tau_7 = 1 - \tau_1 - \tau_2$
2	$\tau_2 = +\frac{3}{4}\tilde{u}_\alpha^* + \frac{\sqrt{3}}{4}\tilde{u}_\beta^*$	$\tau_3 = -\frac{3}{4}\tilde{u}_\alpha^* + \frac{\sqrt{3}}{4}\tilde{u}_\beta^*$	$\tau_0 + \tau_7 = 1 - \tau_2 - \tau_3$
3	$\tau_4 = -\frac{3}{4}\tilde{u}_\alpha^* - \frac{\sqrt{3}}{4}\tilde{u}_\beta^*$	$\tau_3 = +\frac{\sqrt{3}}{2}\tilde{u}_\beta^*$	$\tau_0 + \tau_7 = 1 - \tau_3 - \tau_4$
4	$\tau_4 = -\frac{3}{4}\tilde{u}_\alpha^* + \frac{\sqrt{3}}{4}\tilde{u}_\beta^*$	$\tau_5 = -\frac{\sqrt{3}}{2}\tilde{u}_\beta^*$	$\tau_0 + \tau_7 = 1 - \tau_4 - \tau_5$
5	$\tau_6 = +\frac{3}{4}\tilde{u}_\alpha^* - \frac{\sqrt{3}}{4}\tilde{u}_\beta^*$	$\tau_5 = -\frac{3}{4}\tilde{u}_\alpha^* - \frac{\sqrt{3}}{4}\tilde{u}_\beta^*$	$\tau_0 + \tau_7 = 1 - \tau_5 - \tau_6$
6	$\tau_1 = +\frac{3}{4}\tilde{u}_\alpha^* + \frac{\sqrt{3}}{4}\tilde{u}_\beta^*$	$\tau_6 = -\frac{\sqrt{3}}{2}\tilde{u}_\beta^*$	$\tau_0 + \tau_7 = 1 - \tau_6 - \tau_1$

The sector, in which the reference vector is located, can quickly be determined by checking some signs:

Sector	$\tilde{u}_\beta^*$	$\sqrt{3}\tilde{u}_\alpha^* + \tilde{u}_\beta^*$	$\sqrt{3}\tilde{u}_\alpha^* - \tilde{u}_\beta^*$
1	+	+	+
2	+	+	−
3	+	−	−
4	−	−	−
5	−	−	+
6	−	+	+

Although the respective times for the active vectors can be uniquely determined from the desired voltage reference, there are some degrees of freedom as far the practical realization of vector modulation is concerned:

- The choice of the zero voltage vector, v_0 or v_7
- The sequence (order) of the participating fundamental vectors within the sample interval. Moreover, the time of the zero vector is often split up in equal halves which are allocated to the beginning and end of an interval, respectively.

The below table provides some potential variants, in this context. The sequences of the vectors are only stated for sectors 1 and 2, exemplarily. The vector sequences for the other sectors can easily be deduced from the symmetries. Note, that in the table all listed vector sequences are depicted with the help of the indices k of the relevant fundamental vectors v_k.

type	Sector 1 $i =$	Sector 2 $i =$
1	0, 1, 2, 7 7, 2, 1, 0 [1]	0, 3, 2, 7 7, 2, 3, 0 [1]
2	7 (and 0^2), 1, 2, 7	0 (and 7^2), 2, 3, 0
3	7 (and 0^2), 2, 1, 7	0 (and 7^2), 3, 2, 0

[1] alternating

[2] During a sector change the last forth-coming zero voltage vector would be replaced with the newly given vector, without having any impact on the motor voltage. This redundant switching procedure can be avoided when the last forth-coming voltage vector is left unchanged during a sector change until the next active vector is applied. Only afterwards, the new zero voltage vector is used in the vector sequences.

Type 1 in the above table with split (in equal halves) and alternating zero voltage vectors in the result exactly corresponds to the pulse width modulation with zero point shift and application of the regular-sampling principle.(refer to the figure below).
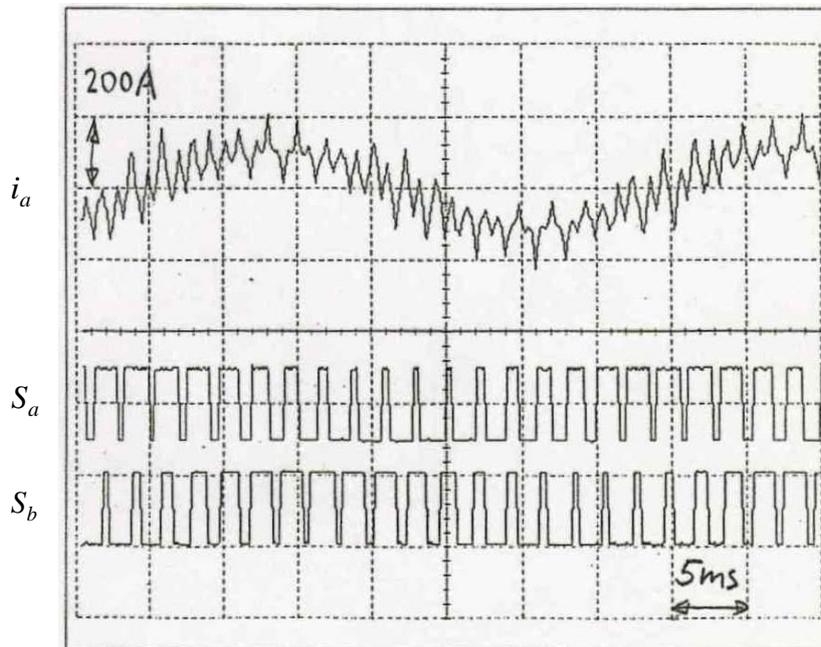
Fig. 4-14: Type 1: Pulse pattern of the vector modulation
Alternating pulse pattern; corresponds to pulse width modulation
(Two out of three switching commands are represented)
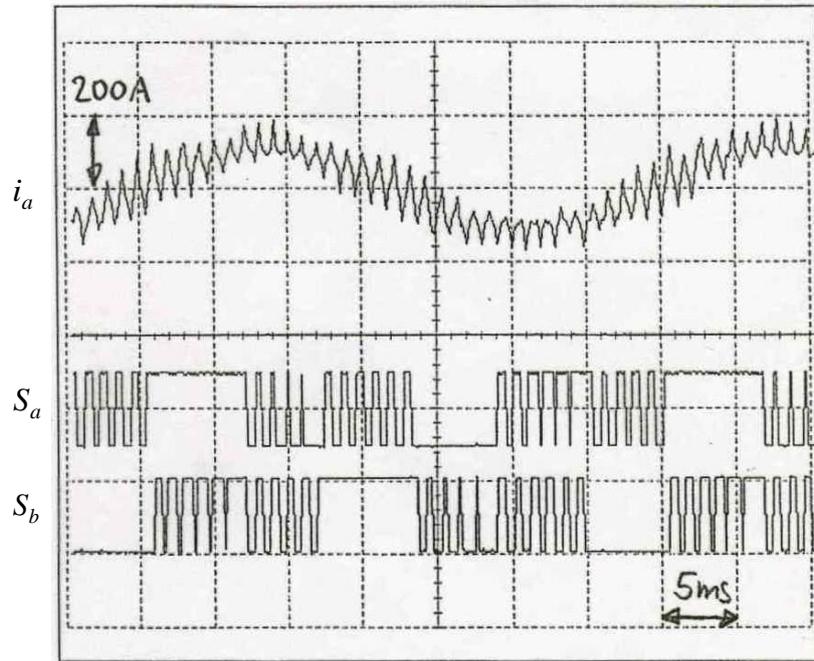
Fig. 4-15: Type 2: Pulse pattern of the vector modulation
(two out of three switching commands are represented)

When switching from one fundamental vector to another, switching procedures in one, two, if necessary also in three inverter legs (phases) can become necessary. The resulting switching frequency of an inverter leg is therefore not directly related to the frequency with which the fundamental vectors are switched.

The following diagram shows the transitions between states of the fundamental vectors. Two states are connected by a line, only if the transition is possible by switching only one leg. For better illustration, the two possible switching states of the zero vectors were not directly put on top of each other.
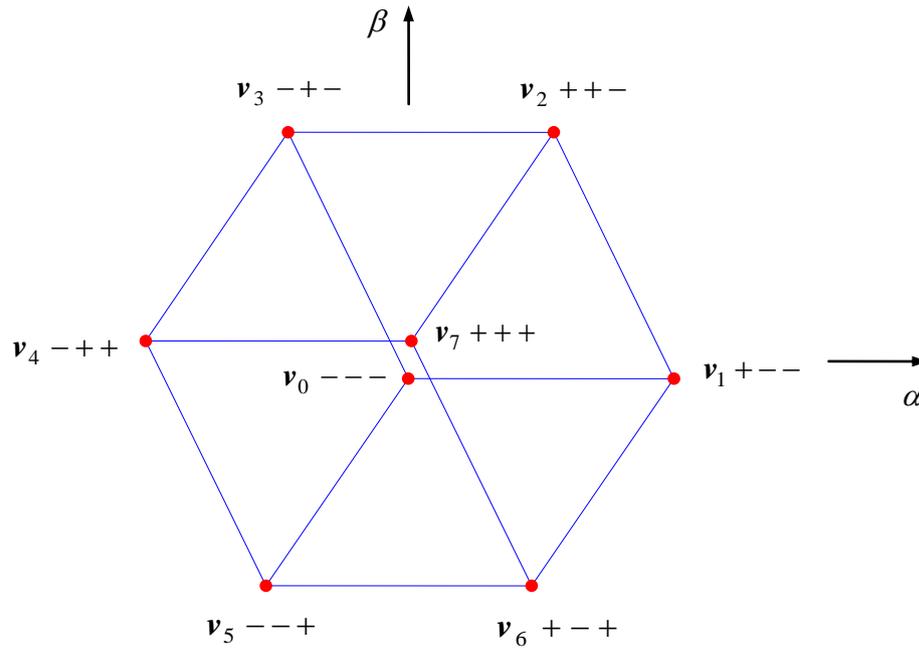
Fig. 4-16: Transition diagram for the fundamental switching states

With the help of this transition diagram, it is easy to determine the number of actual switching events of the inverter legs. For example, the Type 1 sequence switches each leg exactly once within one sampling interval leading to a total of three switching instants. As for Types 2 and 3 a total of four switching events takes place in each interval. However, in these cases switching events during sector transitions, i.e. when the voltage reference vector changes from one sector to another, are eliminated. Shall the sampling frequency be denoted by

$$f_a = \frac{1}{T_a}$$

while f_1 represents the fundamental frequency of the signal to be modulated. Then, the switching frequencies of the inverter legs can be calculated according to the below table.

type of space vector modulation	inverter leg switching frequency
1	$f_s = \frac{1}{2} f_a$
2	$f_s = \frac{2}{3} f_a - f_1$
3	$f_s = \frac{2}{3} f_a - f_1$

4.4   Regular Sampling

When speaking of *regular sampling* we refer to two aspects affecting the interaction of control and pulse width modulation or space vector modulation.

- The synchronization of the modulation carrier with a *discrete-time setting* of the reference voltages (in vector modulation this is automatically given).

- The synchronization of *discrete-time measurement samples* with the modulation carrier.

First Aspect: Nowadays, drive controls are no longer realized with analog circuit designs, which works in a continuous-time manner, but with the help of microcontrollers or DSP technologies. These controls rely on recursive control rules which are executed in a discrete-time manner (sampling), i.e. new reference values are provided only at a certain clock cycle. Since the controller can influence the motor currents only via the switching inverter elements, it is not reasonable from an economic point of view to execute the control cycle more often than the inverter's maximum switching frequency. Therefore, the sampling time T_a is synchronized with the switching period T_s, whereas two variants (see figures below) can be applied:

$$T_a = T_s \quad \text{or} \quad T_a = \frac{1}{2}T_s \tag{4.16}$$

For simplification, the functional principles shall be developed and explained based on a single phase PWM (one inverter leg). The results are directly applicable to three phases case, as well.
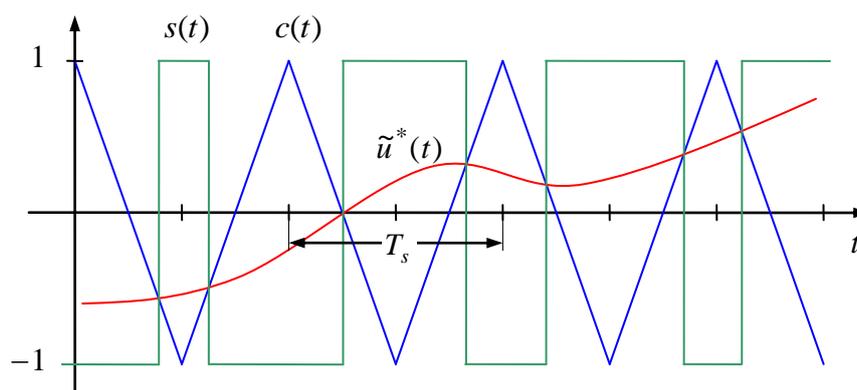
Fig. 4-17: Pulse width modulation with continuous-time reference value
(For not limiting the general validity, a random transient process is illustrated,
instead of a simple sinusoidal one)

These reference values do not have any influence on the control commands
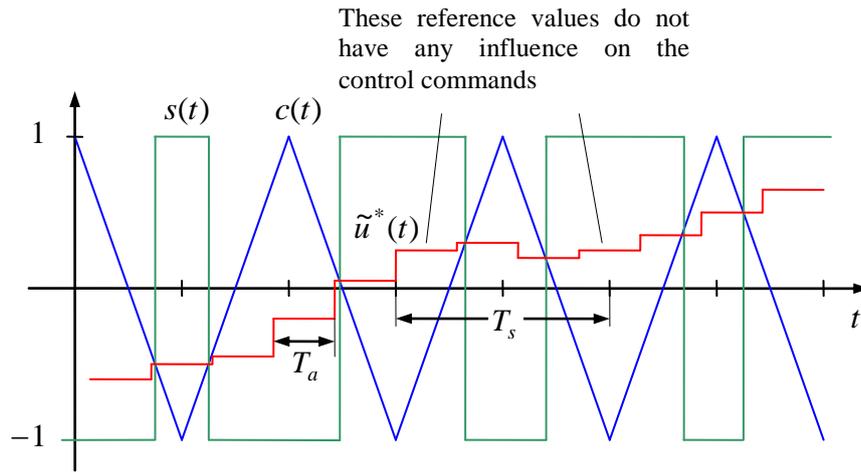
Fig. 4-18: Pulse width modulation with discrete-time, non-synchronized reference values

Each reference value determines exactly one switching edge
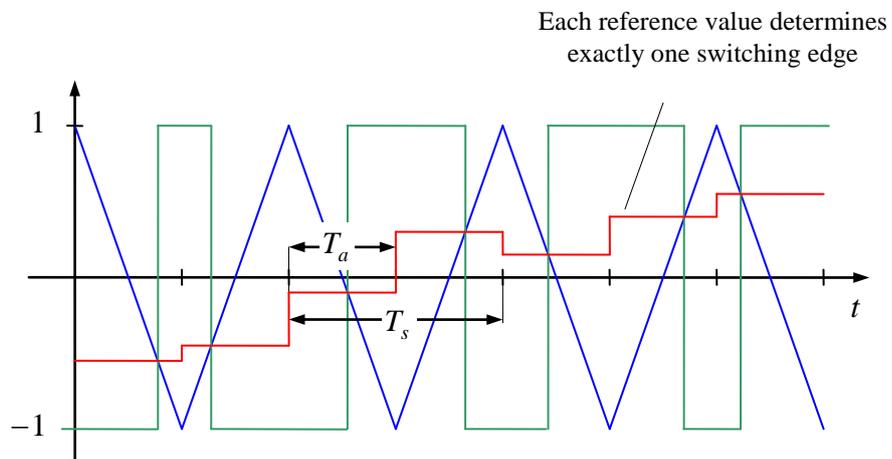
Fig. 4-19: Pulse width modulation with synchronized reference values (Regular Sampling) with $T_a = T_s / 2$
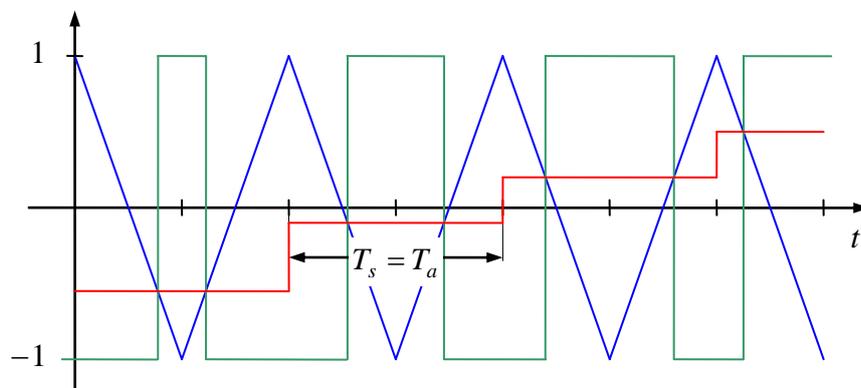
Fig. 4-20: Pulse width modulation with synchronized reference values (Regular Sampling) with $T_a = T_s$

The discrete-time application of reference values leads to a delay in the system, which shall be further examined in the following:
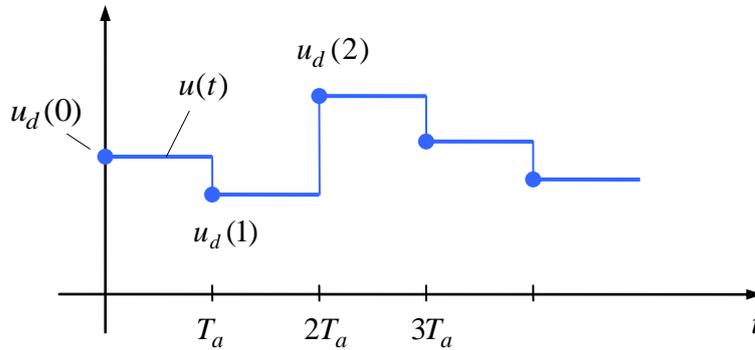
Fig. 4-21: Discrete-time reference

The discrete-time reference values shall be $u_d(k)$, the continuous-time function $u(t)$ is represented by the sum of time-shifted step functions $\sigma(t - t_0)$:

$$u(t) = \sum_k u_d(k) \left[\sigma(t - kT_a) - \sigma(t - (k+1)T_a) \right] \tag{4.17}$$

Transition to the Laplace domain:

$$U(s) = L(u)(s) = \int_{-\infty}^{\infty} u(t)\, e^{st}\, dt$$

$$U(s) = \sum_k u_d(k)\, \frac{1}{s} \left[e^{-skT_a} - e^{-s(k+1)T_a} \right] = \sum_k u_d(k) e^{-skT_a}\, \frac{1}{s} \left[1 - e^{-sT_a} \right] \tag{4.18}$$

The series

$$\sum_k u_d(k) e^{-skT_a} \tag{4.19}$$

represents the *z*-transform (or Laurent-transform) of the sequence $u_d(k)$ at the point $z = e^{sT_a}$:

$$U_d(z) = \sum_k u_d(k) z^{-k} \tag{4.20}$$

The term

$$H(s) = \frac{1}{sT_a}\left[1 - e^{-sT_a}\right]$$
(4.21)

can be considered as the transfer function of a sample and hold process (despite the fact that no continuous-time reference value exists that could be sampled, since the discrete-time reference value is determined directly from a discrete-time controller).

Therefore, it follows:

$$U(s) = T_a H(s) U_d\left(e^{sT_a}\right)$$
(4.22)

In order to see the influence of amplitude and phase more clearly, $H(j\omega)$ can be written in the following form, as well:

$$H(j\omega) = \frac{1}{j\omega T_a}\left[1 - e^{-j\omega T_a}\right] = \frac{1}{j\omega T_a}\left[e^{j\omega T_a/2} - e^{-j\omega T_a/2}\right]e^{-j\omega T_a/2}$$

$$= \frac{2}{j\omega T_a}\sin\left(\frac{\omega T_a}{2}\right)e^{-j\omega T_a/2} = \mathrm{Si}\left(\frac{\omega T_a}{2}\right)e^{-j\omega T_a/2}$$

Alternatively,

$$H(j\omega) = \mathrm{Si}\left(\pi\frac{\omega}{\omega_a}\right)e^{-j\pi\frac{\omega}{\omega_a}}$$
(4.23)

whereas

$$\omega_a = \frac{2\pi}{T_a}$$
(4.24)

Quite frequently, approximations of $H(s)$ are used:

$$H(s) = \frac{1}{sT_a}\left[1 - e^{-sT_a}\right] = e^{-sT_a/2}\frac{1}{sT_a}\left[e^{sT_a/2} - e^{-sT_a/2}\right]$$

$$= e^{-sT_a/2}\frac{1}{sT_a}\left[1 + \frac{sT_a}{2} + \frac{1}{2}\left(\frac{sT_a}{2}\right)^2 - 1 + \frac{sT_a}{2} - \frac{1}{2}\left(\frac{sT_a}{2}\right)^2 + O_3(s)\right]$$
(4.25)

$$= e^{-sT_a/2}\left(1 + O_2(s)\right) \approx e^{-sT_a/2}$$

$O_n(s)$ denotes the remaining terms of the n-th and higher order in s. Through this result, we can conclude that $H(s)$ can be approximated by a dead-time element (T_t - element) with dead time $T_a/2$, whereas terms of second and higher order are neglected.

The 1st-order Padé approximation for the exponential function

$$e^{-sT_a} \approx \frac{1 - sT_a/2}{1 + sT_a/2} \tag{4.26}$$

provides an alternative approximation for $H(s)$

$$H(s) \approx \frac{1}{sT_a}\left[1 - \frac{1 - sT_a/2}{1 + sT_a/2}\right] = \frac{1}{sT_a}\left[\frac{1 + sT_a/2 - 1 + sT_a/2}{1 + sT_a/2}\right] = \frac{1}{1 + sT_a/2}$$

Here, $H(s)$ is approximated through a T_1-element (1st-order delay element) with the time constant $T_a/2$.

Hence, the discrete-time reference value can be approximated either by a dead time element or a delay element, whereas in both cases the significant time constant $T_a/2$ occurs.
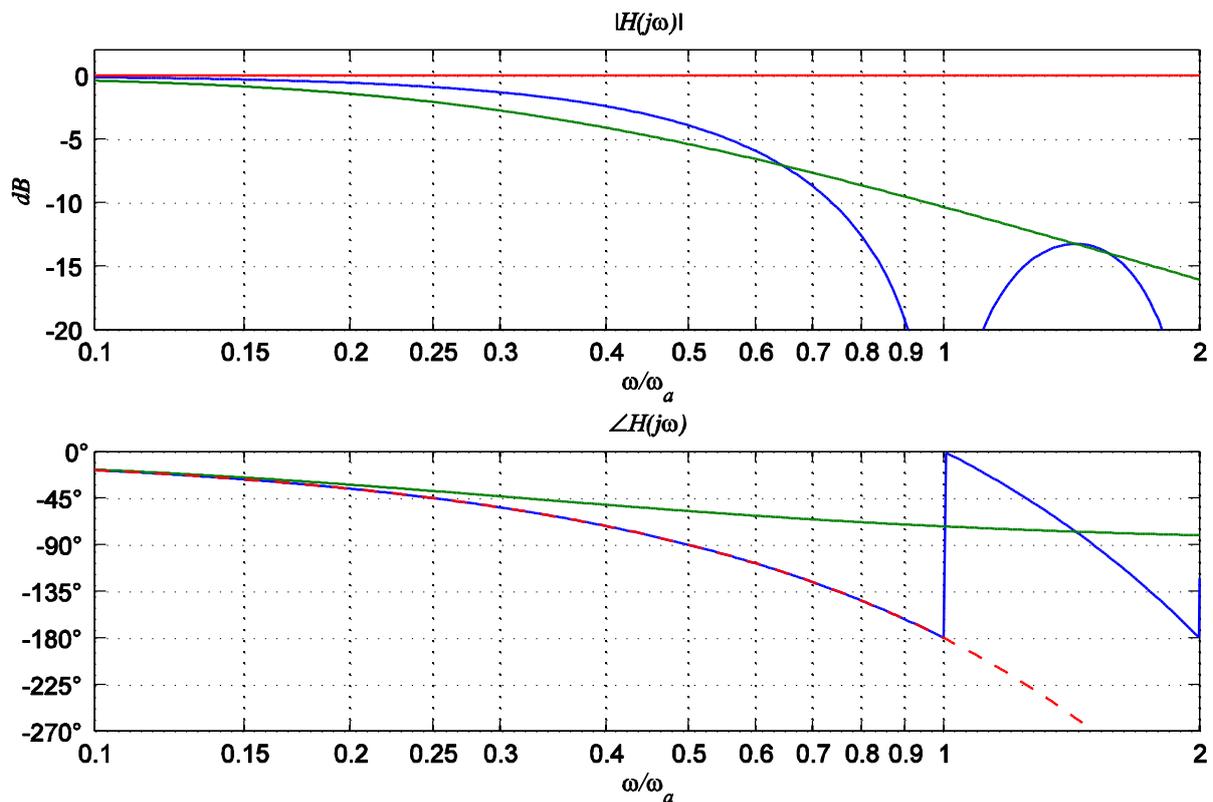
Fig. 4-22: Frequency characteristics of the sample and hold process und its approximations

    blue: $H(j\omega)$ without approximation

    green: approximation through T_1-element with $T_a/2$ as time constant

    red: approximation through T_t-element with $T_a/2$ as dead time

As it becomes evident from the frequency characteristics, both approximations reproduce the actual behavior of the sample and hold process in a different way.

The dead time approximation at least exactly reproduces the behavior of the phase (for frequencies below twice the Nyquist frequency $\omega/\omega_a < 1$). In the range of $\omega/\omega_a < 0.44$, the amplitude error is less than +3 dB.

The useful range of the T_1- approximation is rather determined by the phase error, which is less than 10° if $\omega/\omega_a < 0.29$. In this area the amplitude error is as smaller than 1.4 dB.

Second aspect of the regular sampling process: the measurement sampling:

For simplification, we assume a purely inductive load with a constant reverse voltage. In this case, a synchronization of the current sampling with the PWM carrier causes the sampled current values to exactly represent the time-local average current values. The current ripple caused by the inverter pulsation is masked by this subtly sampling process making analog filtering redundant. On the contrary, the application of an analog pre-filter would cause the current sampling method to no longer work as originally intended. Although the harmonic pulsation components would be smoothed, the pre-filter would cause a phase shift in the fundamental component, leading to errors in the control loop.
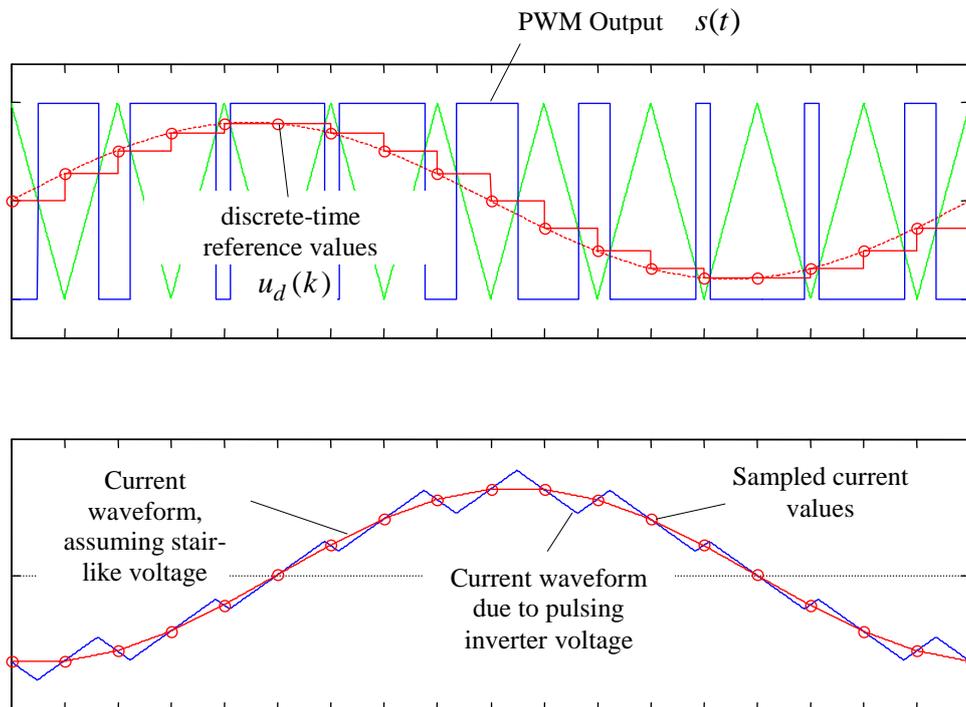
Fig. 4-23: Current sampling with regular-sampling technique

4.5   Dead Time in Digital Control Loops

If the control scheme is implemented on a microcontroller or microprocessor, then a certain time is required to process the control algorithm. Therefore, a measured value can affect the voltage reference only after this time period has passed. In an appropriate manner, all these processes are synchronized with the clock cycle given by the pulse width modulation or vector modulation. This way, the digital control introduces a dead time of one sampling step. Together with the discrete-time application of the reference voltage for the PWM (s. Section 4.4) a total dead time of 1.5 sampling steps of the control loop results.

Fig. 4-24: Flow chart of measurements sampling, control algorithm and PWM

At varying DC input voltages the dead time related to the discrete-time processing causes a further problem. Both, for the vector- and pulse width modulation, the voltage reference $\boldsymbol{u}^*$ initially needs to be referred to the input voltage u_{dc}. Therefore, the DC voltage value, which is known by the time when the reference voltage is applied, is used. If the input voltage has been sampled synchronously together with the current measurements, then the voltage value at the previous sampling instant is given as:

$$\tilde{\boldsymbol{u}}_d^*(k) = \frac{\boldsymbol{u}_d^*(k)}{u_{dc}(k-1)/2} \tag{4.27}$$

However, this normalized voltage reference is converted into a corresponding pulse sequence not before the next sampling interval. If the input voltage does not change or only slowly changes until that point, no problem occurs. When dealing with highly fluctuating input voltages, however, a voltage error is caused during the pulse width modulation, accordingly.

4.6   Voltage Errors Due to Interlocking Times

The switching behavior of an inverter can be realized by giving complimentary gate pulses to the two transistors of an inverter, as shown in the below figure. To avoid short circuits due to dead times in the control and the drivers and to ensure an orderly commutation, the previously conducting transistor is opened/blocked and the complementary transistor changes its state only after an *interlocking time* t_0. The timing of the actual commutation depends on whether the current flows from a transistor to a diode, or vice versa. The stages of operation are illustrated in the following pictures.
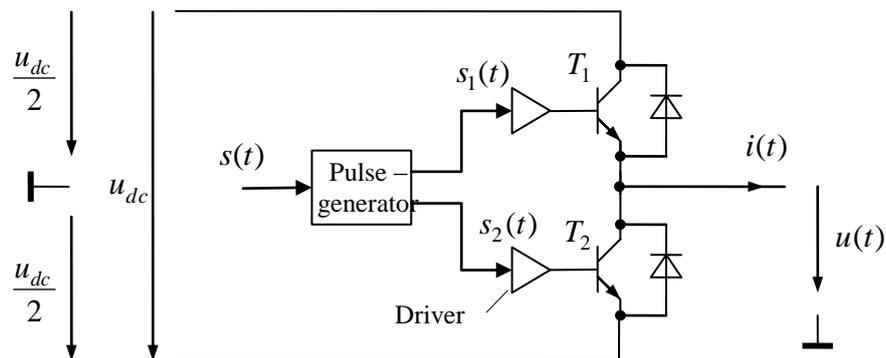
Fig. 4-25: Pulse generator and driver

Output voltage as a function of transistor states

T_1	T_2	u	
1	0	$+u_{dc}/2$	
0	1	$-u_{dc}/2$	
0	0	$-u_{dc}/2\,\mathrm{sgn}(i)$ [1]	open branch [2]
1	1		branch short circuit [3]

[1] As long as the current is flowing, it determines the output voltage via the conducting diode. Once the current stops flowing, i.e. the two diodes are blocking, the output voltage is no longer determined by the inverter but by the reverse voltage of the connected load.

[2] The open state is the idle or off-mode. In case of operation error, the converter is switched to that state.

[3] The short circuit usually leads to the destruction of the transistors, or in consequence even to the destruction of the entire equipment. This must be avoided at all costs.
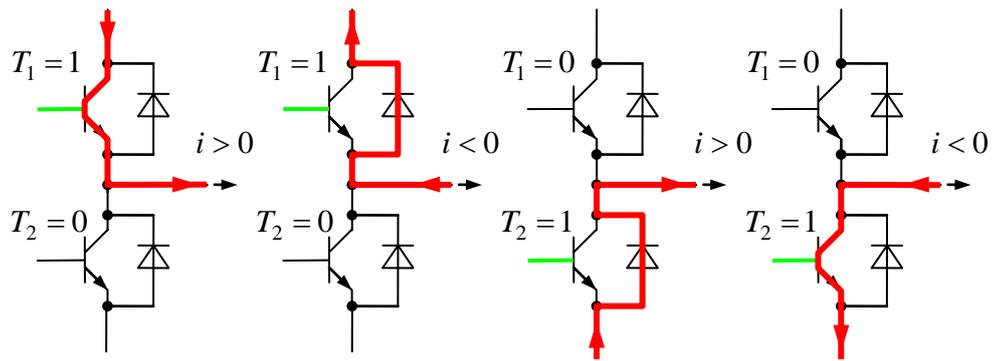
Fig. 4-26: Current paths depending on the switching state
and the current flow direction
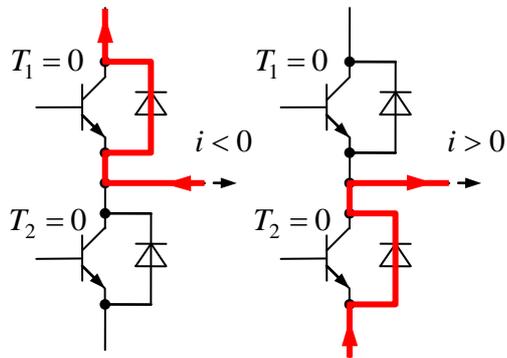
Fig. 4-27: Current paths depending on the current flow direction
in case of blocked transistors
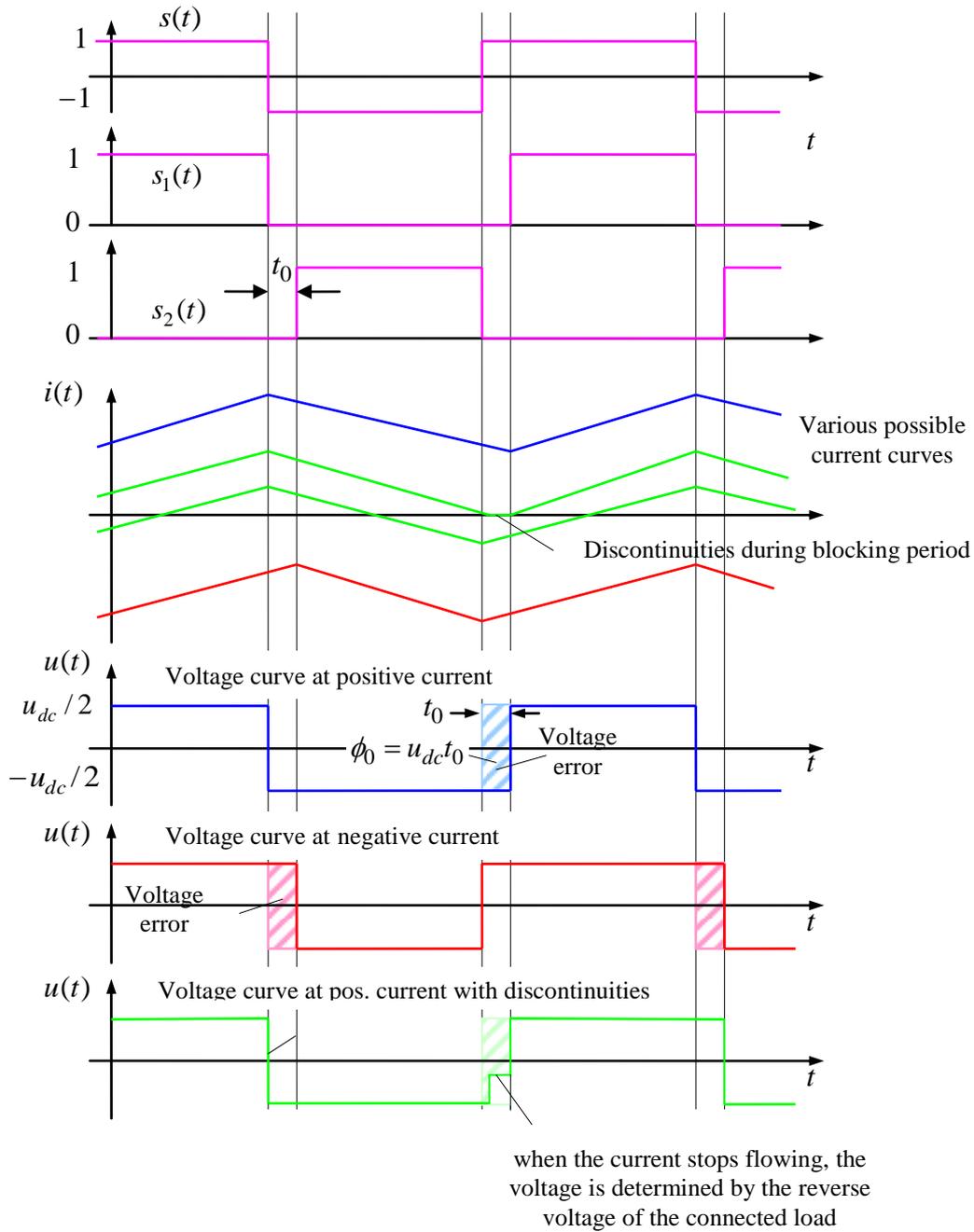
Fig. 4-28: Voltage curves due to interlocking times

The interlocking time introduces an error in the average value of the output voltage. The error affects by always opposing the current flow (just like an additional load). As long as the sign of the current does not change during the pulse period, the following equation holds (in average) under the assumption of an ideal commutation:

$$\Delta u = \overline{u} - s^* u_{dc} = -sign(i)\frac{t_0}{T_s}u_{dc} = -sign(i)t_0 f_s u_{dc} \tag{4.28}$$

Hereby, it shall be assumed that the DC voltage Δu_{dc} does not change significantly during a pulse period. In case the current changes sign within a switching period, then the above error equation is no longer valid. If the current is close to zero then the current curve might even exhibit discontinuities during interlocking periods. Please note that this consideration, as well, can only be regarded as an approximation, as the commutation procedures in the individual transistors and diodes are still assumed to be ideal.

Typical values:

Valve	f_s	t_0
GTO-Thyristor	200-500 Hz	$15-30\,\mu s$
IGBT	5-15 kHz	$2-5\,\mu s$
MOSFET	20-1000 kHz	$\leq 1\,\mu s$

The typical values of the resulting voltage errors can be in the range of 10% or even more! Compensating these errors seems to be simple at a first glance, but turns out to be quite challenging when dealing with small currents, i.e. if the average value of the current lies within the fluctuation range. In this case, the prediction of zero-crossings / discontinuities of the current can only be performed with moderate accuracy.

The voltage errors appear in each of the three phases:

$$\Delta u_{a,b,c} = -sign(i_{a,b,c}) t_0 f_s u_{dc} \tag{4.29}$$

Due to the star connected circuit, always two currents have different signs. The transformation of the individual phase voltage errors into the orthogonal vector representation results in a voltage vector Δu, whose magnitude results from the transformation T_{23}:

$$\left| \Delta u \right| = \frac{4}{3} \Delta u = \frac{4}{3} t_0 f_s u_{dc} \tag{4.30}$$

The direction of the error voltage is determined by the sign of the current or by the sector in which the current vector is located (see below figure). The voltage error, oriented in the opposite direction of the current vector, can now be approximated, as follows:

$$\Delta u = -\frac{i}{|i|} \frac{4}{3} t_0 f_s u_{dc} \tag{4.31}$$
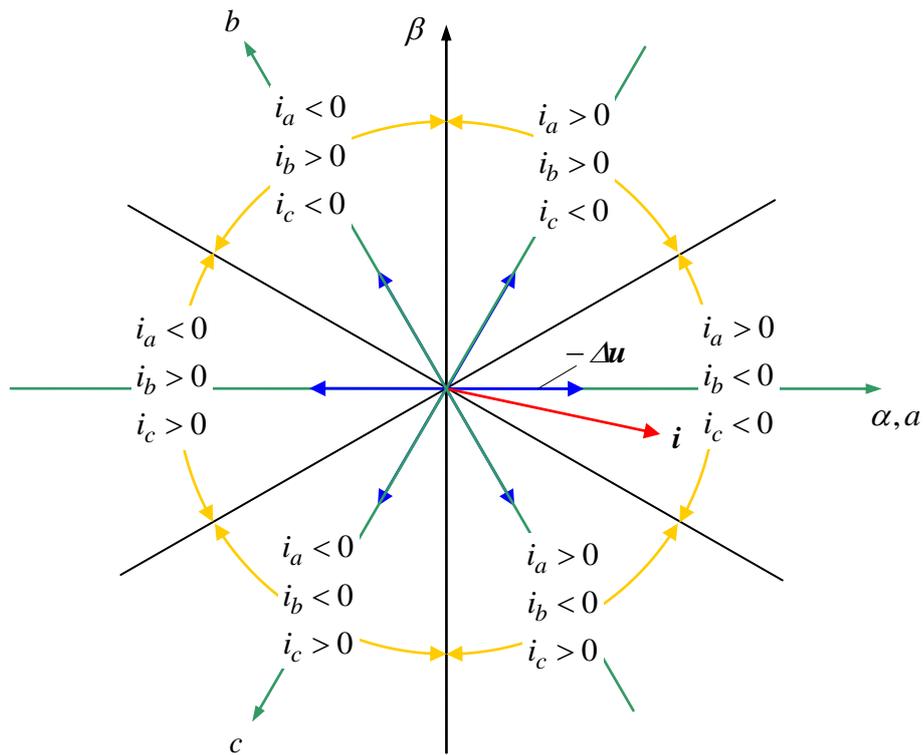
Fig. 4-29: The voltage error can be compensated by adding it to the reference value of the PWM,

$$\boldsymbol{u}^{**} = \boldsymbol{u}^* + \Delta\boldsymbol{u} = -\frac{\boldsymbol{i}}{|\boldsymbol{i}|}\frac{4}{3}t_0 f_s u_{dc} \tag{4.32}$$

It is, however, recommended for small currents, for which the impact direction of the voltage error is uncertain due the current fluctuation range, to slowly fade out this compensation depending on the current amplitude.

4.7 Dynamic State-Space Averaging of the Pulse-Width Modulated Inverter

For instantaneous values, the following equations hold:

$$u_{a,b,c}(t) = \frac{1}{2} s_{a,b,c}(t) u_{dc}(t) \tag{4.33}$$

$$i_{dc}(t) = \frac{1}{2} \sum_{a,b,c} s_k(t) i_k(t) \tag{4.34}$$

Averaging over one pulse period:

$$\overline{u}_{a,b,c}(t) = \frac{1}{2} \overline{s}_{a,b,c}(t) u_{dc}(t) = \frac{1}{2} s_{a,b,c}^*(t) u_{dc}(t) \tag{4.35}$$

$$\overline{i}_{dc}(t) = \frac{1}{2} \sum_{a,b,c} \overline{s}_k(t) i_k(t) = \frac{1}{2} \sum_{a,b,c} s_k^*(t) i_k(t) \tag{4.36}$$

Hereby, it must be assumed that the DC voltage $u_{dc}(t)$ and the corresponding motor currents $i_{a,b,c}(t)$, respectively, do not or at least only change negligibly slow during a pulse period.

State-Space Average (SSA) model in α / β - coordinates:

$$\overline{u}_{\alpha,\beta}(t) = \frac{1}{2} s_{\alpha,\beta}^*(t) u_{dc}(t) \tag{4.37}$$

$$\overline{i}_{dc}(t) = \frac{3}{4} \left(s_\alpha^*(t) i_\alpha(t) + s_\beta^*(t) i_\beta(t) \right) \tag{4.38}$$

State-Space Average model in d/q-coordinates:

$$\overline{u}_{d,q}(t) = \frac{1}{2} s_{d,q}^*(t) u_{dc}(t) \tag{4.39}$$

$$\overline{i}_{dc}(t) = \frac{3}{4} \left(s_d^*(t) i_d(t) + s_q^*(t) i_q(t) \right) \tag{4.40}$$
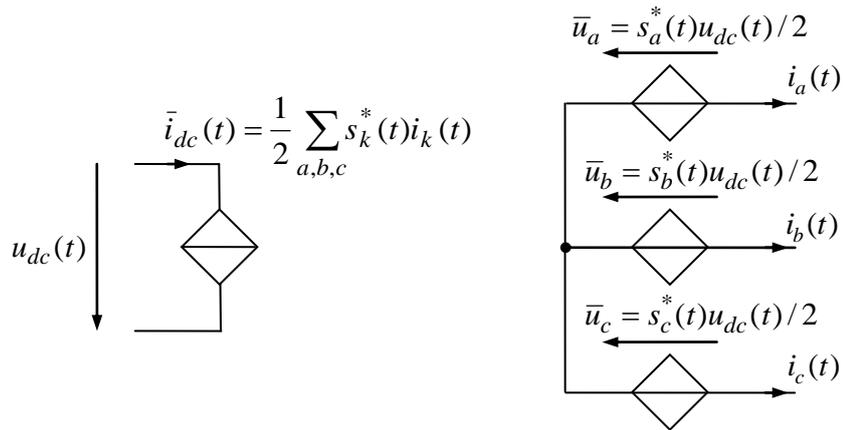
Fig. 4-30: Equivalent circuit diagram for State-Space Average modeling
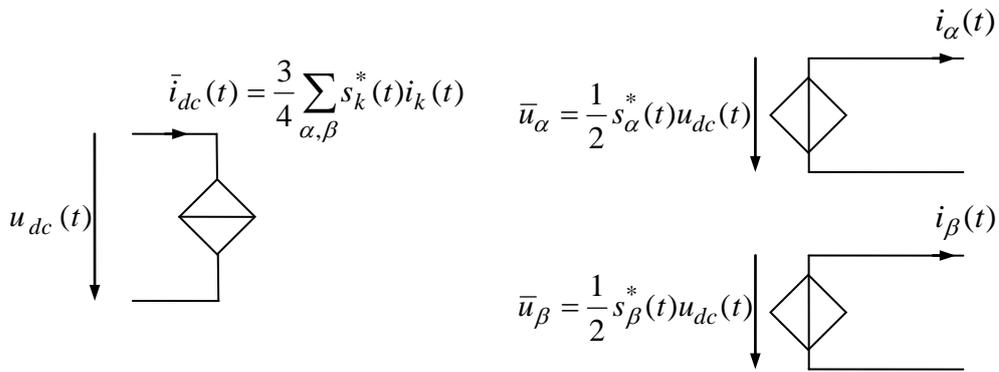
Fig. 4-31: Equivalent circuit diagram for State-Space Average
modeling in orthogonal coordinates

4.8 Harmonics

4.8.1 Harmonics at Constant Reference Values

Harmonics of the switching function $s(t)$ at constant reference values: Due to the operating principle of the pulse width modulation, it is implicitly guaranteed that the reference value is equal to the mean value of the generated switching function:

$$\bar{s} = s*$$
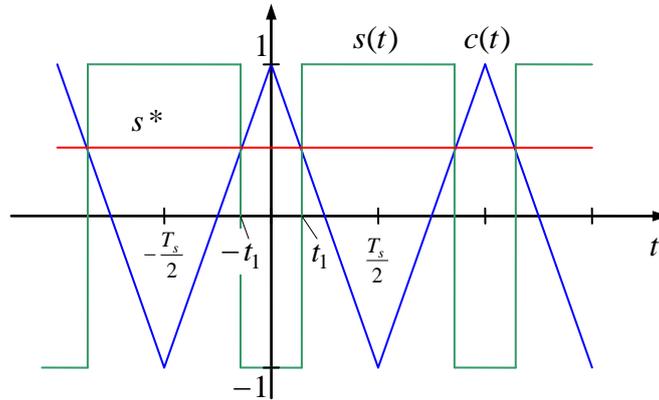
Fig. 4-32: Pulse width modulation with continuous-time reference

In addition to that, the PWM also causes harmonics due to its switching characteristics. The pulse frequency f_s and $\omega_s = 2\pi f_s$, respectively, as well as their multiples occur. The complex Fourier coefficients of the harmonics $k\omega_s$, while $k \neq 0$, result to:

$$S(k\omega_s) = \frac{1}{T_s} \int_{-T_s/2}^{T_s/2} e^{-jk\omega_s t} s(t)\, dt$$

$$= \frac{1}{T_s} \left(\int_{-T_s/2}^{-t_1} e^{-jk\omega_s t}\, dt - \int_{-t_1}^{t_1} e^{-jk\omega_s t}\, dt + \int_{t_1}^{T_s/2} e^{-jk\omega_s t}\, dt \right)$$

$$= \frac{1}{T_s} \left(\int_{-T_s/2}^{T_s/2} e^{-jk\omega_s t}\, dt - 2 \int_{-t_1}^{t_1} e^{-jk\omega_s t}\, dt \right)$$

$$= -\frac{2}{T_s} \int_{-t_1}^{t_1} e^{-jk\omega_s t}\, dt = \frac{2}{T_s jk\omega_s} \left(e^{-jk\omega_s t_1} - e^{+jk\omega_s t_1} \right)$$

$$S(k\omega_s) = -\frac{2}{\pi k} \sin k\omega_s t_1 = -\frac{2}{\pi k} \sin 2\pi k f_s t_1 \qquad (4.41)$$

With,

$$t_1 = \frac{T_s}{4}(1 - s^*) \tag{4.42}$$

it further follows

$$S(k\omega_s) = -\frac{2}{\pi k} \sin\left(\frac{\pi k}{2}(1 - s^*)\right) \tag{4.43}$$

The Fourier coefficient for the zero frequency is the already known mean value:

$$S(0) = \bar{s} = s^*$$

The time function is obtained via the Fourier series

$$s(t) = \sum_{k=-\infty}^{\infty} S(k\omega_s) e^{jk\omega_s t} = -\frac{2}{\pi k} \sum_{k=-\infty}^{\infty} \sin\left(\frac{\pi k}{2}(1 - s^*)\right) e^{jk\omega_s t} \tag{4.44}$$

Since,

$$S(k\omega_s) = S(-k\omega_s) \tag{4.45}$$

we can also write,

$$s(t) = S(0) + 2\sum_{k=1}^{\infty} S(k\omega_s) \cos k\omega_s t = s^* - \frac{4}{\pi k} \sum_{k=1}^{\infty} \sin\left(\frac{\pi k}{2}(1 - s^*)\right) \cos k\omega_s t$$

Alternatively,

$$s(t) = s^* - \frac{2}{\pi k} \sum_{k=1}^{\infty} \sin\left(\pi k(1 - s^*)\right) \cos(2k\omega_s t) - \frac{4}{\pi(2k+1)} \sum_{k=0}^{\infty} \sin\left(\pi \frac{2k+1}{2}(1 - s^*)\right) \cos((2k+1)k\omega_s t)$$

$$= s^* + \frac{2}{\pi k} \sum_{k=1}^{\infty} (-1)^k \sin\left(\pi k s^*\right) \cos(2k\omega_s t) - \frac{4}{\pi(2k+1)} \sum_{k=0}^{\infty} (-1)^k \cos\left(\pi\left(k + \tfrac{1}{2}\right)s^*\right) \cos((2k+1)k\omega_s t)$$

Approximation for small s^*

$$s(t) \approx s^* + 2s^* \sum_{k=1}^{\infty} (-1)^k \cos(2k\omega_s t) - \frac{4}{\pi(2k+1)} \sum_{k=0}^{\infty} (-1)^k \cos((2k+1)k\omega_s t) \tag{4.46}$$

This means, that in a first approximation the odd multiples of the switching frequency do not depend on the desired value s^*. They are approximately constant, while the even multiples grow proportionately with the desired value.

The voltage harmonics result from the switching function via

$$U(k\omega_s) = \frac{U_{dc}}{2} S(k\omega_s),$$ (4.47)

whereas the input DC voltage is assumed to be constant. However, in case harmonics of $u_{dc}(t)$ itself exist, the output voltage results through the convolution operation

$$U(k\omega_s) = \frac{1}{2}\left(U_{dc} * S\right)(k\omega_s) = \frac{1}{2}\sum_{l=-\infty}^{\infty} U(k\omega_s - l\omega_s) S(l\omega_s).$$ (4.48)

We are often not directly interested in the harmonics of the voltage, but rather of the currents. For an inductive load L (with constant input DC voltage), they can be obtained through

$$I(k\omega_s) = \frac{U(k\omega_s)}{jk\omega_s L} = \frac{U_{dc}}{2L}\frac{j}{\pi^2 k^2}\sin\left(\frac{\pi k}{2}(1 - s*)\right)$$ (4.49)
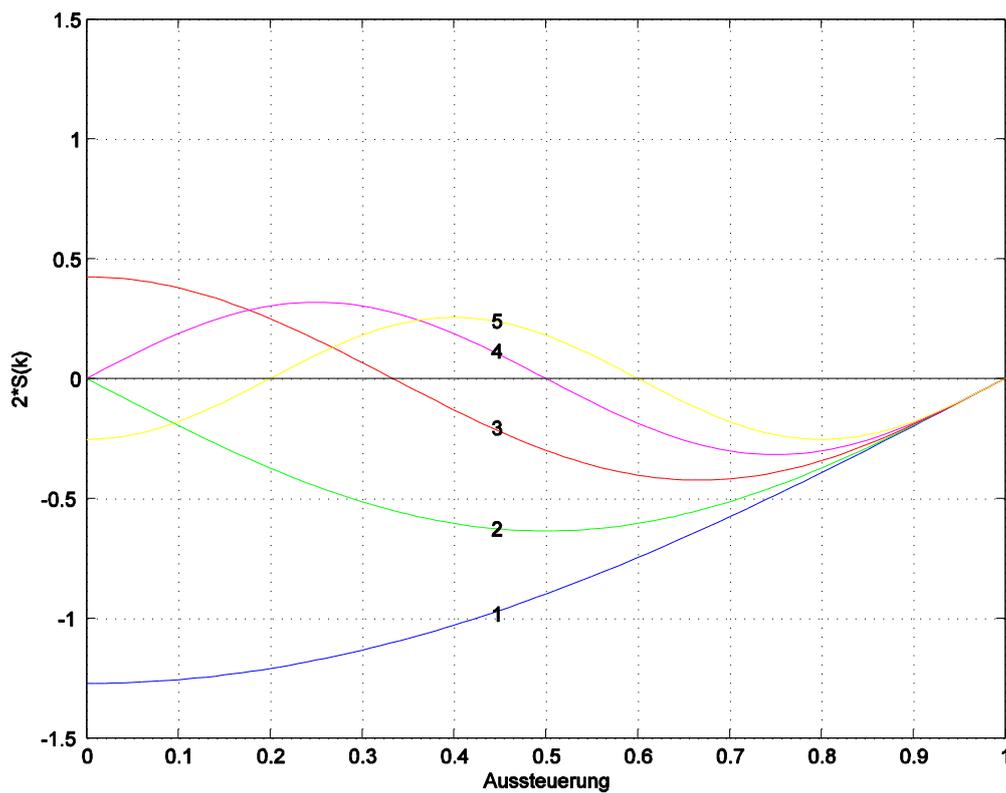
Fig. 4-33: Harmonics due to pulse width modulation

The harmonics of the input DC current

$$i_{dc}(t) = s(t)i(t)$$

can be exactly determined via convolution:

$$I_{dc}(k\omega_s) = (I * S)(k\omega_s) = \sum_{l=-\infty}^{\infty} S(k\omega_s - l\omega_s) I(l\omega_s) = \sum_{l=-\infty}^{\infty} S(k\omega_s - l\omega_s) \frac{U(l\omega_s)}{jl\omega_s L}$$

$$I(k\omega_s) == \frac{U_{dc}}{2jL} \sum_{l=-\infty}^{\infty} \frac{1}{l\omega_s} S(k\omega_s - l\omega_s) S(l\omega_s) \tag{4.50}$$

As an estimate, it may be sufficient to assume the output current

$$i(t) \approx I_0 \tag{4.51}$$

to be nearly constant. Then, the spectrum of the input current, as well as the output voltage directly results from the spectrum of the switching function

$$I_{dc}(k\omega_s) = I_0 \, S(k\omega_s) \tag{4.52}$$

4.8.2 Harmonics at Sinusoidal Reference Values

Assuming a steady state condition, modulation with amplitude A and fundamental frequency f_1:

$$s*(t) = A\cos \omega_1 t = A\cos 2\pi f_1 t = \frac{A}{2}\left(e^{j\omega_1 t} + e^{-j\omega_1 t}\right) \tag{4.53}$$

If the number of pulses per fundamental period,

$$n_p = \frac{\omega_s}{\omega_1} = \frac{f_s}{f_1} = \frac{T_1}{T_s} \tag{4.54}$$

is integral, it is referred to as *synchronized pulsing*. In this case, the pulse rate is a multiple of the fundamental frequency. In the spectrum, only multiples of the fundamental frequency would occur, accordingly.

However, it shall initially be assumed that the frequencies are not following any rational pattern. Then, the pulse sequence is not periodic in a fundamental frequency period. The Fourier coefficients are determined over a sufficiently long averaging time:

$$S(\omega) = \lim_{T\to\infty} \frac{1}{T} \int_{-T/2}^{T/2} e^{-j\omega t} s(t)\, dt \tag{4.55}$$

Fourier coefficients of fundamental frequency multiples:

$$S(k\omega_1) = \lim_{T\to\infty} \frac{1}{T} \int_0^T e^{-jk\omega_1 t} s(t)\, dt$$

$$= \lim_{M\to\infty} \frac{1}{M} \sum_{m=0}^{M} \frac{1}{T_1} \int_0^{T_1} e^{-jk\omega_1 t} s(t+mT_1)\, dt$$

$$S(k\omega_1) = \frac{1}{T_1} \int_0^{T_1} e^{-jk\omega_1 t} \lim_{M\to\infty} \frac{1}{M} \sum_{m=0}^{M} s(t+mT_1)\, dt \qquad (4.56)$$

Consequently, averaging of the switching function $s(t)$ over many periods precisely leads to the reference value of the pulse width modulation:

$$s^*(t) = \lim_{M\to\infty} \frac{1}{M} \sum_{m=0}^{M} s(t+mT_1) \qquad (4.57)$$

It therefore follows,

$$S(k\omega_1) = \frac{1}{T_1} \int_0^{T_1} e^{-jk\omega_1 t} s^*(t)\, dt = S^*(k\omega_1) \qquad (4.58)$$

The Fourier coefficients of the fundamental frequency multiples, thus, exactly correspond to the Fourier coefficients of the reference value of the pulse width modulation. In other words, the pulse width modulation has no influence, in this context. If the reference is a purely sinusoidal signal, as assumed above, then this very signal is reflected in the switching function; the reference is mapped exactly with respect to amplitude and phase:

$$S(\omega_1) = S(-\omega_1) = \frac{A}{2} \qquad (4.59)$$

Then, the coefficients for multiples of the fundamental frequency are zero:

$$S(k\omega_1) = 0 \text{ for } |k| \neq 1$$

In particular, no time delay, as sometimes mistakenly attributed to the pulse width modulation, is recognizable; this would be noticeable in form of a phase shift. A time delay is introduced solely by the discrete-time application of reference values (see Section 4), but not trough the pulse width modulation, itself.

For the practical verification of these relationships, the assumed infinite averaging time must not be overlooked. When limiting the measurement duration to only one or few fundamental periods, multiples of the fundamental frequency will be measureable.

In addition to the multiples of the fundamental frequency, intermodulation products occur between switching- and fundamental frequency. The Fourier series of the switching function $s(t)$ for a constant $s*$ shall serve as a starting point, in this context:

$$s(t) = s* + \frac{2}{\pi k}\sum_{k=1}^{\infty}(-1)^k \sin\left(\pi k s^*\right)\cos(2k\omega_s t) - \frac{4}{\pi(2k+1)}\sum_{k=0}^{\infty}(-1)^k \cos\left(\pi\left(k+\tfrac{1}{2}\right)s^*\right)\cos\left((2k+1)k\omega_s t\right)$$

$$\approx s* + 2s*\sum_{k=1}^{\infty}(-1)^k \cos(2k\omega_s t) - \frac{4}{\pi(2k+1)}\sum_{k=0}^{\infty}(-1)^k \cos\left((2k+1)k\omega_s t\right) \qquad (4.60)$$

With,

$$s^*(t) = A\cos\omega_1 t \qquad (4.61)$$

it follows,

$$s(t) = A\cos\omega_1 t + \frac{2}{\pi k}\sum_{k=1}^{\infty}(-1)^k \sin\left(\pi k A\cos\omega_1 t\right)\cos(2k\omega_s t)$$

$$- \frac{4}{\pi(2k+1)}\sum_{k=0}^{\infty}(-1)^k \cos\left(\pi\left(k+\tfrac{1}{2}\right)A\cos\omega_1 t\right)\cos\left((2k+1)k\omega_s t\right)$$

$$\approx A\cos\omega_1 t\left[1 + 2\sum_{k=1}^{\infty}(-1)^k \cos(2k\omega_s t)\right] - \frac{4}{\pi(2k+1)}\sum_{k=0}^{\infty}(-1)^k \cos\left((2k+1)k\omega_s t\right) \qquad (4.62)$$

In a first approximation intermodulation products continue to occur as odd multiples of the switching frequency f_s and ω_s, respectively. However, the even multiples are shifted around the fundamental frequency, causing side band around each of these frequencies, respectively. If we take higher orders in the above approximation into account, further intermodulation products would occur.

5 Control of Permanent Magnet Synchronous Motor in Rotating Coordinates

So far, we have examined the steady-state behavior of the motor. It was, however, not discussed how to ensure that a desired operating state actually appears. This is the task of the control. The control can be a position-, velocity- or speed control. The position and speed control can be set up largely independent of a particular motor in a cascaded structure, where they represent superordinate entities of a torque control. Therefore, latter shall be focused on in the following.

The torque is proportional to the torque-generating current component. Therefore, a torque reference T^* may be converted into a current reference following

$$i_{sq}^* = \frac{2}{3 p \psi_p} T^*$$ (5.1)

The task of the torque control is thus converted into the task of regulating the current.

5.1 Current Control

The task of the current control is to regulate the components of the motor voltage u_{sd}, u_{sq} in a way that the desired current components i_{sd}, i_{sq} are set. The requested value i_{sq}^* results from the torque. The desired value of the d-component is adjusted, if necessary, according to the requirements with respect to flux weakening (see Section 2.10). At first, the voltage control range shall be provided, i.e.

$$i_{sd}^* = 0$$ (5.2)

can be assumed. In order to perform the current control task, the control or actuating variables of the current controller can be considered as voltage references u_{sd}^*, u_{sq}^* for the PWM unit. In return, the PWM unit generates corresponding switching functions (also known as duty cycles) which are applied to the transistors of the inverter.

For simplification, we shall assume in the following, that the requested values are converted into actual values correctly by the PWM and the inverter (in terms of the dynamic State-Space Average modeling), i.e.

$$u_{sd} = u_{sd}^*, \ u_{sq} = u_{sq}^*$$ (5.3)

In a first step, the plant model (that is the system to be controlled) needs to be derived. It is advantageous to do so by means of the current differential equations in rotor-fixed/rotating coordinates (see Section 2.2):

$$L_s \dot{i}_{sq} = u_{sq} - R_s \, i_{sq} - \omega L_s i_{sd} - \omega \psi_p$$

$$L_s \dot{i}_{sd} = u_{sd} - R_s \, i_{sd} + \omega L_s i_{sq}$$ (5.4)

Regarding the control task, we are, thus, dealing with a *coupled system* with two control or actuating variables u_{sd}, u_{sq} and two controlled variables i_{sd}, i_{sq}. The coupling effect can, however, be compensated with the help of a simple voltage feedback and feed-forward control, respectively, according to

$$
\begin{aligned}
u_{sd}^* &= u_{sd}^0 + \Delta u_{sd}^* \\
u_{sq}^* &= u_{sq}^0 + \Delta u_{sq}^*
\end{aligned}
\quad \text{with} \quad
\begin{aligned}
u_{sd}^0 &= -\omega L_s i_{sq} \\
u_{sq}^0 &= \omega L_s i_{sd} + \omega \psi_p
\end{aligned}
\tag{5.5}
$$

In consequence, two decoupled SISO (Single Input Single-Output) plant models are obtained.

$$
\begin{aligned}
L_s \dot{i}_{sd} &= -R_s\, i_{sd} + \Delta u_{sd}^* \\
L_s \dot{i}_{sq} &= -R_s\, i_{sq} + \Delta u_{sq}^*
\end{aligned}
\tag{5.6}
$$

Both represent $P\text{-}T_1$ elements with the transfer function

$$
G_i(s) = \frac{1}{R_s} \frac{1}{1 + s\tau_s}
\tag{5.7}
$$

whereas,

$$
\tau_s = \frac{L_s}{R_s}
\tag{5.8}
$$

represents the *stator time constant*. The remaining control task can now be easily solved, by designing a PI-controller for each of the plant models.

$$
G_{ci}(s) = K_{Pi} \frac{1 + sT_n}{sT_n}
\tag{5.9}
$$
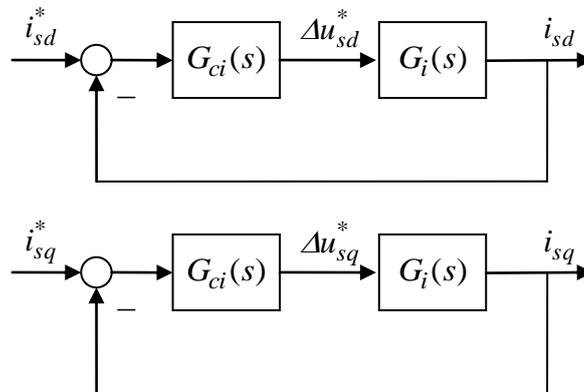
Fig. 5-1: Simplified current control block diagram

This simplified model serves as basis for the design of the controller parameters, i.e. the controller gain K_{Pi} and controller reset time T_n. For the realization of the control scheme, the transformation of the d/q-components into the stator-fixed coordinate system and vice versa, also needs to be regarded, of course.

5.2 Discrete-Time Controller Realization

Quite often, the control design is abstracted from the actual discrete-time control realization on a processor by applying continuous-time design rules and methods (see above). Only after the dimensioning of the control parameters, e.g. integrators are approximated by summing units. In this case, we speak of a *quasi-continuous* design approach. This approach is justified if the typical time constants of the system lie within a certain number of sampling steps. The limitations of this approach are reached at the latest, however, if the control actions are to be executed within only very few sampling steps (such as in deadbeat controls). In such cases, discrete-time design methods must be applied, which shall, not be discussed any further here.

However, even when using a quasi-continuous design approach, the effects of the discrete-time control realization should be taken into account through a total dead-time of one and a half sampling intervals (see Sections 4.4 and 4.5). Although this dead-time results from the controller realization, it can theoretically be added to the plant model as it does not represent a degree of freedom for the controller design:

$$G_{ci}(s) = K_{Pi} \frac{1 + sT_n}{sT_n} e^{-1.5T_a s} \tag{5.10}$$

This dead-time can be recognized not only within each individual control loop for the d-and q-component, but also in the transform into or from the rotor coordinates. If the transformation of the voltage references from the d/q-system into the stator-fixed α/β-system is performed with the currently available rotation angle ε, then after the dead time, the rotor has rotated further by an angle of $1.5T_a\omega$. Depending on the rotational speed ω, an incorrectly oriented voltage would then be applied to the motor. Therefore, during the reverse transformation of the voltage references into the stator-fixed system an angle offset of

$$\Delta\varepsilon = 1.5T_a\omega \tag{5.11}$$

should be taken into account, to ensure a correct voltage orientation. It may be possible to neglect this angle offset, if depending on the speed range of the motor, angular errors of only few degrees result. The integrators in the current controllers will then compensate for these errors. At high speeds and depending on the sampling frequency, however, the angle offset can increase significantly up to two-digit numbers. In this case, it is advisable to explicitly account for this angle offset in the control design.

5.3   Overall Control Structure

The following figure summarizes the previous considerations in a block diagram, also adding a speed controller.
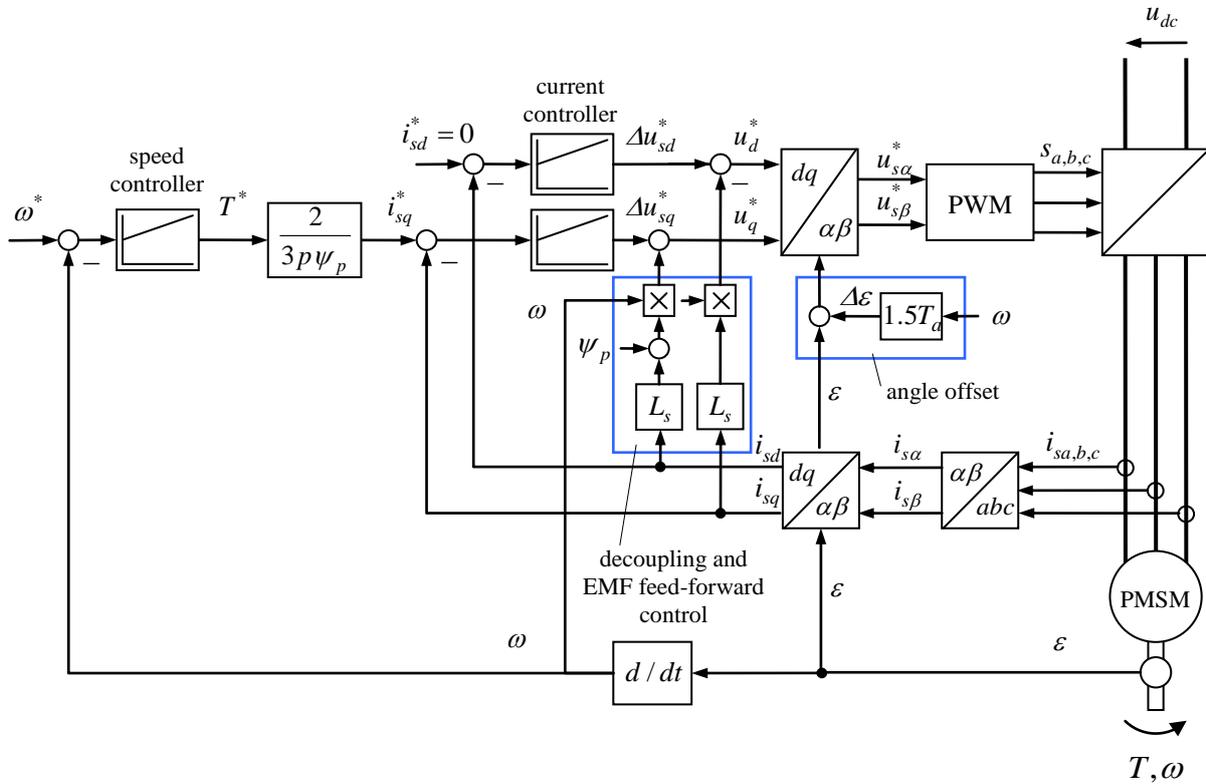
Fig. 5-2: Basic structure of the control loop in rotor-fixed coordinates for the voltage control range (without flux weakening mode)

6 Direct Torque Control (DTC)

6.1 Control Concept

As an alternative to the above described control concept in rotating coordinates with subordinate current controllers and PWM, the *Direct Torque Control* (DTC) shall be discussed in the following.

Once again, the torque equation represents the starting point for the following considerations:

$$T = \frac{3}{2} p \left(\psi_{p\alpha} i_{s\beta} - \psi_{p\beta} i_{s\alpha} \right) = \frac{3}{2} p \, \boldsymbol{\psi}_p \times \boldsymbol{i}_s \tag{6.1}$$

With,

$$\boldsymbol{\psi}_s = L_s \boldsymbol{i}_s + \boldsymbol{\psi}_p \tag{6.2}$$

further equivalent representations for the torque are obtained:

$$T = \frac{3}{2} p \, \boldsymbol{\psi}_p \times \boldsymbol{i}_s = \frac{3}{2} p \left(\boldsymbol{\psi}_s - L_s \boldsymbol{i}_s \right) \times \boldsymbol{i}_s = \frac{3}{2} p \, \boldsymbol{\psi}_s \times \boldsymbol{i}_s \tag{6.3}$$

or

$$T = \frac{3}{2} p \boldsymbol{\psi}_p \times \boldsymbol{i}_s = \frac{3p}{2L_s} \boldsymbol{\psi}_p \times \left(\boldsymbol{\psi}_s - \boldsymbol{\psi}_p \right) = \frac{3p}{2L_s} \boldsymbol{\psi}_p \times \boldsymbol{\psi}_s \tag{6.4}$$

This last representation is the starting point for the DTC method.
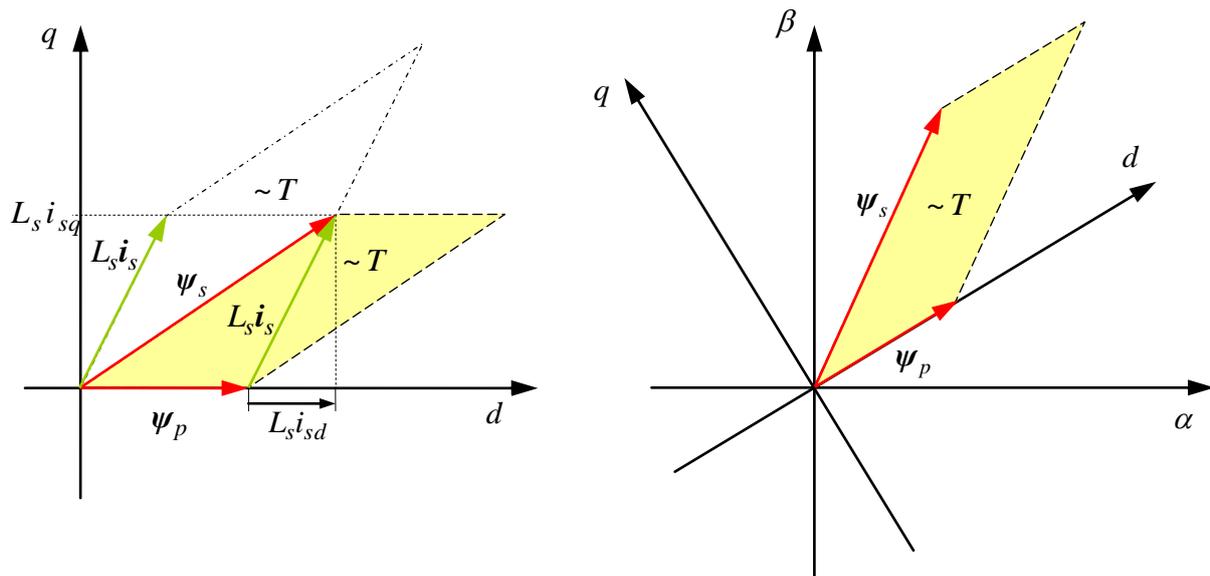
Fig. 6-1: Geometric interpretation of the torque as the cross product between the flux and current or between the flux vectors

The following equation holds:

$$\dot{\psi}_s = u_s - R_s i_s \approx u_s$$

(6.5)

The chosen voltage vector, thus, determines the direction of the flux change. As possible voltage vectors only the fundamental voltages v_k are considered. In the example shown below, vectors v_3, v_4 increase the torque while vectors v_1, v_6 decrease it. Geometrically speaking, this is due to the fact that in the first case the plane of the parallelogram increases, while in the second case it decreases.

If the zero voltage vector v_0, or v_7 is chosen, then the stator flux ψ_s approximately remains in its position. The change in torque then only depends on the movement of the vector of the permanent magnet flux ψ_p, due to the mechanical rotation of the motor. With reference to the below example and assuming a fixed stator flux pointer, the torque would decrease at positive rotations $\dot{\varepsilon} = \omega > 0$ and increase at negative rotations. Apart from the torque, the flux magnitude

$$\psi_s = |\psi_s|$$

increase or decreases, as well, depending on the choice of the voltage vector.
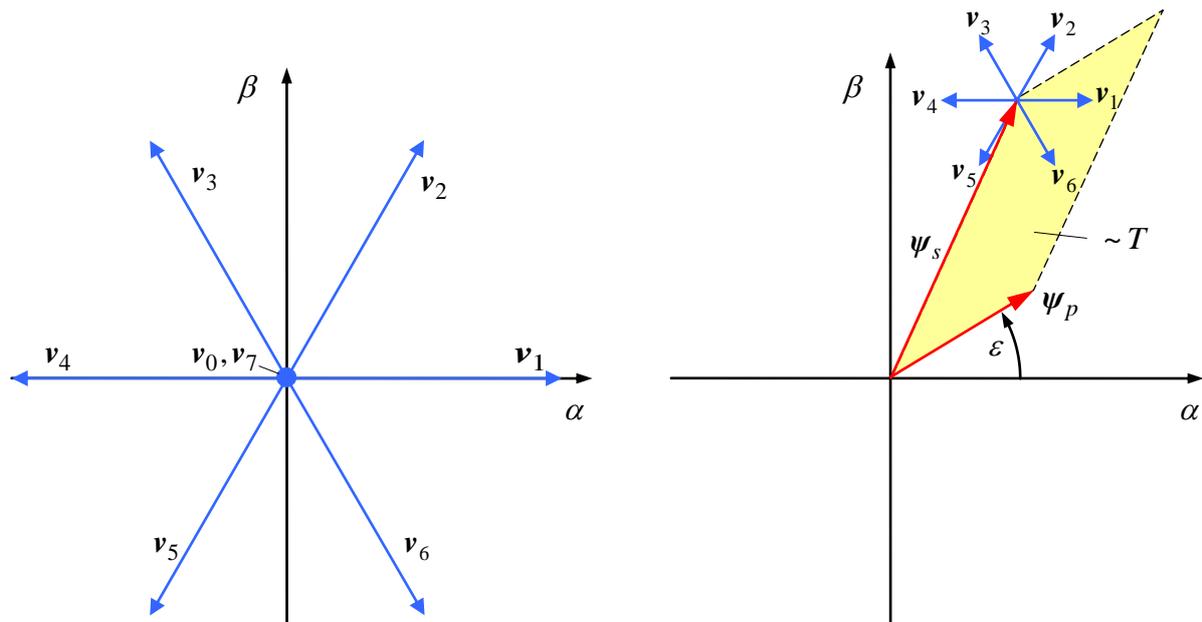
Fig. 6-2: Control concept of the DTC method

Depending on the sector (see figure below, the sector definition used here differs from that of the vector modulation), in which the stator flux vector is currently located, the effects of various voltage vectors on torque and flux are summarized in the following table.
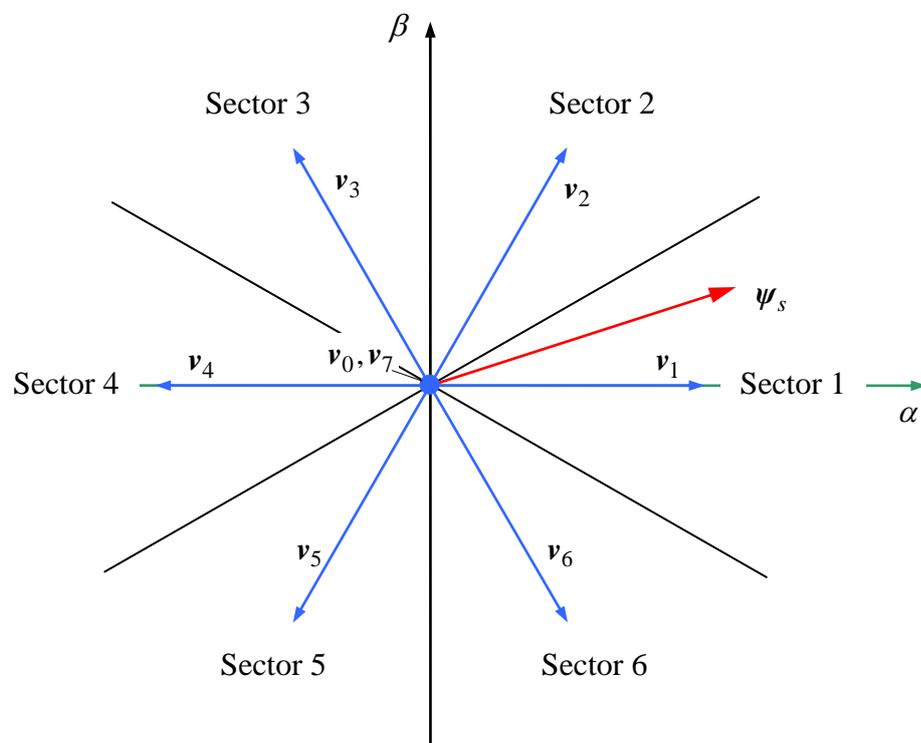
Fig. 6-3: Sector definition for the DTC method

Sector	$\dot{T} > 0$ $\dot{\psi}_s > 0$	$\dot{T} > 0$ $\dot{\psi}_s < 0$	$\dot{T} < 0$ $\dot{\psi}_s > 0$	$\dot{T} < 0$ $\dot{\psi}_s < 0$	$\dot{T} < 0$ if $\omega > 0$ $\dot{T} > 0$ if $\omega < 0$ $\dot{\psi}_s \approx 0$
1	v_2	v_3	v_6	v_5	v_0, v_7
2	v_3	v_4	v_1	v_6	v_0, v_7
3	v_4	v_5	v_2	v_1	v_0, v_7
4	v_5	v_6	v_3	v_2	v_0, v_7
5	v_6	v_1	v_4	v_3	v_0, v_7
6	v_1	v_2	v_5	v_4	v_0, v_7

Torque and flux magnitude are now forced to remain within certain tolerance bands around its reference values with the help of Hysteresis controls. The switching strategy for the torque is as follows: Under the assumption of a positive direction of rotation and torque values too far below the desired reference, an active voltage vector is applied (see table) to increase the torque, in consequence. If the upper threshold of the tolerance band has been reached, the zero voltage vector is applied (last column of the above table), decreasing the torque in positive direction of rotation, accordingly. At the same time, the flux vector remains in its attained position. The flux magnitude cannot be influenced in this state, which is acceptable, as it can be considered during the next choice of the active voltage vector.

This switching strategy requires the permanent knowledge of the direction of rotation, as with respect to the change in torque in the zero voltage state, the relationships exactly invert depending on the direction of rotation. On the other hand, the direction of rotation can be inferred from the behavior of the torque in the zero voltage state: If the torque decreases within the zero voltage state, the direction of rotation must be positive; otherwise, the motor rotates in the negative direction. This can be achieved by modifying the switching strategy, which then relies on three thresholds, as shown in the figure below. An explicit knowledge of the direction of rotation is now no longer necessary.
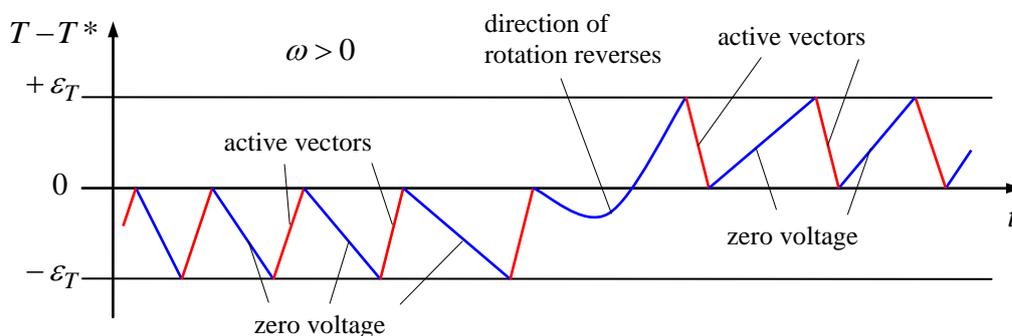
Fig. 6-4: Switching strategy for the torque
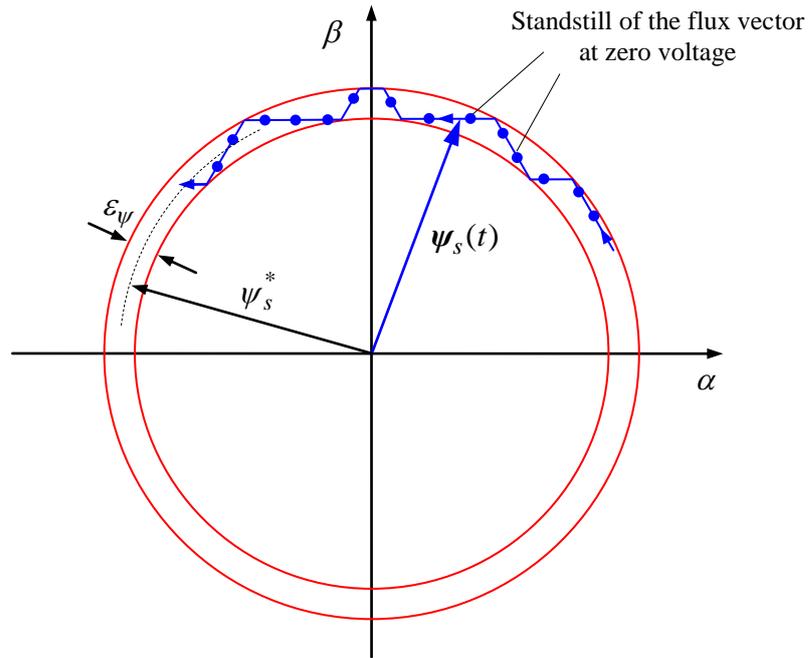
Fig. 6-5: Typical flux trajectory in DTC methods

The resulting control structure is shown in the figure below. Note, that no pulse-width modulation occurs. The switching strategy directly generates the control commands for the inverter.
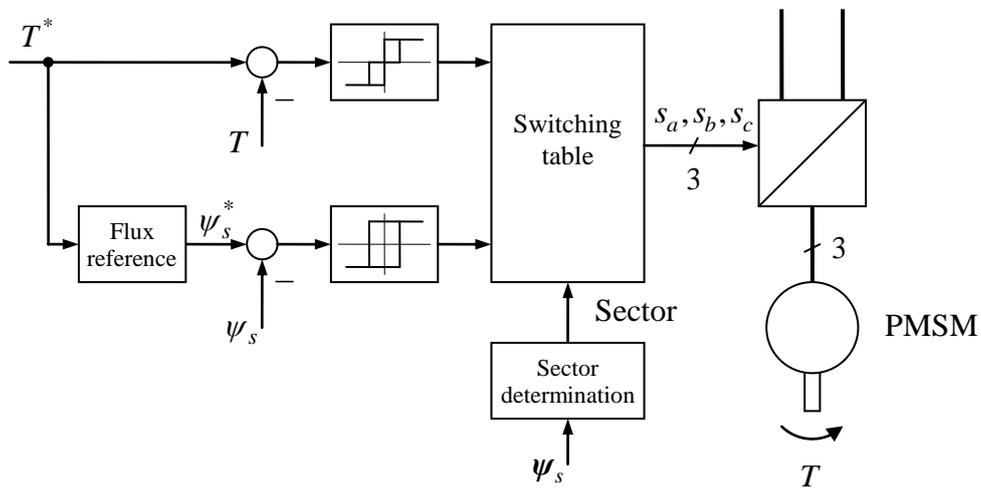
Fig. 6-6: Structure of Direct Torque Control (DTC)

For loss optimal control, the flux reference should be adjusted as a function of the torque. Assuming $i_{sd} = 0$, the flux is given as,

$$\psi_s^2 = \psi_p^2 + L_s^2 i_{sq}^2 = \psi_p^2 + \left(\frac{2L_s T}{3p\psi_p}\right)^2$$

Accordingly, the flux reference should be adjusted depending on the torque reference T^*, as follows:

$$\psi_s^* = \sqrt{\psi_p^2 + \left(\frac{2L_s T^*}{3p\psi_p}\right)^2} \qquad (6.6)$$

When the voltage limit is reached, the flux needs to be reduced, accordingly (flux weakening).

In contrast to PWM, the resulting switching frequency of the DTC method is not exactly defined. In order to limit the switching losses, it may be useful to monitor the switching frequency and adjust the widths of the tolerance bands of the hysteresis controllers, accordingly. This can be accomplished with the help of a simple counter. In terms of control engineering, the counter represents an *I*-controller.
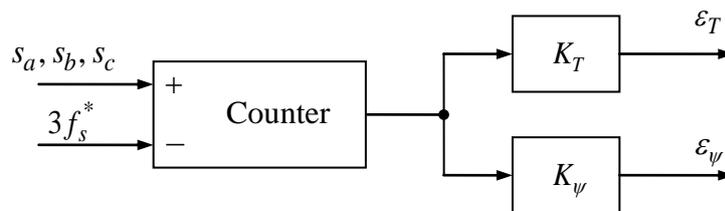
Controlling the switching frequency

6.2 Flux and Torque Observers

The control structure developed in Section 6.1 is not yet complete, because so far we assumed that the stator flux ψ_s and torque T values are known. Although, these quantities are measurable in principle, due to cost reasons, one will usually refrain from doing so by means of sensors in real applications. Instead, they have to be calculated from other available variables. Such an arrangement is referred to as *observer* in control theory.

Measurable quantities are the stator currents i_s and stator voltages u_s. Due to cost reasons, it is desirable to avoid the measurement of the stator voltage, as well. However, one can compute the voltage value from the knowledge of the inverter switching states s_a, s_b, s_c and the DC-link voltage u_{dc}. In this context, the stator voltage shall therefore be regarded as a known variable.

To clearly distinguish in the following between the actual variables x in the technical system and observed or assumed variables, the latter (estimated or observed) variables will be denoted by $\hat{x}$. As measurements can also contain errors, this (hat) denotation will also be applied to measured quantities, as well as assumed machine parameters.

In order to determine the necessary stator flux vector $\boldsymbol{\psi}_s$ for the DTC, the evaluation of the machine equations comes into consideration[5]:

Current Model

By current model, we refer to the equation to determine the stator flux,

$$\hat{\boldsymbol{\psi}}_s = \hat{L}_s \hat{\boldsymbol{i}}_s + \hat{\boldsymbol{\psi}}_p \tag{6.7}$$

or in stator-fixed components,

$$\hat{\psi}_{s\alpha} = \hat{L}_s \hat{i}_{s\alpha} + \hat{\psi}_{p\alpha} = \hat{L}_s \hat{i}_{s\alpha} + \hat{\psi}_p \cos\varepsilon \tag{6.8}$$

$$\hat{\psi}_{s\beta} = \hat{L}_s \hat{i}_{s\beta} + \hat{\psi}_{p\beta} = \hat{L}_s \hat{i}_{s\beta} + \hat{\psi}_p \sin\varepsilon \tag{6.9}$$

It becomes obvious, that apart from the current measurement, the acquisition of the rotation angle also becomes necessary. In addition to that, the machine parameters permanent flux ψ_p and stator inductance L_s need to be known.

With the stator flux determined in this way, the torque can now be estimated via the torque equation

$$\hat{T} = \frac{3p}{2\hat{L}_s} \hat{\boldsymbol{\psi}}_p \times \hat{\boldsymbol{\psi}}_s = \frac{3p\hat{\psi}_p}{2\hat{L}_s} \left(\hat{\psi}_{s\beta} \cos\varepsilon - \hat{\psi}_{s\alpha} \sin\varepsilon \right) \tag{6.10}$$

These equations must then be implemented as an observer to complete the control structure of Section 6.1.

Voltage Model

By voltage model, we refer to the alternative determination of the stator flux via the stator voltage equation

$$\dot{\hat{\boldsymbol{\psi}}}_s = \hat{\boldsymbol{u}}_s - \hat{R}_s \hat{\boldsymbol{i}}_s \tag{6.11}$$

---

[5] Apart from the direct replication of the system equations, the concepts *Luenberger observer* and *Kalman filter* are also known from control theory. These concepts, as well, can be applied to this problem. In the course of these lecture notes, these concepts will, however, not be further discussed.

The voltage must therefore be integrated to obtain the flux:

$$\hat{\boldsymbol{\psi}}_s(t) = \int_{t_0}^{t} \left(\hat{\boldsymbol{u}}_s(\tau) - \hat{R}_s \hat{\boldsymbol{i}}_s(\tau) \right) d\tau + \hat{\boldsymbol{\psi}}_{s0} \tag{6.12}$$

The advantages are obvious: Only the stator resistance is required as machine parameter. The rotation angle is not a necessary measurement. In the remaining DTC control structure, as well, the rotation angle is not necessary, as no transformation into a rotating coordinate system is performed. We can therefore completely abandon the use of a rotary encoder. This case is referred to as *sensorless control*. Those types of control schemes are highly appreciated not only for cost but also robustness reasons (encoder failures, wire break) and constructive degrees of freedom.

The mentioned advantages are countered by a number of disadvantages to be faced: On the one hand, the initial value of the flux $\hat{\boldsymbol{\psi}}_{s0}$ is unknown in most cases. On the other hand, the observer is mainly represented by a simple integrator, which is characterized as a simple stable system in control theory. Specifically this means that a potential offset error in the voltage determination,

$$\hat{\boldsymbol{u}}_s = \boldsymbol{u}_s + \Delta \boldsymbol{u}_s \tag{6.13}$$

no matter how small it is, lead to an arbitrarily large flux error after a sufficiently long time

$$\Delta \boldsymbol{\psi}_s(t) = (t - t_0)\, \Delta \boldsymbol{u}_s \tag{6.14}$$

In this form, the strategy is of no practical use. For this reason, the original differential equation is modified by means of a stabilizing feedback term:

$$\dot{\hat{\boldsymbol{\psi}}}_s = \hat{\boldsymbol{u}}_s - \hat{R}_s \hat{\boldsymbol{i}}_s - \frac{1}{\tau_B} \hat{\boldsymbol{\psi}}_s \tag{6.15}$$

The system with the input $\hat{\boldsymbol{e}}_s = \hat{\boldsymbol{u}}_s - \hat{R}_s \hat{\boldsymbol{i}}_s$ and the output $\hat{\boldsymbol{\psi}}_s$ is now stable, which can be best seen in the Laplace domain:

$$s\hat{\boldsymbol{\psi}}_s(s) = \hat{\boldsymbol{u}}_s(s) - \hat{R}_s \hat{\boldsymbol{i}}_s(s) - \frac{1}{\tau_B} \hat{\boldsymbol{\psi}}_s(s)$$

$$\hat{\boldsymbol{\psi}}_s(s) = \frac{1}{s + 1/\tau_B} \left[\hat{\boldsymbol{u}}_s(s) - \hat{R}_s \hat{\boldsymbol{i}}_s(s) \right] = \frac{1}{s + 1/\tau_B} \hat{\boldsymbol{e}}_s \tag{6.16}$$

The observer pole is now at $s = -1/\tau_B$; the system is exponentially stable. A voltage offset error then only causes a limited stationary flux error

$$\Delta\boldsymbol{\psi}_s = \tau_B \Delta\boldsymbol{u}_s \tag{6.17}$$

Looking at this equation, it seems reasonable to choose the time constant τ_B as small as possible, in order to achieve the smallest possible flux error as a result of a voltage offset. Moreover, the (step) response to the in most cases incorrect initial observer value $\hat{\boldsymbol{\psi}}_{s0}$ decays with the time constant τ_B.

One should not overlook, that the additional introduced feedback distorts the original system behavior. Assuming the measurements is accurate, i.e. $\hat{\boldsymbol{u}}_s = \boldsymbol{u}_s, \hat{\boldsymbol{i}}_s = \boldsymbol{i}_s$ an estimation error of

$$\hat{\boldsymbol{\psi}}_s(s) - \boldsymbol{\psi}_s(s) = \left[\frac{1}{s+1/\tau_B} - \frac{1}{s} \right] \left[\boldsymbol{u}_s(s) - R_s\boldsymbol{i}_s(s) \right] = \left[\frac{1}{s+1/\tau_B} - \frac{1}{s} \right] \boldsymbol{e}_s \tag{6.18}$$

would result. In the frequency range $\omega > 1/\tau_B$, the error can be neglected, due to

$$\frac{1}{j\omega+1/\tau_B} \approx \frac{1}{j\omega}$$

On the other hand, for decreasing frequencies below $\omega < 1/\tau_B$, the error becomes increasingly large and the flux estimation useless, in consequence. After this consideration, τ_B should therefore be chosen as large as possible to obtain a preferably large usable frequencies range. This directly reflects the possible speed range in which such an observer works reliably: For standstill and frequencies $\omega_{rs} < 1/\tau_B$, the observer does not work properly. Only at a minimum speed of $\omega_{rs} > 1/\tau_B$ this observer can be used.

For achieving both design objectives, a trade-off has to be made. In fact, in the practical implementation, lots of efforts are made to achieve small voltage errors and to thus allow large values of τ_B. For this purpose, it is usually not sufficient to model the inverter only by its ideal switching behavior, but both the transient switching behavior and the forward voltage drops must be considered.

In the context of DTC in the literature, the voltage model often serves as the basis for the observer design and is even presented as an inherent part of it. There is, however, no reason for that. The DTC principle can very well be combined with the current model as an observer, as well. Compared to the voltage model, the drawback lies in the necessity to measure the rotor position. On the other hand, the current model observer can then be used within the entire frequency range – even at standstill.

7 Protective Measures

The operation of an electric drive generally requires measures for monitoring operation, to detect unacceptable operating conditions and to safely shut down the system, in consequence. Variables to be monitored are, for example:

- Motor and inverter output currents
- Supply voltage (DC input voltage)
- Motor temperature
- Converter temperature
- Rotor speed

The protective measures are aiming at protecting the system against damage or in case of a component damage which has already occurred (e.g. a defect capacitor or transistor) to minimize the spread of the damage to other components and to avoid endangering people. As a rule of thumb one can say, that protective measures are becoming more complex as the drive size increases. With larger drives, it is crucial to consider during the design phase, how they can be protected (e.g. extinguishing electric arcs). In micro drives, the ohmic resistance of the motor may already limit the current sufficiently and thus dispense with the need for further measures.

Protective measures should be implemented on a control level independent of the motor control, itself. The reason is that the processor responsible for the motor control is often too slow for time-critical operations and could, thus, even be the cause of a fault, itself. In the ideal case, protective measures are designed in a way that they can autonomously and safely shut down the system, completely independent of a functioning motor control (*fail safe*).

In particular, the monitoring of the inverter output and motor currents represent the most time-critical requirements. Since the thermal time constants of the junctions of the power semiconductors are extremely short, an overstepping of the permissible limits by only a few milliseconds can already lead to the destruction of the device. Moreover, in case of a short-circuit (due to control errors or damage of other components) the application of unwanted voltages can lead to rapidly increasing inverter currents in a way that within only a few microseconds the current flow cannot be interrupted anymore. On the other hand, since operational limits are to be exploited as far as possible due to economic reasons, the distance between operationally permissible maximum currents and unsafe over- or excess currents is often quite small. Therefore, a safety shutdown in this field must respond very quickly. By the way, excess currents occasionally also occur as random fluctuations as a result of never completely avoidable disturbances in the control loop.

In the following, possible measures for responding to excess currents are being discussed.

7.1   Pulse Blocking or Motor Short-Circuiting

The commonly used protective measure when dealing with excess currents is to block all the transistors of the bridge (*pulse blocking*). Due to the inductive behavior of the load, the motor current initially flows through the diodes in a bridge. But if the input DC voltage is greater than the induced motor voltage then this voltage difference counteracts the current flow forcing the motor current to quickly extinct (usually within a few milliseconds). This is the commonly applied protective measure, for example, in induction motors, see Section 4.6.

If a permanent magnet synchronous motor is operated at a speed range where the main voltage is smaller than the input DC voltage, $\omega \psi_p < u_{dc} / \sqrt{3}$, the current will also extinct. In contrast, if the motor is operated in the flux weakening range, $\omega \psi_p > u_{dc} / \sqrt{3}$, the induced voltage will feed current across the diode bridge back to the DC side. The entire motor voltage (consisting of main voltage and armature reactions) is still determined by the DC link capacitor, which more or less quickly charges, as long as the power on the DC side is not discharged by other means (i.e. feed back into the power supply or dissipation in a braking unit). In cases, where the occurring braking effect slows down the drive and the induced voltage drops below the critical value, in consequence, a limited increase in voltage may be tolerated. An estimation can be accomplished in this context by comparing the dominant kinetic energy of the drive to the storage capacity of the capacitor.

For drives where the load keeps on rotating the drive even after the fault case occurs and the drive cannot or should not be stopped, this measure is not acceptable. It is then conceivable to separate the motor from the inverter through a switch. However, this measure is associated with relatively high costs.

An alternative is to short circuit the motor by applying voltages to either all three bottom or upper transistors of the bridge. The short-circuit as a protective measure requests the inverter to be fully functional. If this is not guaranteed, problems occur: If the malfunction was caused by the failure of an inverter valve, a forced motor short-circuit could as well result in a bridge short-circuit which might destroy the inverter, irreversibly. A motor short-circuit can also not be considered, if the energy supply of the inverter control and therefore its operational functionality cannot be guaranteed.

Therefore, the behavior of permanent magnet synchronous motors in case of short-circuits shall be investigated, in the following.

7.2   Steady State Short-Circuit Currents

If the motor is shorted symmetrically (i.e. with all three terminals at the same time) and after the decay of transients, the steady-state voltage equations

$$0 = R_s\, i_{sd} - \omega L_s i_{sq}$$

$$0 = R_s\, i_{sq} + \omega L_s i_{sd} + \omega \psi_p$$

and the steady-state short-circuit currents as a function of the rotational frequency

$$i_{sdk} = -\frac{\omega^2 L_s \psi_p}{\omega^2 L_s^2 + R_s^2} = -i_0 \frac{\omega^2 \tau_s^2}{1 + \omega^2 \tau_s^2} \tag{7.1}$$

$$i_{sqk} = -\frac{\omega R_s \psi_p}{\omega^2 L_s^2 + R_s^2} = -i_0 \frac{\omega \tau_s}{1 + \omega^2 \tau_s^2} \tag{7.2}$$

$$i_{sk} = \sqrt{i_{dk}^2 + i_{qk}^2} = i_0 \frac{\omega \tau_s}{\sqrt{1 + \omega^2 \tau_s^2}} \tag{7.3}$$

with,

$$i_0 = \frac{\psi_p}{L_s} \quad , \quad \tau_s = \frac{L_s}{R_s} \tag{7.4}$$

result. Based on these equations, the steady-state short-circuit torque

$$T_k = -\frac{3p\,\psi_p i_0}{2} \frac{1}{\omega \tau_s + \frac{1}{\omega \tau_s}} = -\frac{3p\,\psi_p i_0}{2} \frac{\omega \tau_s}{1 + \omega^2 \tau_s^2} \tag{7.5}$$

results. For a sufficiently large rotational frequency $\omega \tau_s \gg 1$, the steady-state short circuit current can be estimated through the speed-independent value i_0.
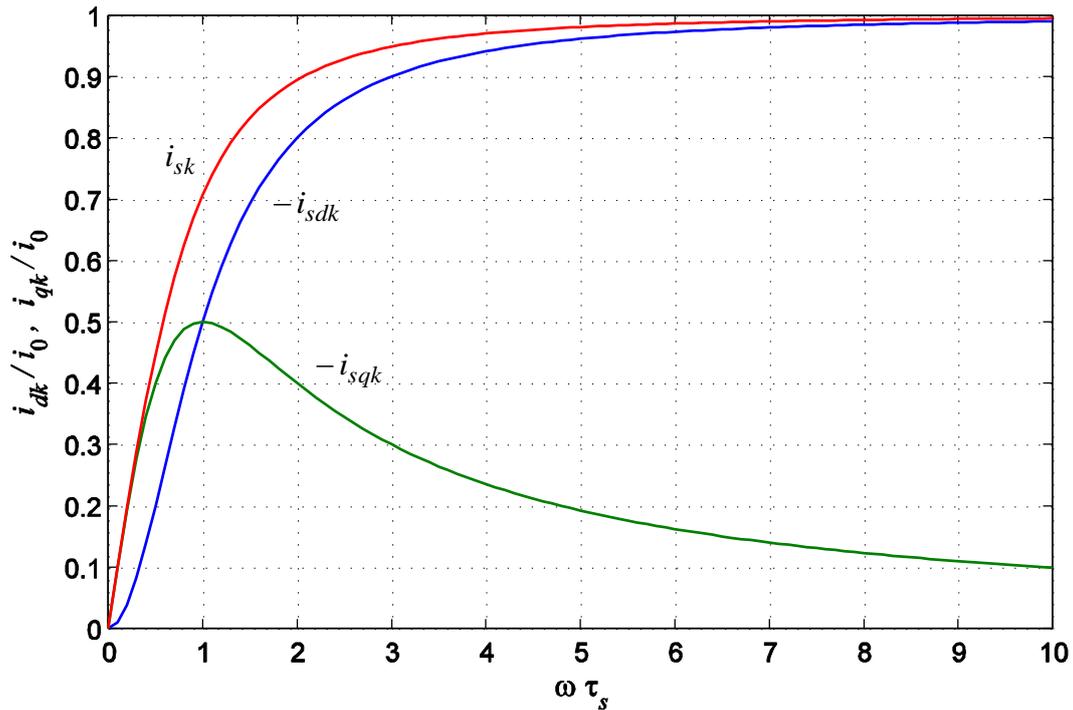
Fig. 7-1: Steady state short-circuit current vs. speed

The motor short-circuit can therefore only be considered if the drive is capable of conducting the steady-state short circuit current, i.e.

$$i_{sk}(\omega) < i_{max}$$

If the drive is operated at high speeds, $\omega\tau_s \gg 1$, the condition

$$i_0 < i_{max} \quad \text{and} \quad k < 1$$

must hold in the limit case. For such motors, the motor short-circuit can be considered as a protective measure. On the other hand, motors with $k > 1$ cannot or only to a very limited extent be flux weakened, anyways, making pulse block to a very suitable protective measure.

7.3   Transient Short-Circuit Currents

Apart from the steady-state short circuit currents, the transient behavior is investigated. The peaks of the transient short-circuit currents can significantly exceed the steady-state values. Starting point are the current differential equations for the shorted motor:

$$L_s\dot{i}_{sd} = -R_s\,i_{sd} + \omega L_s i_{sq} \tag{7.6}$$

$$L_s\dot{i}_{sq} = -R_s\,i_{sq} - \omega L_s i_{sd} - \omega\psi_p \tag{7.7}$$

A particular solution of this differential equation is already known and represented by the steady-state short-circuit currents of the previous section. It is therefore sufficient to only consider the homogeneous differential equations

$$L_s \dot{i}_{dh} = -R_s \, i_{dh} + \omega L_s i_{qh} \tag{7.8}$$

$$L_s \dot{i}_{qh} = -R_s \, i_{qh} - \omega L_s i_{dh} \tag{7.9}$$

and

$$\dot{i}_{dh} = -\frac{1}{\tau_s} i_{dh} + \omega i_{qh} \tag{7.10}$$

$$\dot{i}_{qh} = -\frac{1}{\tau_s} i_{qh} - \omega i_{dh} \,, \tag{7.11}$$

respectively. The homogeneous solution leads to a with the frequency ω oscillating and with the time constant τ_s decaying process:

$$i_{dh}(t) = e^{-t/\tau_s} \left(i_{dh0} \cos \omega t + i_{qh0} \sin \omega t \right) \tag{7.12}$$

$$i_{qh}(t) = e^{-t/\tau_s} \left(i_{qh0} \cos \omega t - i_{dh0} \sin \omega t \right) \tag{7.13}$$

In the *d/q*-plane, the solution is represented by a spiral trajectory around the origin. Superimposing the steady-state solution, the center of the spiral is shifted to the point (i_{sdk}, i_{sqk}). The initial values of this homogeneous solution result from the current components at the beginning of the short-circuit and the steady-state short-circuit currents according to

$$i_{dh0} = i_{sd0} - i_{dk} \tag{7.14}$$

$$i_{qh0} = i_{sq0} - i_{qk} \tag{7.15}$$

For estimating the maximum peak value a high rotor speed is assumed, keeping the damping effect within a single period at a low level. If now, a short-circuit occurs out of a state of maximum current,

$$i_{sd0} = 0, \quad |i_{sq0}| = i_{\max} \,,$$

i.e.

$$i_{qh0} = i_{sq0} - i_{qk} \approx \pm i_{max} \tag{7.16}$$

$$i_{dh0} = i_{sd0} - i_{dk} \approx -i_0 \tag{7.17}$$

a vector length for the homogeneous component of about $\sqrt{i_{max}^2 + i_0^2}$ results. When this vector is eventually oriented towards the negative d-direction, an estimation of the transient current peak can be obtained.

$$\hat{i}_s < i_0 + \sqrt{i_{max}^2 + i_0^2} = i_{max}\left(k + \sqrt{1 + k^2} \right) \tag{7.18}$$

Even larger peaks would result for initial values $i_{sd0} > 0$. As these values do not represent reasonable operating points, however, they remain ignored.

The above peak power estimation is obtained asymptotically for very large speeds and may lead to very large peak currents. Depending on the actually used speed range and stator time constant, the values can be lower, though.

Whether the drive will survive this transient overstepping of the current limit, cannot be answered in general, but must be examined in each particular case. On the one hand, this overstepping will decay in most cases after only a few milliseconds. On the other hand, the transistors are no longer pulsed after applying the short circuit, causing switching losses to completely disappear. In consequence, higher short-term conduction losses can possibly be tolerated.

Another alternative would be, depending on the rotational frequency, to either apply the pulse-block or the motor short-circuit as protective measure. In the flux weakening range small transient current peaks would then occur, as they originate from more favorable initial values in the left half of the current limit circle. For this staggered measure, however, the availability of the rotational frequency is required. If a simultaneous goal is to protect oneself against sensor failures, then this approach is therefore questionable.
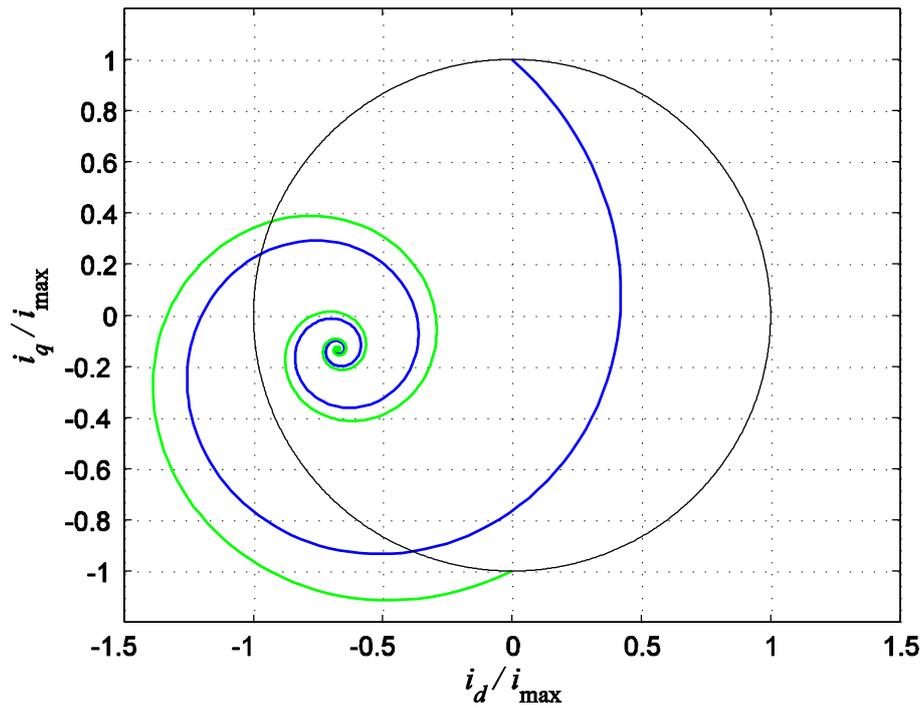
Fig. 7-2: Exemplary trajectories of short-circuit currents for
$\omega\tau_s = 5$, $k = 0.7$ and two different initial values
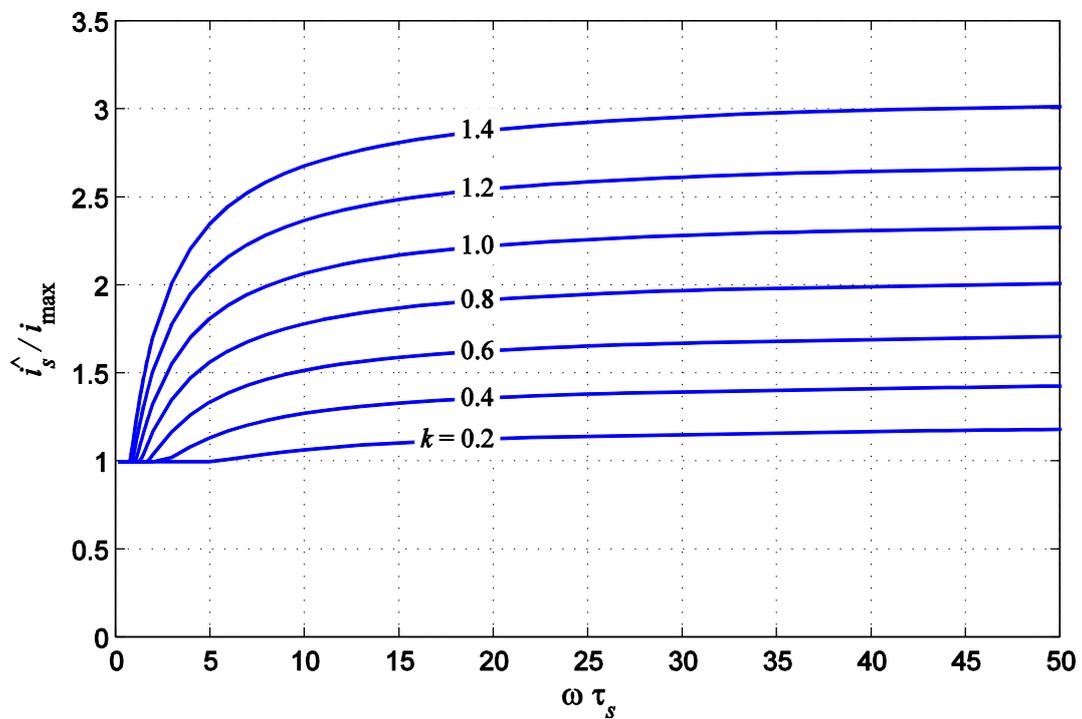
Fig. 7-3: Maximum transient short-circuit current peak as a function of k and $\omega\tau_s$

8   Induction Motor

8.1   Modeling with Orthogonal Windings

Modeling of the stator and rotor with orthogonal windings:
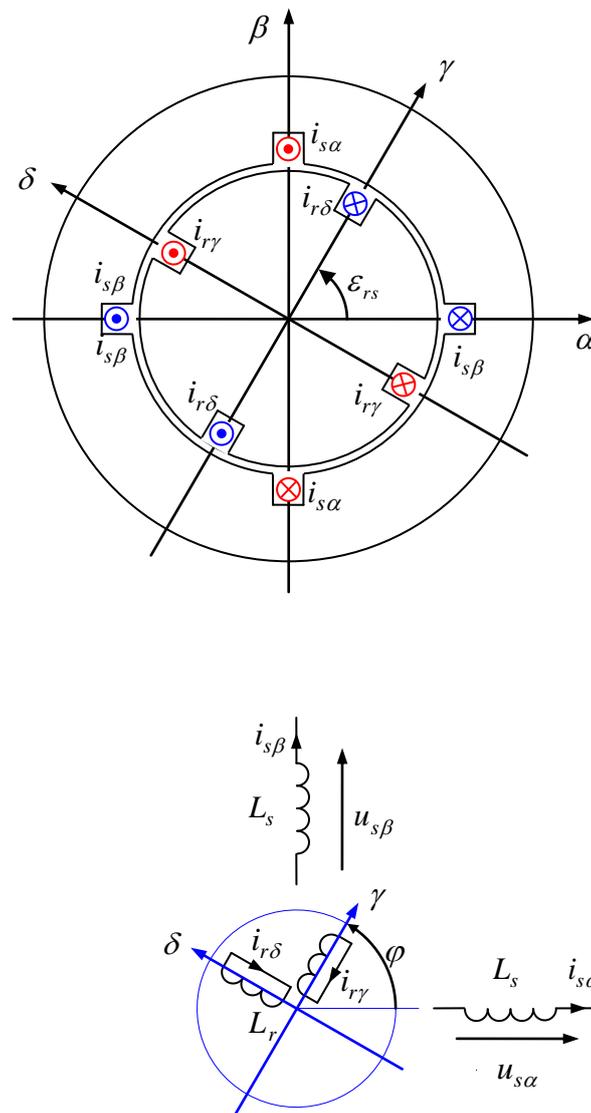
Fig. 8-1: Simplified model of induction motor with squirrel cage rotor

α / β: stator-fixed coordinates

γ / δ: rotor-fixed coordinates (for the rotor coordinate system, the *d/q* notation is not used, since these terms are needed for another coordinate system later)

Faraday's induction law for stator and rotor also considering ohmic resistances:

$$\dot{\boldsymbol{\psi}}_s^s = \boldsymbol{u}_s^s - R_s \boldsymbol{i}_s^s \tag{8.1}$$

$$\dot{\boldsymbol{\psi}}_r^r = \boldsymbol{u}_r^r - R_r \boldsymbol{i}_r^r = -R_r \boldsymbol{i}_r^r \tag{8.2}$$

The superscript should make clear, in which coordinate system the vector is represented. For a random vector $\boldsymbol{x}$ it therefore follows,

$$\boldsymbol{x}^s = \begin{bmatrix} x_\alpha \\ x_\beta \end{bmatrix} \quad \text{und} \quad \boldsymbol{x}^r = \begin{bmatrix} x_\gamma \\ x_\delta \end{bmatrix}$$

As usual, the different representations can be transformed into each other via the rotational transformation,

$$\boldsymbol{Q}(\varepsilon) = \begin{bmatrix} \cos \varepsilon & -\sin \varepsilon \\ \sin \varepsilon & \cos \varepsilon \end{bmatrix}$$

$$\boldsymbol{x}^s = \boldsymbol{Q}(\varepsilon_{rs}) \, \boldsymbol{x}^r \tag{8.3}$$

For example, the stator flux can be represented in the rotor coordinate system: $\boldsymbol{\psi}_s^r$

So far, two-dimensional real-valued vectors were used for modeling the processes. For the induction motor, however, the complex notation has certain advantages. The two coordinates of a vector are then converted into a complex vector:

$$\underline{x}^s(t) = x_\alpha(t) + j x_\beta(t) \tag{8.4}$$

The rotational transformation is then very simply performed by multiplication with the exponential function:

$$\underline{x}^r(t) = e^{-j\varepsilon_{rs}(t)} \underline{x}^s(t) \,, \quad \underline{x}^s(t) = e^{j\varepsilon_{rs}(t)} \underline{x}^r(t) \tag{8.5}$$

For the transformation of the time derivatives, it follows:

$$\dot{\underline{x}}^r(t) = -j\omega_{rs} e^{-j\varepsilon_{rs}(t)} \underline{x}^s(t) + e^{-j\varepsilon_{rs}(t)} \dot{\underline{x}}^s(t)$$
$$\dot{\underline{x}}^r(t) = -j\omega_{rs} \underline{x}^r(t) + e^{-j\varepsilon_{rs}(t)} \dot{\underline{x}}^s(t) \tag{8.6}$$

Similarly,

$$\dot{\underline{x}}^s(t) = j\omega_{rs} \underline{x}^s(t) + e^{j\varepsilon_{rs}(t)} \dot{\underline{x}}^r(t) \tag{8.7}$$

The most important equations are once again summarized in Section 9.

In complex notation, the voltage equations are completely analogous to the vector form

$$\dot{\underline{\psi}}_s^s = \underline{u}_s^s - R_s \underline{i}_s^s \tag{8.8}$$

$$\dot{\underline{\psi}}_r^r = \underline{u}_r^r - R_r \underline{i}_r^r = -R_r \underline{i}_r^r \tag{8.9}$$

If the differential equation for the rotor flux is transformed into the stator system, it follows

$$\dot{\underline{\psi}}_r^s = j\omega_{rs}\underline{\psi}_r^s - R_r \underline{i}_r^s \tag{8.10}$$

Similarly, the differential equation for the stator flux can be transformed into the rotor system:

$$\dot{\underline{\psi}}_s^r = -j\omega_{rs}\underline{\psi}_s^r + \underline{u}_s^r - R_s \underline{i}_s^r \tag{8.11}$$

Instead of writing down the equations in the stator or rotor coordinate system, it may be useful to use another random coordinate system K, which is rotated against the stator by an angle ε_{ks} and against the rotor by an angle $\varepsilon_{kr} = \varepsilon_{ks} - \varepsilon_{rs}$. The axes of the coordinate system K are denoted d and q. The actual meaning of these denotations remains to be seen, though.
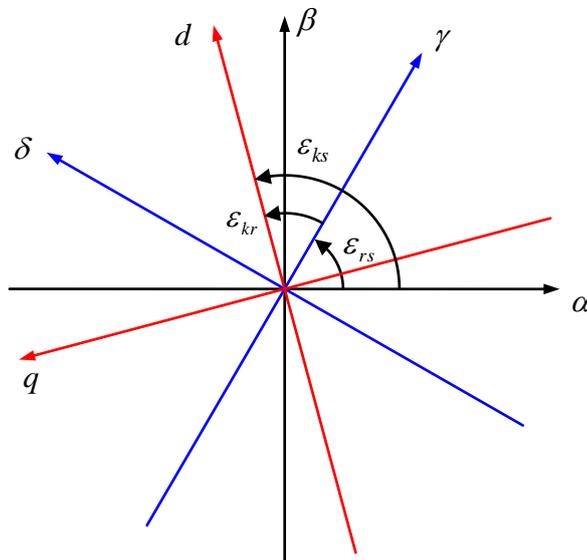
Fig. 8-2: In this coordinate system, the two flux differential equations can now be written as

$$\dot{\underline{\psi}}_s^k = j\omega_{sk}\underline{\psi}_s^k + \underline{u}_s^k - R_s \underline{i}_s^k \tag{8.12}$$

$$\dot{\underline{\psi}}_r^k = j\omega_{rk}\underline{\psi}_r^k - R_r \underline{i}_r^k \tag{8.13}$$

In addition to the differential equations, the relations between the currents and fluxes are required. In principle, the induction motor can be regarded as a transformer. Due to symmetry reasons, we may assume that the orthogonal components do not influence each other and that the inductances are independent of the spatial direction. This leads to

$$\underline{\psi}_s = L_s \underline{i}_s + L_m \underline{i}_r \tag{8.14}$$

$$\underline{\psi}_r = L_m \underline{i}_s + L_r \underline{i}_r \tag{8.15}$$

L_s : Stator-self inductance

L_r : Rotor-self inductance

L_m : Mutual inductance; due to principle reasons, the mutual inductance is the same in both
   equations

In the above equations, the superscripts are omitted, because the equations are valid in every reference system. However, all complex vectors of an equation have to be presented in the very same reference system.
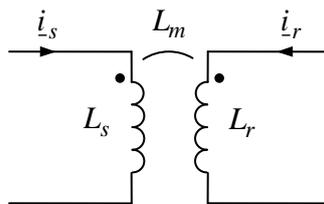
Fig. 8-3: Coupling between stator and rotor windings
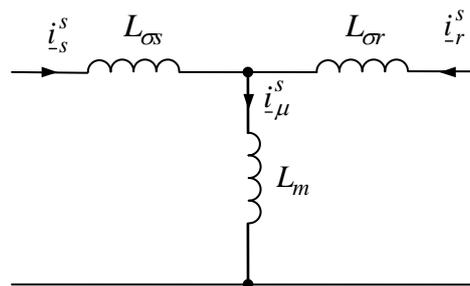
Fig. 8-4: T-equivalent circuit of the transformer coupling

Introduction of *leakage inductances*

$$L_{\sigma s} = L_s - L_m \tag{8.16}$$

$$L_{\sigma r} = L_r - L_m \tag{8.17}$$

and the *leakage coefficients*

$$\sigma = \frac{L_s L_r - L_m^2}{L_s L_r} = 1 - \frac{L_m^2}{L_s L_r} = \frac{L_m(L_{\sigma s} + L_{\sigma r}) + L_{\sigma s} L_{\sigma r}}{L_s L_r} \tag{8.18}$$

It follows:

$$\underline{\psi}_s = L_{\sigma s} \underline{i}_s + L_m(\underline{i}_s + \underline{i}_r) \tag{8.19}$$

$$\underline{\psi}_r = L_{\sigma r} \underline{i}_r + L_m(\underline{i}_s + \underline{i}_r) \tag{8.20}$$

The portions

$$\underline{\psi}_{\sigma s} = L_{\sigma s} \underline{i}_s \ , \quad \underline{\psi}_{\sigma r} = L_{\sigma r} \underline{i}_r \tag{8.21}$$

are the *leakage fluxes,* while

$$\underline{\psi}_m = L_m(\underline{i}_s + \underline{i}_r) \tag{8.22}$$

is the *mutual flux*. The sum of stator and rotor current

$$\underline{i}_\mu = \underline{i}_s + \underline{i}_r \tag{8.23}$$

is also called *magnetizing current*, as this current is responsible for the magnetization of the mutual inductance.
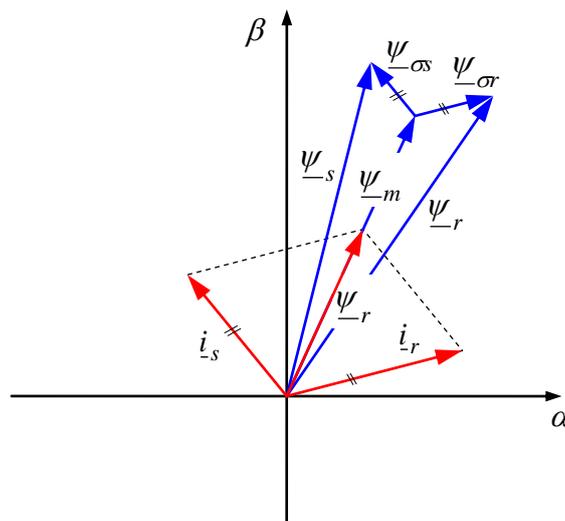
Fig. 8-5: Vector diagram of currents and fluxes

Solving the flux equations for the currents leads to

$$i_s = \frac{L_r \underline{\psi}_s - L_m \underline{\psi}_r}{L_s L_r - L_m^2} \tag{8.24}$$

$$i_r = \frac{L_s \underline{\psi}_r - L_m \underline{\psi}_s}{L_s L_r - L_m^2} \tag{8.25}$$

Inserting the leakage coefficients, it follows

$$i_s = \frac{1}{\sigma L_s}\left[\underline{\psi}_s - \frac{L_m}{L_r}\underline{\psi}_r\right] \tag{8.26}$$

$$i_r = \frac{1}{\sigma L_r}\left[\underline{\psi}_r - \frac{L_m}{L_s}\underline{\psi}_s\right] \tag{8.27}$$

The above developed equations result in the following equivalent circuit diagrams. Please note, that due to the complex notation, the equivalent circuits are applicable for two spatial axes, respectively. The equivalent circuits describe the steady-state as well as the dynamic behavior in general. Due to the arrangement of the mutual and leakage inductances, we refer to this group of circuit diagrams as a T-equivalent circuit diagrams.
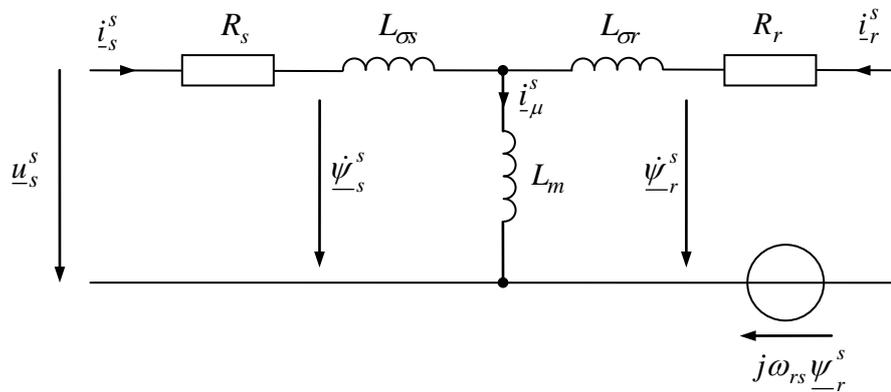
Fig. 8-6: Equivalent circuit diagram of the induction motor in the stator coordinate system
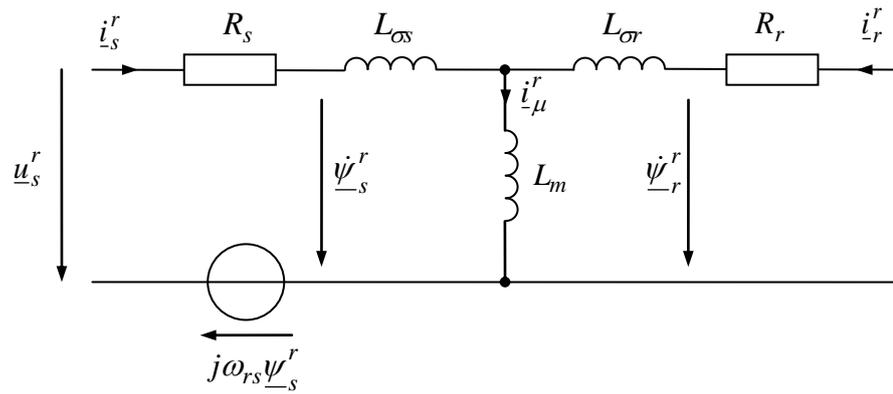
Fig. 8-7: Equivalent circuit diagram of the induction motor in the rotor coordinate system
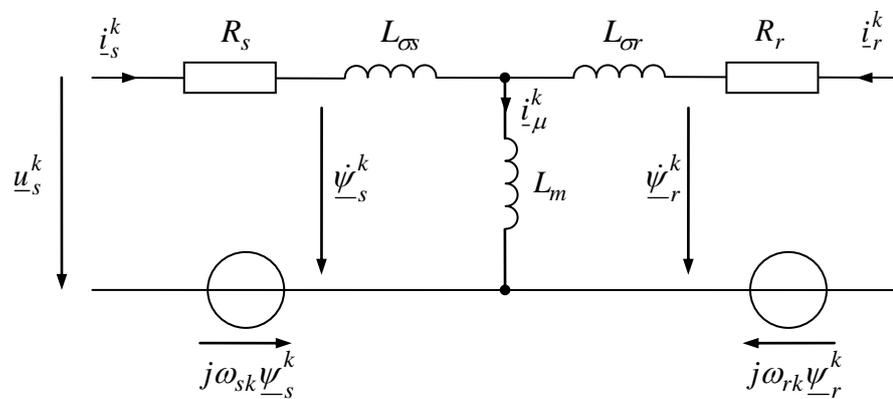
Fig. 8-8: Equivalent circuit diagram of the induction motor in random K coordinate system

8.2 Torque Generation

The torque of an induction motor can again be identified from the power balance. Starting point are, for example, the voltage equations in rotor coordinates (any other reference system could be used as well):

$$\underline{u}_s^r = \underline{\dot{\psi}}_s^r + j\omega_{rs}\underline{\psi}_s^r + R_r\underline{i}_s^r$$

$$0 = \underline{u}_r^r = \underline{\dot{\psi}}_r^r + R_r\underline{i}_r^r$$

In order to calculate the power terms, the equations are multiplied with the conjugated complex currents, respectively (see Section 8.6).

$$\underline{u}_s^r\underline{\bar{i}}_s^r = \underline{\dot{\psi}}_s^r\underline{\bar{i}}_s^r + j\omega_{rs}\underline{\psi}_s^r\underline{\bar{i}}_s^r + R_s\underline{i}_s^r\underline{\bar{i}}_s^r$$

$$0 = \underline{\dot{\psi}}_r^r\underline{\bar{i}}_r^r + R_r\underline{i}_r^r\underline{\bar{i}}_r^r$$

As all terms appearing in these equations are invariant with respect to the choice of the reference system, the superscript labeling of the reference system may be omitted:

$$\underline{u}_s\underline{\bar{i}}_s = \underline{\dot{\psi}}_s\underline{\bar{i}}_s + j\omega_{rs}\underline{\psi}_r\underline{\bar{i}}_r + R_s\underline{i}_s\underline{\bar{i}}_s$$

$$0 = \underline{\dot{\psi}}_r\underline{\bar{i}}_r + R_r\underline{i}_r\underline{\bar{i}}_r$$

The summation of the real parts in the equations and the identification of the individual terms leads to

$$P_{el} = \dot{W}_{magn} + P_d + P_{mech} \tag{8.28}$$

with the supplied electrical power

$$P_{el} = \frac{3}{2}\operatorname{Re}\left(\underline{u}_s\underline{\bar{i}}_s\right) \tag{8.29}$$

the dissipated power (power loss)

$$P_d = \frac{3}{2}\operatorname{Re}\left(R_s\underline{i}_s\underline{\bar{i}}_s + R_r\underline{i}_r\underline{\bar{i}}_r\right) = \frac{3}{2}\left(R_s\left|\underline{i}_s\right|^2 + R_r\left|\underline{i}_r\right|^2\right) \tag{8.30}$$

and the alteration of the magnetic energy

$$\dot{W}_{magn} = \frac{3}{2}\operatorname{Re}\left(\underline{\dot{\psi}}_s\underline{\bar{i}}_s + \underline{\dot{\psi}}_r\underline{\bar{i}}_r\right) \tag{8.31}$$

Moreover, the integration provides the energy content as

$$W_{magn} = \frac{3}{4}\left(L_m\left|\underline{i}_s + \underline{i}_r\right|^2 + L_{\sigma s}\left|\underline{i}_s\right|^2 + L_{\sigma r}\left|\underline{i}_r\right|^2 \right)$$
(8.32)

Consequently, the mechanical power must be

$$P_{mech} = \frac{3}{2}\operatorname{Re}\left(j\omega_{rs}\underline{\psi}_s\underline{\bar{i}}_s\right) = \frac{3}{2}\omega_{rs}\operatorname{Im}\left(-\underline{\psi}_s\underline{\bar{i}}_s\right) = \frac{3}{2}\omega_{rs}\operatorname{Im}\left(\underline{\bar{\psi}}_s\underline{i}_s\right)$$
(8.33)

Alternatively,

$$P_{mech} = T\omega_{mech} = T\frac{\omega_{rs}}{p}$$
(8.34)

In consequence, the torque can be calculated via

$$T = \frac{3}{2}p\operatorname{Im}\left(\underline{\bar{\psi}}_s\underline{i}_s\right)$$
(8.35)

This is the same torque equation as for the synchronous motor. It can be evaluated in different coordinate systems according to

$$T = \frac{3}{2}p\left(\psi_{s\alpha}i_{s\beta} - \psi_{s\beta}i_{s\alpha}\right) = \frac{3}{2}p\left(\psi_{s\gamma}i_{s\delta} - \psi_{s\delta}i_{s\gamma}\right)$$
(8.36)

This torque corresponds to the torque of the synchronous motor. Instead of once again evaluating the power balance, it would have been valid to directly use the torque equation of the synchronous motor, as only stator quantities occur in this equation. For the torque, it is irrelevant in this context how the torque generating magnetic fields are formed in the stator.

Substituting

$$\underline{\psi}_s = \sigma L_s\underline{i}_s + \frac{L_m}{L_r}\underline{\psi}_r$$
(8.37)

leads to a further representation of the torque equation:

$$T = \frac{3}{2}p\frac{L_m}{L_r}\operatorname{Im}\left(\underline{\bar{\psi}}_r\underline{i}_s\right)$$
(8.38)

Alternatively, it can be written component-wise in the random K coordinate system:

$$T = \frac{3}{2}p\frac{L_m}{L_r}\left(\psi_{rd}i_{sq} - \psi_{rq}i_{sd}\right)$$
(8.39)

8.3   Flux-Oriented Coordinate System

The above representations of the torque by means of the stator and rotor flux

$$T = \frac{3}{2}p\left(\psi_{sd}i_{sq} - \psi_{sq}i_{sd}\right) = \frac{3}{2}p\frac{L_m}{L_r}\left(\psi_{rd}i_{sq} - \psi_{rq}i_{sd}\right) \tag{8.40}$$

give rise to the definition of a flux oriented coordinate system, similar to the one of the synchronous motor. Now, the alignment of the so far free K coordinate system is determined in a way that the d-axis is oriented along the direction of the flux. The q-component of the flux is zero, in consequence. As the torque can now be expressed by the stator flux as well as the rotor flux, this leads to two different variants depending on whether the d/q-axes are oriented along the direction of the stator or rotor flux:

Stator flux orientation

Is the d-axis choses as the direction of the stator flux (see Fig. 8-9 left figure), we refer to the *stator flux orientation.* In that case it is

$$\psi_{sd} = \left|\underline{\psi}_s\right| = \psi_s \quad \text{und} \quad \psi_{sq} = 0 \tag{8.41}$$

and we get the torque

$$T = \frac{3}{2}p\psi_{sd}i_{sq} \tag{8.42}$$

Rotor flux orientation

We refer to the *rotor flux orientation* if the d-axis is aligned with the rotor flux, i.e.

$$\psi_{rd} = \left|\underline{\psi}_r\right| = \psi_r \quad \text{und} \quad \psi_{rq} = 0 \tag{8.43}$$

Then, the torque results as

$$T = \frac{3}{2}p\frac{L_m}{L_r}\psi_{rd}i_{sq} \tag{8.44}$$

The current component i_{sq} can be interpreted as the torque generating current component, same as for the permanent magnet synchronous motor. The meaning of the component i_{sd} will be elaborated later. It should be noted, however, that the d/q-components in the two torque representations (8.42) and (8.44) refer to different coordinate axes (see Fig. 8-9). In the following, only the rotor flux orientation shall be considered. The stator flux orientation will not be discussed.

Stator flux orientation   Rotor flux orientation
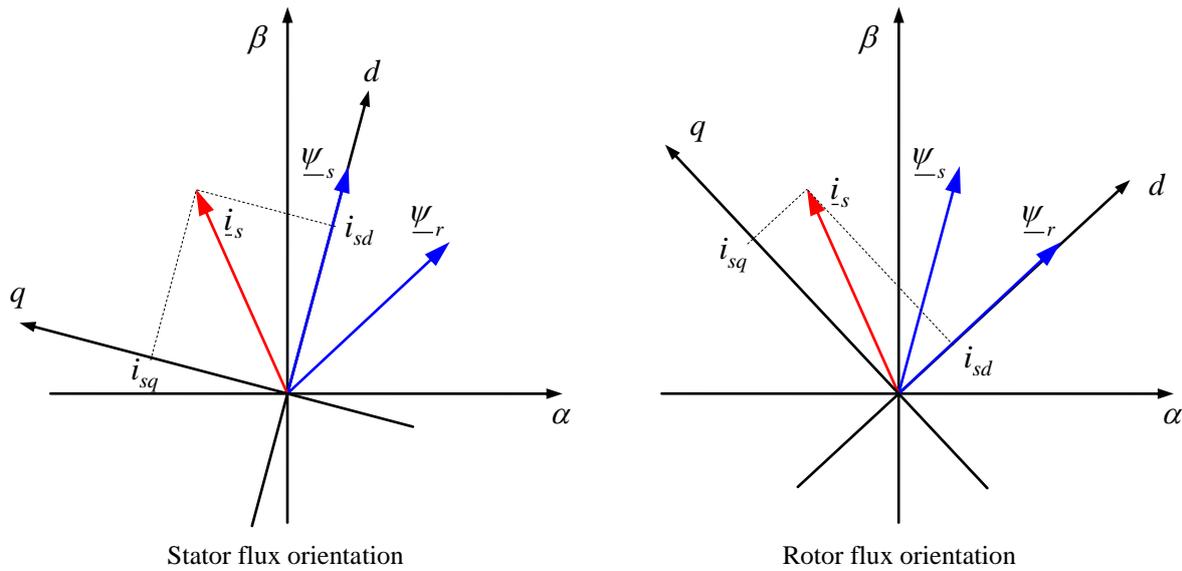
Fig. 8-9: Flux-oriented reference frames

8.4   Dynamic Modeling in Rotor Flux-Oriented Coordinates

The dynamic equations in a random coordinate system were already developed:

$$\dot{\underline{\psi}}_s^k = j\omega_{sk}\underline{\psi}_s^k + \underline{u}_s^k - R_s \underline{i}_s^k \tag{8.45}$$

$$\dot{\underline{\psi}}_r^k = j\omega_{rk}\underline{\psi}_r^k - R_r \underline{i}_r^k \tag{8.46}$$

Now the coordinate system K is aligned following the rotor flux orientation (8.43). The complex rotor flux vector has only a real part when representing it in its own rotor flux-oriented reference frame:

$$\underline{\psi}_r^K = \underline{\psi}_r^{\psi_r} = \psi_{rd} + j\psi_{rq} = \psi_r \tag{8.47}$$

Apart from the transition to the rotor flux system new state variables shall also be introduced. So far, the differential equations were stated with stator and rotor flux as state variables. However, with regard to the torque representation, the stator current and rotor flux shall now be used as state variables, instead. To do so, the rotor current and stator flux are being eliminated with the help of the equations

$$\underline{i}_r = \frac{1}{L_r}\underline{\psi}_r - \frac{L_m}{L_r}\underline{i}_s \tag{8.48}$$

$$\underline{\psi}_s = \sigma L_s \underline{i}_s + \frac{L_m}{L_r}\underline{\psi}_r \tag{8.49}$$

The equations originate from the inductance relations.

Rotor circuit

By substituting the rotor current in the rotor flux differential equation, it follows

$$
\begin{aligned}
\dot{\underline{\psi}}_r^k &= j\omega_{rk}\underline{\psi}_r^k - \frac{R_r}{L_r}\underline{\psi}_r^k + \frac{R_r L_m}{L_r}\underline{i}_s^k \\
&= \left(j\omega_{rk} - \frac{R_r}{L_r} \right)\underline{\psi}_r^k + \frac{R_r L_m}{L_r}\underline{i}_s^k
\end{aligned}
\tag{8.50}
$$

The hereby occurring term

$$
\tau_r = \frac{L_r}{R_r}
\tag{8.51}
$$

represents the *rotor time constant*. Thus, the differential equation takes the form

$$
\dot{\underline{\psi}}_r^k = \left(j\omega_{rk} - \frac{1}{\tau_r} \right)\underline{\psi}_r^k + \frac{L_m}{\tau_r}\underline{i}_s^k
\tag{8.52}
$$

This equation subdivided into a real and an imaginary part, i.e. *d*- and *q*-component. It has to be noted that the rotor flux by definition has no *q*-component:

$$
\dot{\psi}_{rd} = \dot{\psi}_r = -\frac{R_r}{L_r}\psi_r + \frac{R_r L_m}{L_r}i_{sd}
\tag{8.53}
$$

$$
\dot{\psi}_{rq} = 0 = \omega_{r\psi_r}\psi_r + \frac{R_r L_m}{L_r}i_{sq}
\tag{8.54}
$$

From the last equation, we can determine the unknown frequency $\omega_{r\psi_r}$. This is the frequency of the rotor relatively to the *d/q* coordinate system. It is also known as *rotor frequency* of *slip frequency*.

$$
-\omega_{r\psi_r} = \omega_{\psi_r r} = \frac{R_r L_m}{L_r}\frac{i_{sq}}{\psi_r}
\tag{8.55}
$$

While the torque generating component i_{sq} together with the rotor flux ψ_r determine the slip frequency, the current component i_{sd} is responsible for forming the rotor flux. They are referred to as *torque generating* and *flux forming* or *magnetizing* current component.
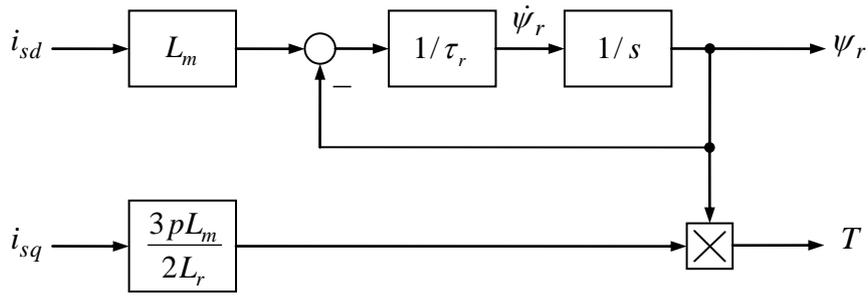
Fig. 8-10: Block diagram for flux forming and torque generation
(rotor side)

Stator circuit

Substituting the stator flux

$$\underline{\psi}_s = \sigma L_s \underline{i}_s + \frac{L_m}{L_r} \underline{\psi}_r \qquad (8.56)$$

in the right and left side of the stator flux differential equation results in

$$\sigma L_s \underline{\dot{i}}_s^k + \frac{L_m}{L_r} \underline{\dot{\psi}}_r^k = j\omega_{sk} \left(\sigma L_s \underline{i}_s^k + \frac{L_m}{L_r} \underline{\psi}_r^k \right) + \underline{u}_s^k - R_s \underline{i}_s^k$$

$$\sigma L_s \underline{\dot{i}}_s^k + \frac{L_m}{L_r} \left(j\omega_{rk} \underline{\psi}_r^k - \frac{R_r}{L_r} \underline{\psi}_r^k + \frac{R_r L_m}{L_r} \underline{i}_s^k \right) = j\omega_{sk} \sigma L_s \underline{i}_s^k + j\omega_{sk} \frac{L_m}{L_r} \underline{\psi}_r^k + \underline{u}_s^k - R_s \underline{i}_s^k$$

$$\sigma L_s \underline{\dot{i}}_s^k = \underline{u}_s^k + j\omega_{sk} \sigma L_s \underline{i}_s^k - \left(R_s + R_r \frac{L_m^2}{L_r^2} \right) \underline{i}_s^k - j\omega_{rs} \frac{L_m}{L_r} \underline{\psi}_r^k + \frac{L_m R_r}{L_r^2} \underline{\psi}_r^k$$

$$\sigma L_s \underline{\dot{i}}_s^k = \underline{u}_s^k - j\omega_{ks} \sigma L_s \underline{i}_s^k - \left(R_s + R_r \frac{L_m^2}{L_r^2} \right) \underline{i}_s^k + \left(-j\omega_{rs} \frac{L_m}{L_r} + \frac{L_m R_r}{L_r^2} \right) \underline{\psi}_r^k$$

$$(8.57)$$

whereas,

$$\omega_{rs} = \omega_{rk} - \omega_{sk}$$

is used. Explicitly solving for the time derivative of the current leads to the current differential equation

$$\underline{i}_s^k = -j\omega_{ks}\underline{i}_s^k + \frac{1}{\sigma L_s}\left[\underline{u}_s^k - \left(R_s + R_r\frac{L_m^2}{L_r^2}\right)\underline{i}_s^k + \left(-j\omega_{rs}\frac{L_m}{L_r} + \frac{L_mR_r}{L_r^2}\right)\underline{\psi}_r^k\right] \tag{8.58}$$

The individual terms can be interpreted as follows: The first term on the right side originates from the apparent current variation, due to the rotation of the reference system. Through multiplication with the imaginary part, the two current components are exactly coupled cross-wise, in consequence. The first term in brackets is the driving external voltage at the equivalent inductance σL_s. Alongside, a resistive voltage drop, also including the rotor resistance takes effect. Moreover, there are direct and rotational reactions from the rotor flux.

Also a typical time constant, the *leakage time constant* can be identified.

$$\tau_\sigma = \frac{\sigma L_s}{R_s + R_r\frac{L_m^2}{L_r^2}} \tag{8.59}$$

It follows:

$$\underline{i}_s^k = -\left(j\omega_{ks} + \frac{1}{\tau_\sigma}\right)\underline{i}_s^k + \frac{1}{\sigma L_s}\left[\underline{u}_s^k + \left(-j\omega_{rs}\frac{L_m}{L_r} + \frac{L_mR_r}{L_r^2}\right)\underline{\psi}_r^k\right] \tag{8.60}$$

The hereby occurring angular frequency ω_{ks} corresponds to

$$\omega_{ks} = \omega_{\psi_r s} = \omega_{rs} + \omega_{\psi_r r} \tag{8.61}$$
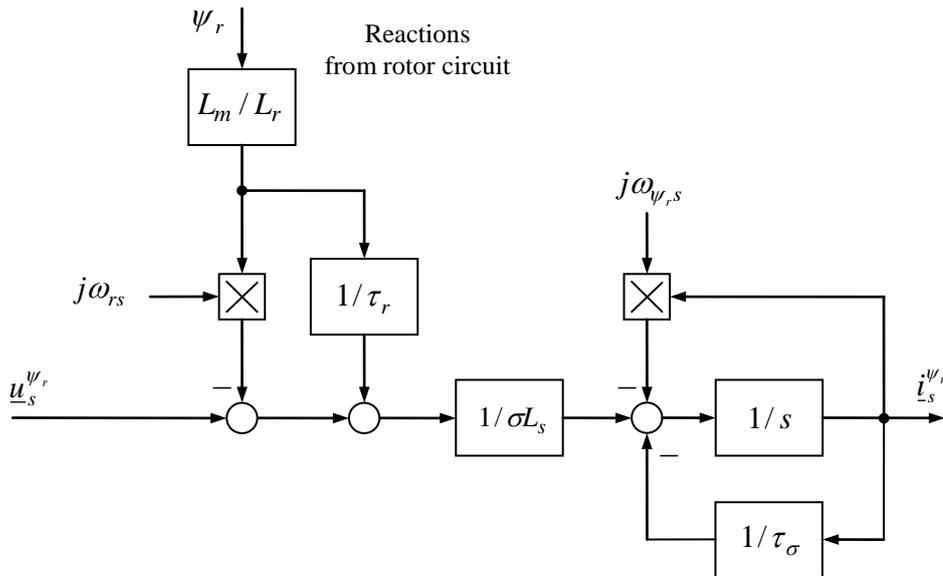
Fig. 8-11: Block diagram of the stator circuit in rotor flux orientation

Current control approach

The above block diagram serves as a basis for the design of a subordinate current control: The reactions from the rotor circuit on the dynamics of the stator current are regarded as a disturbances and can be compensated through a disturbance feed-forward control ("EMF feed-forward") in the controller. Furthermore, the coupling of the current components by the angular frequency $\omega_{\psi,s}$ can be compensated by an opposing decoupling measure. Both terms are summarized in the decoupling or feed-forward control portion $\underline{u}_s^{k0}$. The total voltage can be written as follows:

$$\underline{u}_s^k = \Delta\underline{u}_s^k + \underline{u}_s^{k0} = \Delta\underline{u}_s^k + j\omega_{ks}\sigma L_s \underline{i}_s^k + \left(j\omega_{rs}\frac{L_m}{L_r} - \frac{L_m R_r}{L_r^2} \right)\underline{\psi}_r^k \tag{8.62}$$

Inserting this voltage in the above current differential equation, a simple decoupled equivalent stator circuit can be obtained:

$$\dot{\underline{i}}_s^k = -\frac{1}{\tau_\sigma}\underline{i}_s^k + \frac{1}{\sigma L_s}\Delta\underline{u}_s^k \tag{8.63}$$

Component-wise:

$$\dot{i}_{sd} = -\frac{1}{\tau_\sigma}i_{sd} + \frac{1}{\sigma L_s}\Delta u_{sd}$$
$$\dot{i}_{sq} = -\frac{1}{\tau_\sigma}i_{sq} + \frac{1}{\sigma L_s}\Delta u_{sq} \tag{8.64}$$

This is structure exactly corresponds to the one already known from the permanent magnet synchronous motor. The remaining control design is carried out, accordingly.

8.5   Transformation of Leakage Inductances

Starting point:

$$\underline{\psi}_s^k = L_s \underline{i}_s^k + L_m \underline{i}_r^k$$
$$\underline{\psi}_r^k = L_m \underline{i}_s^k + L_r \underline{i}_r^k$$

(8.65)

$$\underline{\dot{\psi}}_s^k = j\omega_{sk}\underline{\psi}_s^k + \underline{u}_s^k - R_s \underline{i}_s^k$$
$$\underline{\dot{\psi}}_r^k = j\omega_{rk}\underline{\psi}_r^k - R_r \underline{i}_r^k$$

The stator quantities, i.e. current and voltage but also the stator flux, shall not be altered, due to their reflections at the motor terminals. Based on the above equations, the rotor quantities are scaled with a constant factor c:

$$\underline{\psi}_s^k = L_s \underline{i}_s^k + cL_m \frac{\underline{i}_r^k}{c}$$
$$c\underline{\psi}_r^k = cL_m \underline{i}_s^k + c^2 L_r \frac{\underline{i}_r^k}{c}$$

(8.66)

$$\underline{\dot{\psi}}_s^k = j\omega_{sk}\underline{\psi}_s^k + \underline{u}_s^k - R_s \underline{i}_s^k$$
$$c\underline{\dot{\psi}}_r^k = j\omega_{rk}c\underline{\psi}_r^k - c^2 R_r \frac{\underline{i}_r^k}{c}$$

and again in the previous form

$$\underline{\psi}_s^k = L_s \underline{i}_s^k + L_m' \underline{i}_r'^k$$
$$\underline{\psi}_r'^k = L_m' \underline{i}_s^k + L_r' \underline{i}_r'^k$$

(8.67)

$$\underline{\dot{\psi}}_s^k = j\omega_{sk}\underline{\psi}_s^k + \underline{u}_s^k - R_s \underline{i}_s^k$$
$$\underline{\dot{\psi}}_r'^k = j\omega_{rk}\underline{\psi}_r'^k - R_r' \underline{i}_r'^k$$

Written with the transformed variables,

$$\underline{\psi}_r'^k = c\underline{\psi}_r^k$$
$$\underline{i}_r'^k = \frac{\underline{i}_r^k}{c}$$
$$R_r' = c^2 R_r$$
$$L_m' = cL_m$$

(8.68)

$$L'_r = c^2 L_r$$

Although, the stator inductance L_s itself is not changed by the transformation, its distribution into mutual and leakage inductance is affected, however.

$$L'_{\sigma s} = L_s - L'_m \tag{8.69}$$

The transformed leakage inductance of the rotor is

$$L'_{\sigma r} = L'_r - L'_m \tag{8.70}$$

By choosing a suitable scaling factor, leakages of the resulting equivalent circuit can be shifted between the stator and rotor circuit.

8.5.1 Model with Leakage Inductance Concentrated on Stator Side

If the leakage inductance on the rotor side shall disappear, then

$$\begin{aligned} L'_{\sigma r} &= L'_r - L'_m = 0 \\ L'_r &= L'_m \\ c^2 L_r &= c L_m \end{aligned} \tag{8.71}$$

In this case, factor c is chosen as

$$c = \frac{L_m}{L_r} \tag{8.72}$$

The transformed variables are

$$\underline{\psi}'_r = \frac{L_m}{L_r} \underline{\psi}_r \tag{8.73}$$

$$\underline{i}'_r = \frac{L_r}{L_m} \underline{i}_r \tag{8.74}$$

$$R'_r = \frac{L_m^2}{L_r^2} R_r \tag{8.75}$$

$$L'_m = L'_r = \frac{L_m^2}{L_r} = L_s \frac{L_m^2}{L_s L_r} = (1-\sigma)L_s \tag{8.76}$$

$$L'_{\sigma s} = L_s - L'_m = L_s - \frac{L_m^2}{L_r} = L_s\left(1 - \frac{L_m^2}{L_s L_m}\right) = \sigma L_s \tag{8.77}$$

Finally, the torque equation simplifies to

$$T = \frac{3}{2} p \operatorname{Im}\left(\underline{\psi}'_r \underline{i}_s\right) \tag{8.78}$$

or

$$T = \frac{3}{2} p \psi'_r i_{sq} \tag{8.79}$$

in the rotor flux oriented coordinate system. Also, the stator current differential equation is simplified by this transformation to

$$\underline{\dot{i}}_s^k = j\omega_{sk}\underline{i}_s^k + \frac{1}{\sigma L_s}\left[\underline{u}_s^k - (R_s + R'_r)\underline{i}_s^k + \left(j\omega_{rs} + \frac{R'_r}{L'_m}\right)\underline{\psi}'_r^k\right] \tag{8.80}$$
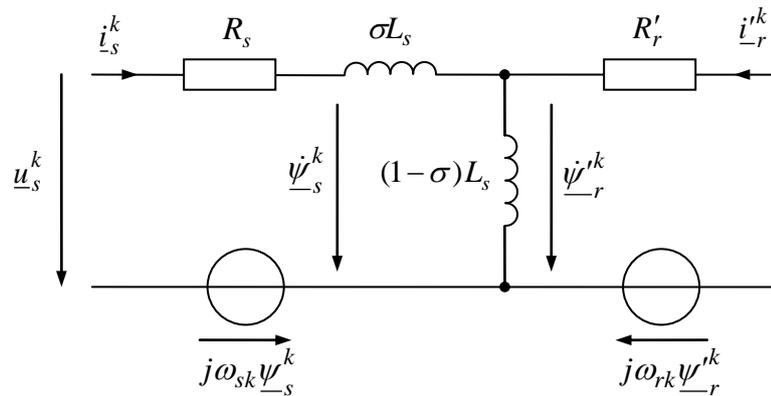
Fig. 8-12: Equivalent circuit of induction motor with leakage concentrated on stator side

Since many relations simplify through the transformation of the leakage inductance to the stator side, the rotor flux oriented control is usually based on this structure from the start.

8.5.2 Model with Leakage Inductance Concentrated on Rotor Side

From the requirement

$$L'_{\sigma s} = L_s - L'_m = 0 \tag{8.81}$$

the scaling factor,

$$c = \frac{L_s}{L_m}$$

(8.82)

results. It follows for the transformed variables

$$\underline{\psi}'_r = \frac{L_s}{L_m}\underline{\psi}_r$$

(8.83)

$$\underline{i}'_r = \frac{L_m}{L_s}\underline{i}_r$$

(8.84)

$$R'_r = \frac{L_s^2}{L_m^2}R_r$$

(8.85)

$$L'_m = L_s$$

(8.86)

$$L'_r = \frac{L_s^2}{L_m^2}L_r = L_s\frac{L_sL_r}{L_m^2} = \frac{1}{1-\sigma}L_s$$

(8.87)

$$L'_{\sigma r} = L'_r - L_s = \frac{\sigma}{1-\sigma}L_s$$

(8.88)

The torque equation is given as

$$T = \frac{3}{2}p\frac{L_m^2}{L_rL_s}\operatorname{Im}\left(\overline{\underline{\psi}}'_r\underline{i}_s\right) = \frac{3}{2}p(1-\sigma)\operatorname{Im}\left(\overline{\underline{\psi}}'_r\underline{i}_s\right)$$

(8.89)

or, alternatively

$$T = \frac{3}{2}p(1-\sigma)\psi'_r i_{sq}$$

(8.90)
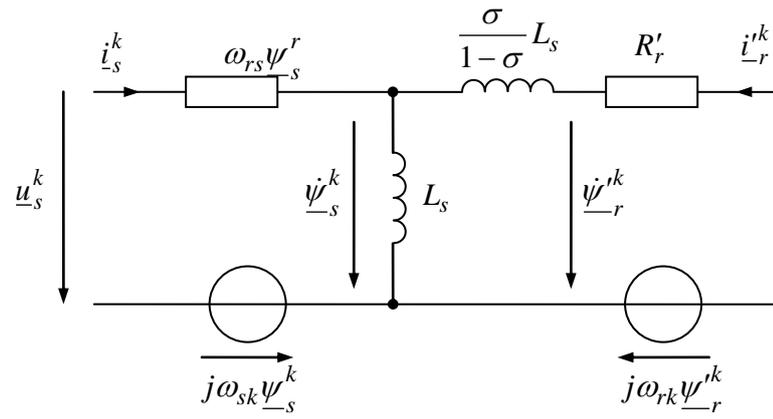
Fig. 8-13: Equivalent circuit of induction motor with leakage concentrated on rotor side

8.6   Consideration of Real Magnetization Behavior

So far, the inductances in the model of the induction motor were assumed as constant. In fact, the iron in the motor may be saturated considerably during operation. This is owed to an economically and technically optimal motor design. Of course, it would be possible to reduce iron saturation by using more material, however, this measure would make the motor heavier and more expensive. Quite often, it is acceptable to consider only the saturation of the mutual inductance while assuming the leakage inductances as constant. Then, the mutual inductance or the mutual flux is dependent on magnetizing current i_μ.
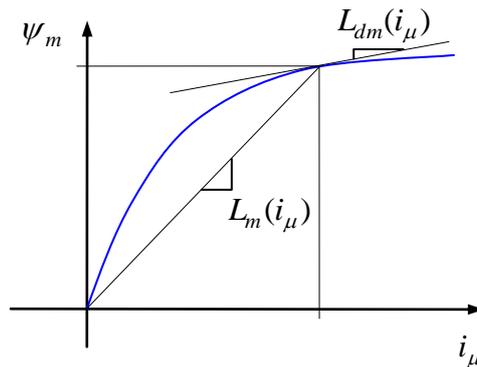
Fig. 8-14: Saturation of the mutual inductance

Altering the magnetization of a material is due to its hysteretic behavior associated with additional losses. In a first approximation, one can assume that these losses increase with the square of the flux magnitude and linearly with the frequency. In the circuit diagram, these additional hysteresis losses can be accounted for by inserting an equivalent resistance R_{Fe} parallel to the mutual inductance.
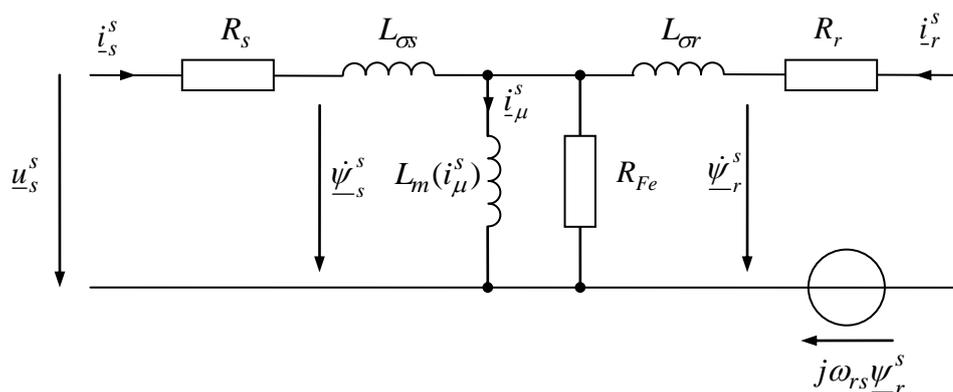
Fig. 8-15: Equivalent circuit diagram considering the saturation of the mutual inductance as well as iron losses

8.7 Steady-State Operating Characteristics

8.7.1 Voltage Equations and Vector Diagrams

In steady state, all quantities in the flux-oriented reference system are settled. In particular, all current components, voltages and fluxes have the same angular velocity. Then, the angular frequency of rotor flux oriented system exactly corresponds to the frequency of current and voltage at the stator terminals. Therefore, in steady-state we can simply use the term *stator frequency*.

$$\omega_s = \omega_{\psi_r s} = \omega_{u_s s} = \omega_{i_s s} \tag{8.91}$$

The frequency between the electrical phasors and the rotor is referred to as rotor frequency or slip frequency.

$$\omega_r = \omega_{\psi_r r} = \omega_{u_s r} = \omega_{i_s r} \tag{8.92}$$

The rotational frequency (related to the electrical system) can now be expressed as

$$\omega_{rs} = \omega_s - \omega_r \tag{8.93}$$

The dimensionless variable

$$s = \frac{\omega_r}{\omega_s} \tag{8.94}$$

is called *slip*.

In steady state, the stationary rotor flux

$$\psi_r = L_m i_{sd} \tag{8.95}$$

arises. The stationary stator voltage follows the equation

$$\underline{u}_s^{\psi_r} = R_s \underline{i}_s^{\psi_r} + j\omega_s \left(\sigma L_s \underline{i}_s^{\psi_r} + \frac{L_m}{L_r} \psi_r \right) \tag{8.96}$$

or in individual components

$$u_{sd} = R_s i_{sd} - \omega_s \sigma L_s i_{sq} \tag{8.97}$$

$$u_{sq} = R_s i_{sq} + \omega_s \left(\sigma L_s i_{sd} + \frac{L_m}{L_r} \psi_r \right)$$

$$= R_s i_{sq} + \omega_s \left(\sigma L_s + \frac{L_m^2}{L_r} \right) i_{sd}$$

$$= R_s i_{sq} + \omega_s L_s i_{sd}$$

Motor operation mode   Generator operation mode
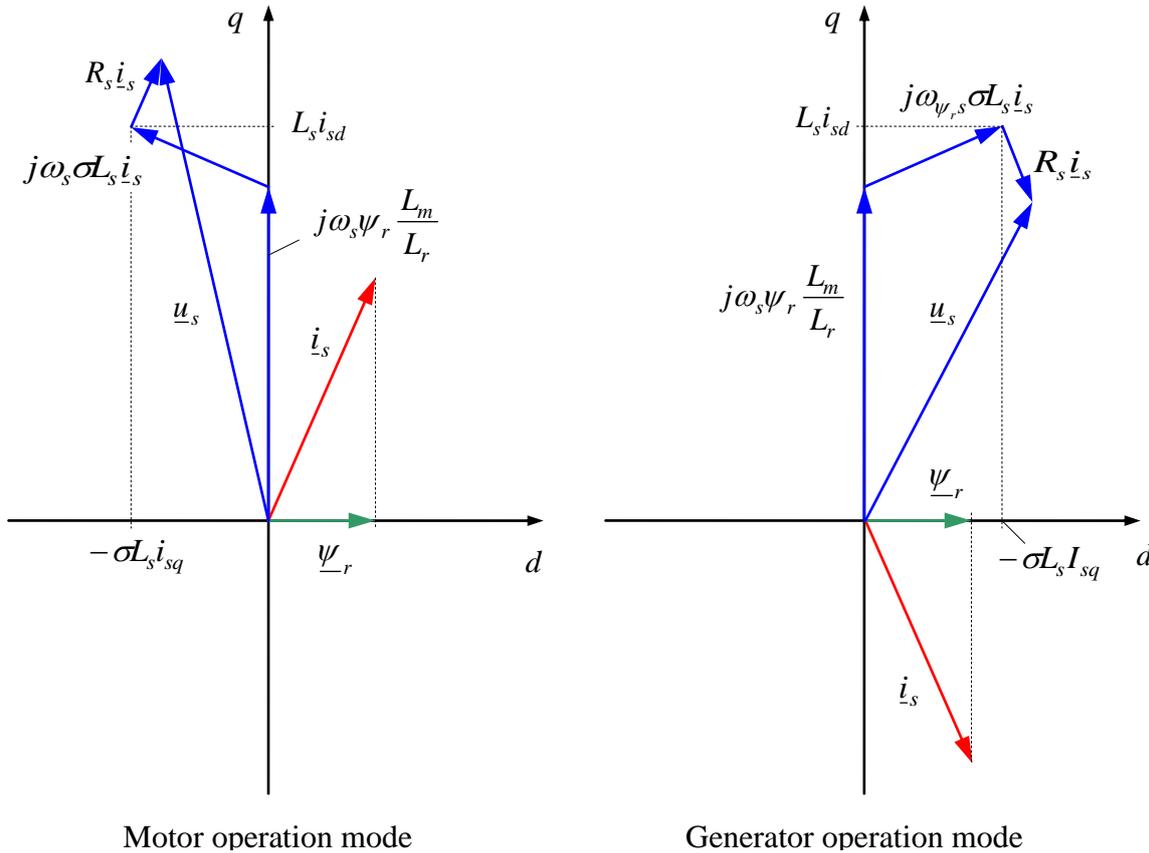
Fig. 8-16: Phasor diagram for steady state operation
(With appropriate scaling of current and flux phasors, the rotor flux can be
represented as a projection of the stator current phasor on the *d*-axis)

In steady state, we can express the torque relationship directly as the product of the current components:

$$T = \frac{3}{2} p \frac{L_m}{L_r} \psi_r i_{sq} = \frac{3}{2} p \frac{L_m^2}{L_r} i_{sd} i_{sq} \tag{8.98}$$

The torque is directly proportional to the rectangular plane spanned by the current phasor in *d/q*-coordinates, provided the remaining parameters are assumed constant.

8.7.2 Steady-State Equivalent Circuit Diagram

Starting point: stator and rotor voltage equations

$$\underline{u}_s^{\psi_r} = R_s \underline{i}_s^{\psi_r} + j\omega_s \underline{\psi}_s^{\psi_r} = R_s \underline{i}_s^{\psi_r} + j\omega_s L_m \left(\underline{i}_s^{\psi_r} + \underline{i}_r^{\psi_r} \right) + j\omega_s L_{\sigma s} \underline{i}_s^{\psi_r}$$

$$0 = \underline{u}_r^{\psi_r} = R_r \underline{i}_r^{\psi_r} + j\omega_r \underline{\psi}_r^{\psi_r} = R_r \underline{i}_r^{\psi_r} + j\omega_r L_m \left(\underline{i}_s^{\psi_r} + \underline{i}_r^{\psi_r} \right) + j\omega_r L_{\sigma r} \underline{i}_r^{\psi_r}$$

Dividing the rotor voltage equation by the slip s leads to

$$0 = \frac{1}{s} R_r \underline{i}_r^{\psi_r} + j\omega_s \underline{\psi}_r^{\psi_r}$$

$$= \frac{1}{s} R_r \underline{i}_r^{\psi_r} + j\omega_s L_m \left(\underline{i}_s^{\psi_r} + \underline{i}_r^{\psi_r} \right) + j\omega_s L_{\sigma r} \underline{i}_r^{\psi_r}$$

These equations can now be interpreted in terms of the normal complex vectors for AC systems. The terms $j\omega_s L_m$, $j\omega_s L_{\sigma s}$, $j\omega_s L_{\sigma r}$ are regarded as complex AC-impedances of the inductances. This leads to the following equivalent circuit, which in contrast to the previously presented equivalent circuit diagrams is only valid under steady state conditions.
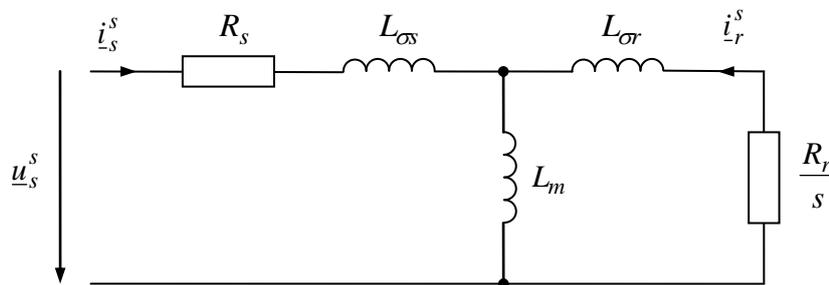
Fig. 8-17: Steady state equivalent circuit diagram of an induction motor

In this equivalent circuit diagram, the stator leakage inductance can be transformed to the rotor side (Section 8.5.2):
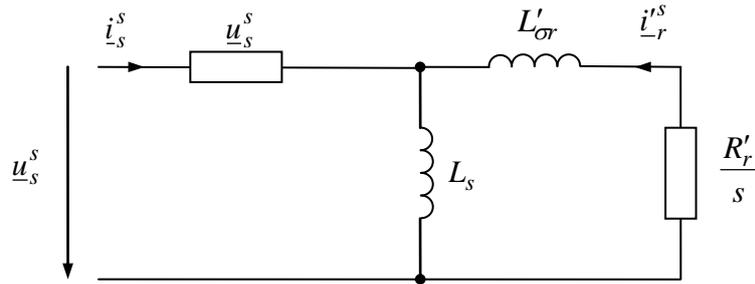
Fig. 8-18: Steady state equivalent circuit diagram of an induction motor
with leakage concentrated on rotor side.

8.7.3 Torque at Constant Voltage and Frequency Supply

In the uncontrolled operation mode, the induction motor can be connected to a three-phase system with constant amplitude and frequency. The torque estimation can be based on the equation

$$T = \frac{3}{2} p \, \mathrm{Im}(\overline{\underline{\psi}}_s \underline{i}_s) = -\frac{3}{2} p \, \mathrm{Im}(\overline{\underline{\psi}}_s \underline{i}_r) , \tag{8.99}$$

whereas the above steady state equivalent circuit diagram with rotor-sided leakage is made use of. The rotor current is determined from the rotor loop, while neglecting the stator resistance R_s.

$$\underline{i}_r'^s = -\frac{1}{\dfrac{R_r'}{s} + j\omega_s L_{\sigma r}'} \underline{u}_s^s \tag{8.100}$$

Then, the stator flux results to

$$\underline{\psi}_s^s = \frac{1}{j\omega_s} \underline{u}_s^s \tag{8.101}$$

It follows

$$
\begin{aligned}
T &= -\frac{3}{2} p \operatorname{Im}\left[\frac{1}{-j\omega_s}\, \bar{u}_s^{\,s}\, \frac{-1}{\dfrac{R_r'}{s} + j\omega_s L_{\sigma r}'}\, u_s^{\,s}\right] \\[2mm]
&= \frac{3}{2} p \frac{u_s^2}{\omega_s} \operatorname{Re}\left[\frac{1}{\dfrac{R_r'}{s} + j\omega_s L_{\sigma r}'}\right] \\[2mm]
&= \frac{3}{2} p \frac{u_s^2}{\omega_s} \operatorname{Re}\left[\frac{s}{R_r' + j\omega_s s L_{\sigma r}'}\right] \\[2mm]
&= \frac{3}{2} p \frac{u_s^2}{\omega_s^2} \operatorname{Re}\left[\frac{\omega_s s}{R_r' + j\omega_s s L_{\sigma r}'}\right] \\[2mm]
&= \frac{3}{2} p \frac{u_s^2}{\omega_s^2} \operatorname{Re}\left[\frac{\omega_s s\left(R_r' - j\omega_s s L_{\sigma r}'\right)}{R_r'^2 + \left(\omega_s s L_{\sigma r}'\right)^2}\right] \\[2mm]
&= \frac{3}{2} p \frac{u_s^2}{\omega_s^2} \frac{\omega_s s R_r'}{R_r'^2 + \left(\omega_s s L_{\sigma r}'\right)^2} \\[2mm]
&= \frac{3}{2} p \frac{u_s^2}{\omega_s^2} \frac{\omega_r R_r'}{R_r'^2 + \left(\omega_r L_{\sigma r}'\right)^2}
\end{aligned}
\tag{8.102}
$$

When using the RMS value of the stator voltage instead of the phasor amplitude,

$$
U_s = \frac{u_s}{\sqrt{2}}
\tag{8.103}
$$

then the equation results in

$$
T = 3p \frac{U_s^2}{\omega_s^2} \frac{\omega_r R_r'}{R_r'^2 + \left(\omega_r L_{\sigma r}'\right)^2}
\tag{8.104}
$$

This is referred to as Kloss's formula. With a constant stator frequency, the maximum torque is reached at a rotor frequency

$$
\omega_{rk} = \frac{R_r'}{L_{\sigma r}'}\,,
\tag{8.105}
$$

also known as *sweep* or *slip frequency*. The corresponding torque at this frequency is called *sweep torque* and amounts to

$$
T_k = \frac{3p}{2L_{\sigma r}'} \frac{U_s^2}{\omega_s^2}
\tag{8.106}
$$

By making use of the introduced sweep quantities, the torque equation can be expressed in the clear form

$$\frac{T}{T_k} = \frac{2}{\dfrac{\omega_r}{\omega_{rk}} + \dfrac{\omega_{rk}}{\omega_r}} = \frac{2}{\dfrac{s}{s_k} + \dfrac{s_k}{s}} \tag{8.107}$$

For small slips $|s| \ll s_k$, the torque behavior can be approximated with the linear function

$$\frac{T}{T_k} \approx 2 \frac{s}{s_k} \tag{8.108}$$
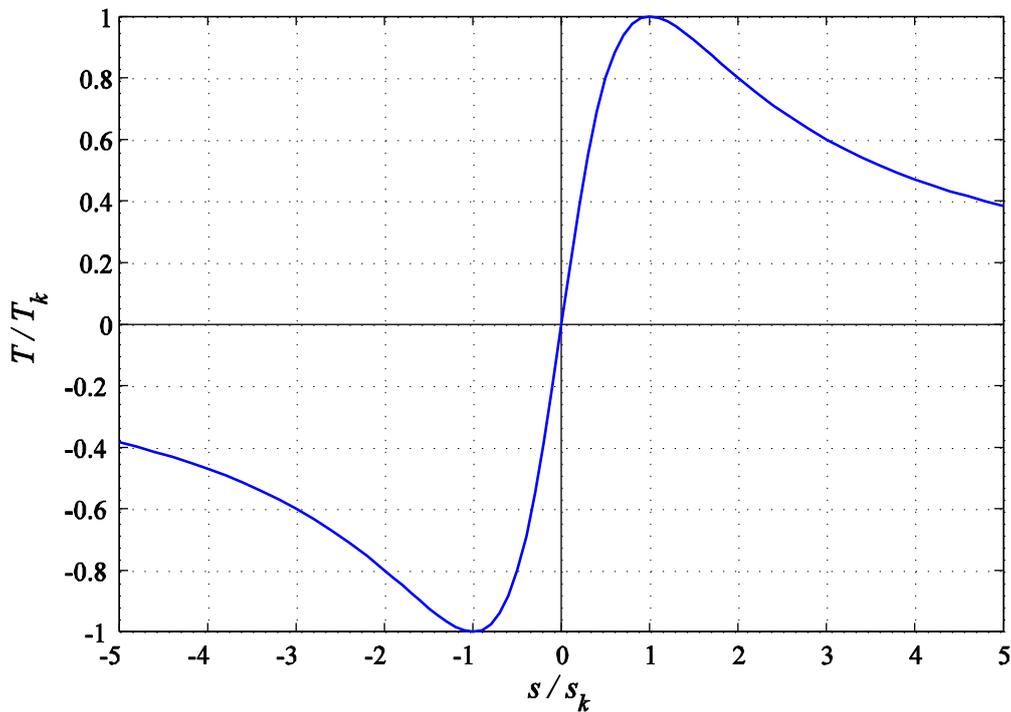
Fig. 8-19: Torque as a function of the slip

8.7.4 Operation with Minimum Losses

In steady state, the torque can be expressed by the product of the current components:

$$T = \frac{3}{2} p \frac{L_m}{L_r} \psi_r i_{sq} = \frac{3}{2} p \frac{L_m^2}{L_r} i_{sd} i_{sq} \tag{8.109}$$

A desired torque can thus be achieved by various combinations of i_{sd}, i_{sq}. We want to investigate at this point, which one of these possible operating points causes the lowest ohmic losses. The ohmic stator and rotor losses are

$$P_d = \frac{3}{2} R_s \left(i_{sd}^2 + i_{sq}^2 \right) + \frac{3}{2} R_r \left(i_{rd}^2 + i_{rq}^2 \right) \tag{8.110}$$

With the help of the equation

$$\underline{\psi}_r = L_m \underline{i}_s + L_r \underline{i}_r \tag{8.111}$$

the rotor currents can be expressed through rotor flux and stator currents. Component-wise this results in

$$i_{rd} = \frac{1}{L_r} \psi_{rd} - \frac{L_m}{L_r} i_{sd} = \frac{1}{L_r} \psi_r - \frac{L_m}{L_r} i_{sd} \tag{8.112}$$

$$i_{rq} = \frac{1}{L_r} \psi_{rq} - \frac{L_m}{L_r} i_{sq} = -\frac{L_m}{L_r} i_{sd} \tag{8.113}$$

In steady state, what shall be focused on in the following, the equation

$$\psi_r = L_m i_{sd} \tag{8.114}$$

also holds, so that the d-component of rotor current is always zero:

$$i_{rd} = 0$$

The ohmic losses can then be solely expressed by the stator currents:

$$P_d = \frac{3}{2} R_s \left(i_{sd}^2 + i_{sq}^2 \right) + \frac{3}{2} R_r i_{rq}^2 = \frac{3}{2} \left[R_s i_{sd}^2 + \left(R_s + R_r \frac{L_m^2}{L_r^2} \right) i_{sq}^2 \right] \tag{8.115}$$

These losses are now to be minimized for a given torque T. Mathematically, this corresponds to an extreme value problem with two variables i_{sd}, i_{sq} and a constraint, which is solved by setting the partial derivatives of the Lagrangian function

$$L(i_{sd}, i_{sq}, \lambda) = T(i_{sd}, i_{sq}) - \lambda P_d(i_{sd}, i_{sq}) \tag{8.116}$$

to zero:

$$\frac{\partial L}{\partial i_{sd}} = \frac{\partial T}{\partial i_{sd}} - \lambda \frac{\partial P_d}{\partial i_{sd}} = 0$$

$$\frac{\partial L}{\partial i_{sq}} = \frac{\partial T}{\partial i_{sq}} - \lambda \frac{\partial P_d}{\partial i_{sq}} = 0$$

This leads to

$$\frac{3}{2} p \frac{L_m^2}{L_r} i_{sq} = \frac{3}{2} 2\lambda R_s i_{sd}$$

$$\frac{3}{2} p \frac{L_m^2}{L_r} i_{sd} = \frac{3}{2} 2\lambda \left(R_s + R_r \frac{L_m^2}{L_r^2} \right) i_{sq} \tag{8.117}$$

Calculating the quotient of both equations eliminates the Lagrangian multiplier λ, leading to

$$\frac{i_{sq}}{i_{sd}} = \frac{R_s}{R_s + R_r \dfrac{L_m^2}{L_r^2}} \frac{i_{sd}}{i_{sq}} \quad ,$$

$$\frac{i_{sq}}{i_{sd}} = \pm \frac{1}{\sqrt{1 + \dfrac{R_r}{R_s} \dfrac{L_m^2}{L_r^2}}} \tag{8.118}$$

The operating points with minimum losses thus lie on the line through the origin in the i_{sd}/i_{sq} plane. Motor and generator operation mode are distinguished by the sign. Now, the current components as a function of the given torque shall be determined. Using the last formula, i_{sq} can be eliminated in the torque formula:

$$T = \frac{3}{2} p \frac{L_m^2}{L_r} i_{sd} i_{sq} = \pm \frac{3}{2} p \frac{L_m^2}{L_r} \frac{1}{\sqrt{1 + \dfrac{R_r}{R_s} \dfrac{L_m^2}{L_r^2}}} i_{sd}^2 \tag{8.119}$$

Solving for i_{sd} results in

$$i_{sd} = \sqrt{|T| \frac{2L_r}{3pL_m^2} \sqrt{1 + \frac{R_r}{R_s} \frac{L_m^2}{L_r^2}}}$$

(8.120)

and

$$i_{sq} = \mathrm{sgn}(T) \sqrt{|T| \frac{\dfrac{2L_r}{3pL_m^2}}{\sqrt{1 + \dfrac{R_r}{R_s} \dfrac{L_m^2}{L_r^2}}}}$$

(8.121)

The optimal rotor flux can therefore be calculated via

$$\psi_r = L_m i_{sd} = \sqrt{|T| \frac{2L_r}{3p} \sqrt{1 + \frac{R_r}{R_s} \frac{L_m^2}{L_r^2}}}$$

(8.122)

The calculations were once again performed under the assumption of constant inductances, which is a useful approximation for small magnetizations. However, near the nominal operating point of the machine, the degree of saturation increases, making it necessary to modify the derived results, similar to section 8.7.5.

As part of the rotor flux oriented control, only the above determined rotor flux would be used as reference for the flux control. In consequence, the flux controller would adjust the necessary magnetizing current i_{sd}, while the torque control adjusts the suitable i_{sq}. The above formulas for i_{sd} and i_{sd} must therefore not be implemented in the control. Instead, only the implementation of the formula for ψ_r as a function of the nominal torque becomes necessary.

When controlling the rotor flux according to this loss minimizing strategy, reduced torque dynamics must be taken into account. As flux changes always follow the relatively large rotor time constant, dynamic torque requirements cannot be realized that quickly. In case highly dynamic torque characteristics are required, a sufficiently large flux should be permanently maintained in the motor, also during idle mode and light load operation.
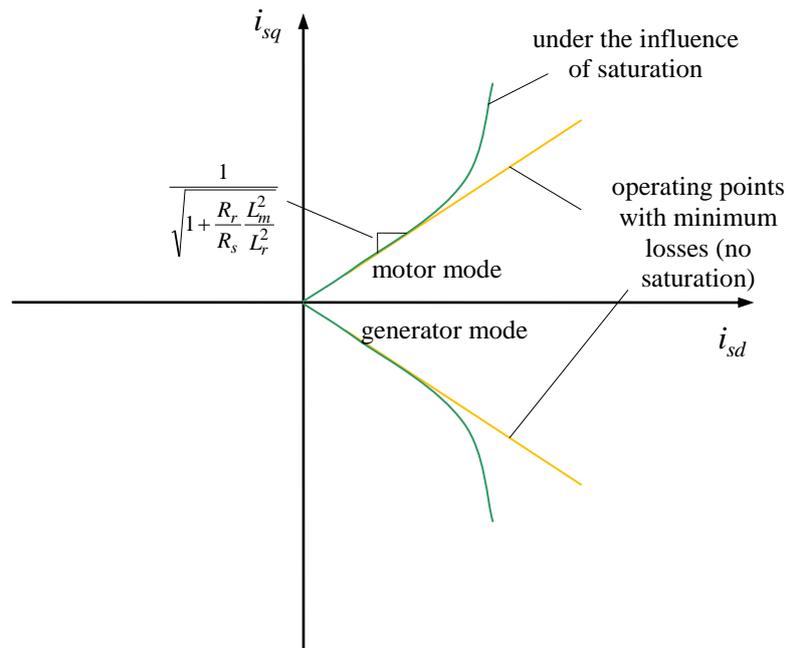
Fig. 8-20: Operating points with minimum losses

8.7.5 Operating at Current Limits

Constant torque curves in the current plane are hyperbolas. However, the inductances due to saturation of the magnetic material are dependent on the current. With assumed constant inductances the maximum torque would be set at a maximum possible current

$$i_{max} > i_s = |\underline{i}_s| = \sqrt{i_{sd}^2 + i_{sq}^2}$$

at the operating point

$$i_{sd} = i_{sq} = \frac{i_{max}}{\sqrt{2}}$$

Since the real constant torque curves due to the iron saturation noticeably deviate from the hyperbolic form, the maximum torque is usually achieved at a point at which the torque-generating current i_{sq} is significantly larger than the magnetizing current i_{sd}.
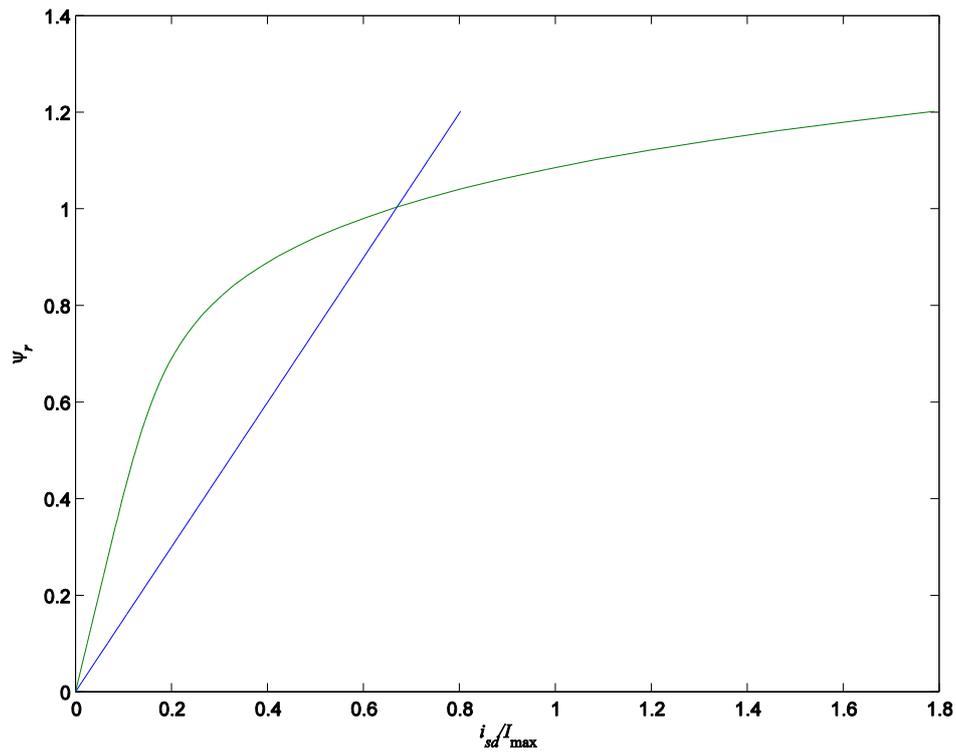
Fig. 8-21: Steady state characteristic of rotor flux over magnetizing current component for linear and saturating inductance
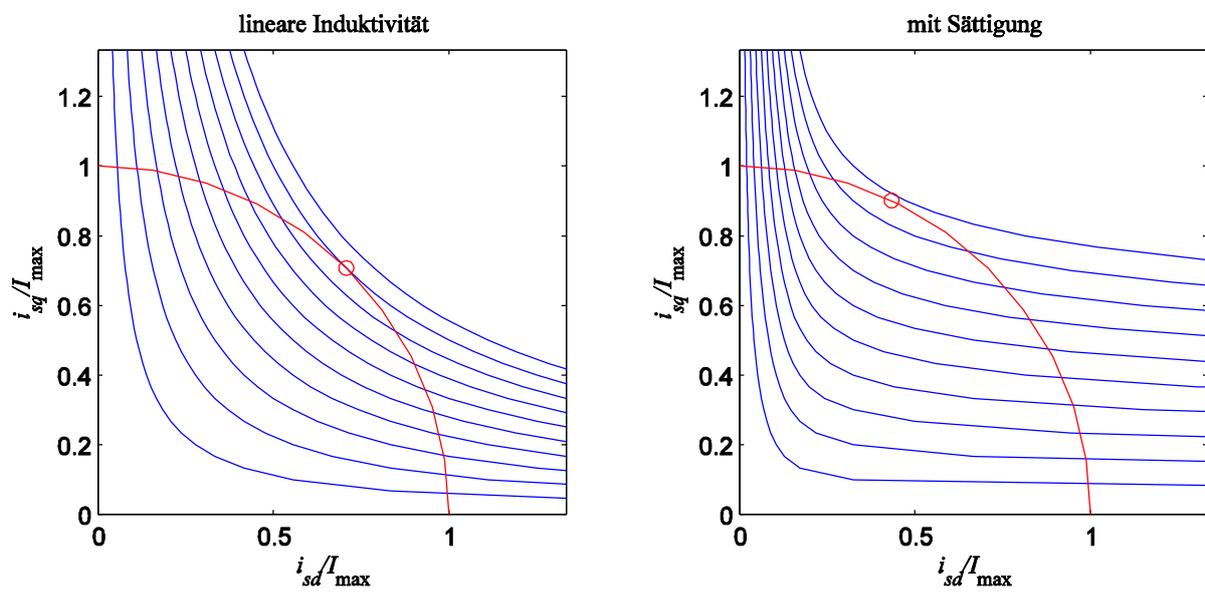
Fig. 8-22: Constant torque curves for linear (left) and saturating inductance (right) incl. point of maximum torque at a given maximum current
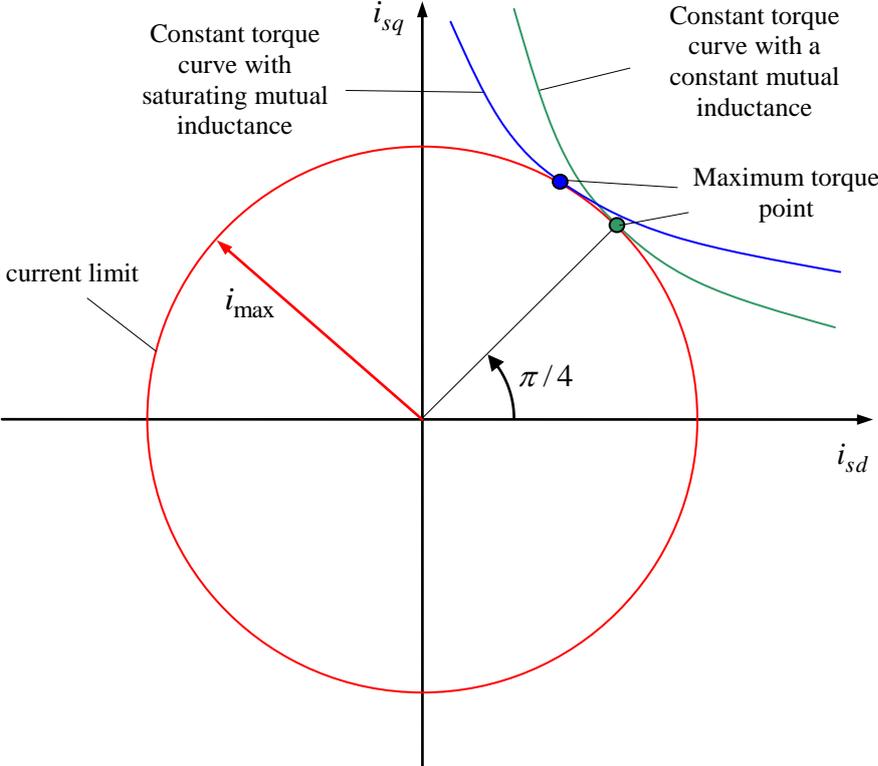
Fig. 8-23: Comparison of maximum torque operating points
for linear and saturating inductance

8.7.6 Operation at the Voltage Limit, Flux Weakening

With a constant rotor flux, the motor voltage increases approximately proportional with the speed. Neglecting resistive voltage drops, the voltage magnitude in steady state results to

$$u_s^2 = u_{sd}^2 + u_{sq}^2 = \omega_s^2 \left[(\psi_r + \sigma L_s i_{sd})^2 + (\sigma L_s i_{sq})^2 \right] = \omega_s^2 \left[(L_s i_{sd})^2 + (\sigma L_s i_{sq})^2 \right]$$

The inverter can only provide a maximum voltage, which is limited by the area of the hexagon (see Section 3). For a simple analysis, we assume a circular restriction.

$$u_s^2 = u_{sd}^2 + u_{sq}^2 \leq u_{max}^2$$

At low speeds or frequencies, the inverter voltage is usually sufficient and the voltage limit is not reached. As the speed increases, the voltage limit is reached at some point. This point is referred to as the rated point of the drive. Greater speeds can be achieved by reducing (weakening) the rotor flux. This however reduces the available torque

$$T = \frac{3}{2} p \frac{L_m}{L_r} \psi_r i_{sq} = \frac{3}{2} p \frac{L_m^2}{L_r} i_{sd} i_{sq} \ ,$$

unless the reduced flux ψ_r can be compensated by an increased current i_{sq}. This is, however, usually not possible or only possible to a limited extent, as the current itself is in turn limited by the current limit i_{max}. One can also represent the voltage limitation within the current plane. This results in a limiting ellipse, which becomes smaller with increasing stator frequency. The main axes of this ellipse is oriented in the i_d- and i_q-direction with magnitudes of

$$\frac{u_{max}}{\omega_s L_s} \quad \text{and} \quad \frac{u_{max}}{\omega_s \sigma L_s}$$
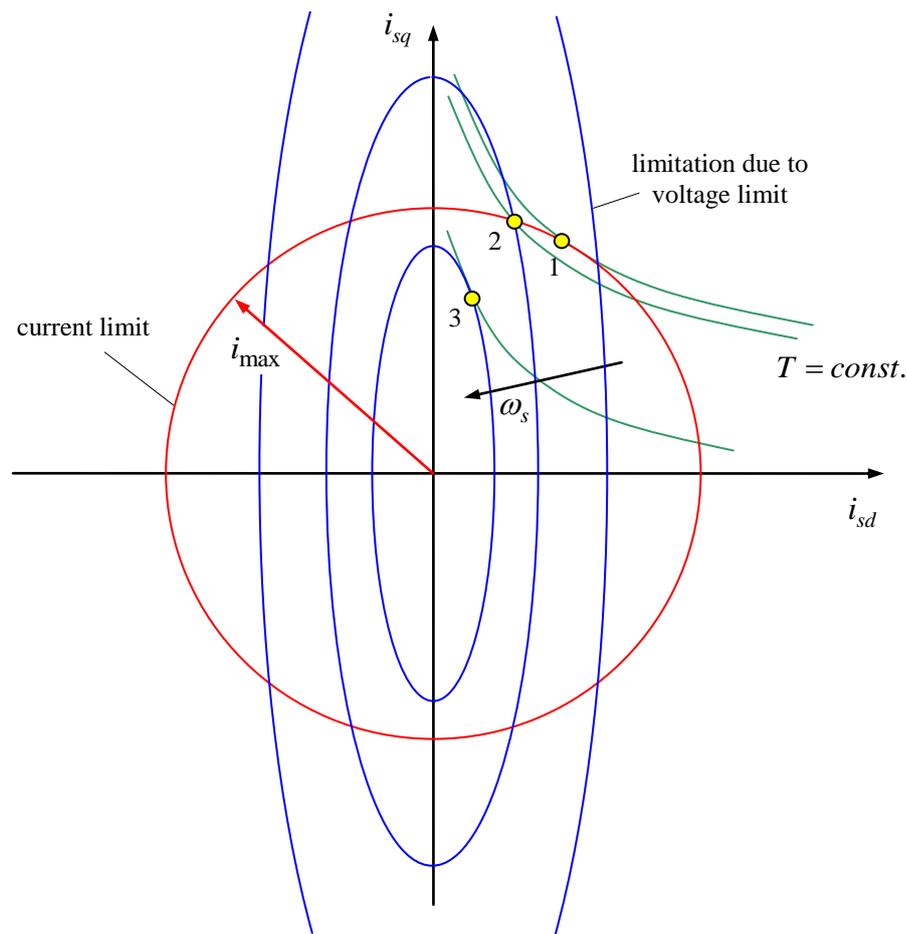
Fig. 8-24: Operation at voltage and current limits

Using the above diagram, three qualitatively different cases can be illustrated:

1. The speed and the stator frequency are small and the available voltage is sufficiently large. In this case the voltage limit does not impose restrictions on how to set currents within the current limit circle. The maximum torque is achieved at the contact point of constant torque curves and current limit circle (point 1). The maximum achievable torque is independent of the frequency in this region. Setting the stator frequency and the rotational frequency equal in a first estimation, then the power increases proportionally with the frequency. The described region is referred to as *voltage control range*, or in accordance with the terms of the DC motor as the *armature control range*.

2. At higher speeds or frequencies the voltage limit comes into effect. Valid phasors have to be located within both the current limit circle and the limiting voltage ellipse. The maximum torque is achieved at the intersection of the two limiting curves. The maximum available torque is reduced with increasing frequency, roughly by $1/\omega_s$. As in this region, the flux-forming current component i_{sd} and the rotor flux ψ_r are reduced depending on the speed, this area is called *flux weakening region*. More

precisely, we refer to this region as the *lower flux weakening region.* The maximum achievable power is approximately constant in the lower flux weakening region.

3. With further increase in frequency, the limiting voltage ellipses become so small that the current limit is of no importance any longer. The maximum torque is achieved at the contact point of voltage ellipses and constant torque curves. This region is called *upper flux weakening region*. The attainable torque is by $1/\omega_s^2$ and the maximum power by $1/\omega_s$.
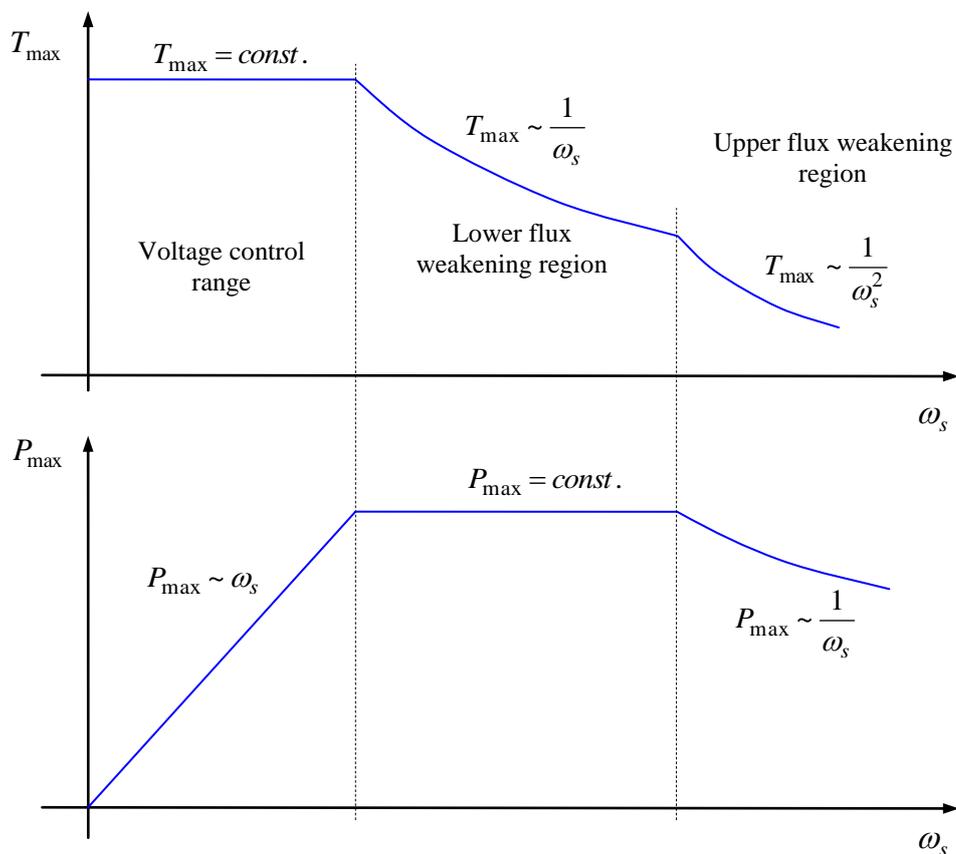
Fig. 8-25: Approximate maximum torque and maximum power curves when operating at current and voltage limits

The utilized flux weakening region during operation is often expressed as the ratio of the maximum speed to the rated speed. For example, we speak of a flux weakening region of 1:3.

Depending on the field of application voltage control range and flux weakening region are designed differently: In case the load torque increases with the speed, which is typical for pumps and fans for example, operation in the flux weakening region is not reasonable, as the torque of the drive would be reduced. Such drives operate almost completely in the voltage control range, in consequence.

For many drives, it is important to utilize the installed power evenly within a preferably large speed range. This is a typical characteristic of traction drives (railways, road vehicles). Such drives are designed for a large lower flux weakening region of 1:3 to 1:5, for example.

The upper flux weakening region, on the other hand, is not or only to a limited extent used in typical applications. The reason lies in the decreasing power as a function of the speed for which hardly any drive task with a suitable load characteristic can be found.

9 Comparison of the Two-Dimensional Vector and Complex Representation

	Vector notation	Complex notation
	$$\boldsymbol{x} = \begin{bmatrix} x_1 \\ x_2 \end{bmatrix}$$	$$\underline{x} = x_1 + jx_2$$
Transformation between two reference systems A und B	$$\boldsymbol{x}^B = \boldsymbol{Q}(-\varepsilon_{BA})\boldsymbol{x}^A$$ with $$\boldsymbol{Q}(\varphi_{BA}) = \begin{bmatrix} \cos\varphi_{BA} & -\sin\varphi_{BA} \\ \sin\varphi_{BA} & \cos\varphi_{BA} \end{bmatrix}$$	$$\underline{x}^B = e^{-j\varphi_{BA}}\,\underline{x}^A$$
Transformation of the time derivative	$$\dot{\boldsymbol{x}}^B = -\dot{\varphi}_{BA}\boldsymbol{J}\boldsymbol{x}^B + \boldsymbol{Q}(\varphi_{BA})\,\dot{\boldsymbol{x}}^A$$	$$\dot{\underline{x}}^B = -j\dot{\varphi}_{BA}\underline{x}^B + e^{-j\varphi_{BA}}\,\dot{\underline{x}}^A$$
Rotation by 90°	$$\boldsymbol{J}\boldsymbol{x} = \boldsymbol{x}\boldsymbol{J} \quad \text{with}$$ $$\boldsymbol{J} = \begin{bmatrix} 0 & -1 \\ 1 & 0 \end{bmatrix}$$	$$j\,\underline{x}$$
Rotation-dilation	$$\begin{bmatrix} a_1 & -a_2 \\ a_2 & a_1 \end{bmatrix}\boldsymbol{x}$$	$$(a_1 + ja_2)\,\underline{x}$$
General mapping	$$\begin{bmatrix} a_{11} & a_{12} \\ a_{21} & a_{22} \end{bmatrix}\boldsymbol{x}$$	N/A
Magnitude	$$\lvert\boldsymbol{x}\rvert = \sqrt{\boldsymbol{x}^{\mathrm{T}}\boldsymbol{x}}$$	$$\lvert\underline{x}\rvert = \sqrt{\bar{\underline{x}}\underline{x}}$$
Scalar/inner product	$$\boldsymbol{x}^{\mathrm{T}}\boldsymbol{y} = x_1 y_1 + x_2 y_2$$	$$\mathrm{Re}\,\bar{\underline{x}}\underline{y} = x_1 y_1 + x_2 y_2$$
Vector/cross product	$$\boldsymbol{x} \times \boldsymbol{y} = x_1 y_2 - x_2 y_1$$	$$\mathrm{Im}\,\bar{\underline{x}}\underline{y} = x_1 y_2 - x_2 y_1$$

10 Fourier and Laplace Transformation of Two-Dimensional Time-Domain Functions

A vector-valued time function

$$\boldsymbol{x}(t) = \begin{bmatrix} x_\alpha(t) \\ x_\beta(t) \end{bmatrix}$$

whose components $x_\alpha(t), x_\beta(t)$ represent real-valued functions can be transformed component-wise into the Fourier or Laplace domain:

$$\underline{X}(s) = \begin{bmatrix} \underline{X}_\alpha(s) \\ \underline{X}_\beta(s) \end{bmatrix} \quad \text{and} \quad \underline{X}(\omega) = \begin{bmatrix} \underline{X}_\alpha(\omega) \\ \underline{X}_\beta(\omega) \end{bmatrix}$$

with the Laplace or Fourier transformation

$$\underline{X}_{\alpha,\beta}(s) = \int_0^\infty x_{\alpha,\beta}(t)\, e^{-st} dt \quad \text{and} \quad \underline{X}_{\alpha,\beta}(\omega) = \int_{-\infty}^\infty x_{\alpha,\beta}(t)\, e^{-j\omega t} dt$$

and the corresponding inverse transformations

$$x_{\alpha,\beta}(t) = \frac{1}{2\pi j} \int_C \underline{X}_{\alpha,\beta}(s)\, e^{st}\, ds \quad \text{and} \quad x_{\alpha,\beta}(t) = \frac{1}{2\pi} \int_{-\infty}^\infty \underline{X}_{\alpha,\beta}(\omega)\, e^{j\omega t}\, d\omega$$

Instead of a component-wise transformation, we can combine the two real-valued time functions $x_\alpha(t), x_\beta(t)$ to a *complex-valued time function*

$$\underline{x}(t) = x_\alpha(t) + j x_\beta(t)$$

and apply the Laplace or Fourier transformation to this complex-valued function:

$$\underline{X}(s) = \int_0^\infty \underline{x}(t)\, e^{-st} dt \quad \text{and} \quad \underline{X}(s) = \int_{-\infty}^\infty \underline{x}(t)\, e^{-j\omega t} d\omega$$

Obviously, the following equation holds:

$$\underline{X}(s) = \underline{X}_\alpha(s) + j \underline{X}_\beta(s)$$

This transformed function $\underline{X}(s)$ is complex-valued as well (such as the real-valued time functions). However, it is not a complex conjugate to itself, as it is common for transformed real-valued time functions. In general, the following equations do not apply:

$$\overline{\underline{X}}(s) = \underline{X}(\overline{s}) \quad \text{and} \quad \overline{\underline{X}}(\omega) = \underline{X}(-\omega)$$

For the Fourier transform in particular, it is not sufficient to only consider the positive frequencies. Instead, the frequency range for all positive and negative frequencies must be taken into account.

The inverse transformations are clearly defined:

$$\underline{x}(t) = \frac{1}{2\pi j} \int_C \underline{X}(s)\,e^{st}\,ds \quad \text{and} \quad \underline{x}(t) = \frac{1}{2\pi} \int_{-\infty}^{\infty} \underline{X}(\omega)\,e^{j\omega t}\,d\omega$$

The original components can be recovered according to

$$x_\alpha(t) = \operatorname{Re}\underline{x}(t)$$
$$x_\beta(t) = \operatorname{Im}\underline{x}(t)$$

The well-known rules of the Laplace and Fourier transform can be applied in the same way for the transformation of complex-valued time functions. The *modulation rule* shall be considered in more detail, however:

It is,

$$\underline{x}(t)e^{-j\omega_0 t} \mapsto \underline{X}(s+j\omega_0) \quad \text{and} \quad \underline{x}(t)e^{-j\omega_0 t} \mapsto \underline{X}(\omega+\omega_0)$$

$$\underline{x}(t)e^{-j\omega_0 t} = x_\alpha(t)\cos\omega_0 t + x_\beta(t)\sin\omega_0 t + j\big(-x_\alpha(t)\sin\omega_0 t + x_\beta(t)\cos\omega_0 t\big)$$
$$= x_d(t) + jx_q(t)$$

with

$$\begin{bmatrix} x_d \\ x_q \end{bmatrix} = \boldsymbol{Q}(-\omega_0 t)\begin{bmatrix} x_\alpha \\ x_\beta \end{bmatrix}, \quad \boldsymbol{Q}(-\varepsilon) = \begin{bmatrix} \cos\varepsilon & \sin\varepsilon \\ -\sin\varepsilon & \cos\varepsilon \end{bmatrix}$$
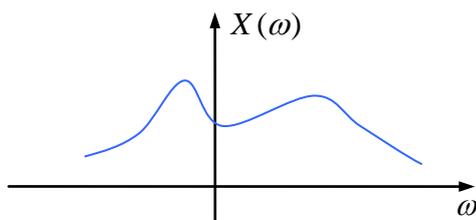
Spectrum in stator-fixed α/β- coordinates
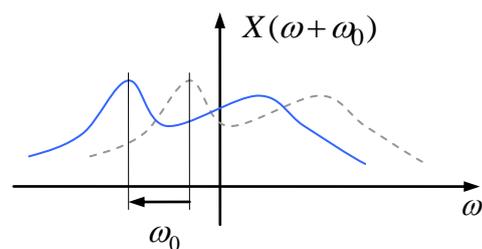
Spectrum in rotating d/q- coordinates

In consequence, a transformation into a reference frame rotating with speed ω_0 leads to a frequency shift of the spectrum by exactly ω_0 (see above figure). In particular, the frequency component at $\omega = \omega_0$ in the spectrum of the stator-fixed quantities now appears as a DC-quantity at $\omega = 0$ in the spectrum of the rotating reference system.

That way, the frequencies in the spectrum can not only be interpreted as *oscillations* with positive or negative frequencies: A positive frequency component corresponds to a rotating vector in the mathematically positive sense, a negative frequency corresponds to a vector rotating in the opposite direction.

When referring to a frequency ω_0, the frequency component at the point $\omega = +\omega_0$ is referred to as the *positive sequence* component, the one at $\omega = -\omega_0$ is referred to as the *negative sequence* component, accordingly.

11 German-English Glossary

Abtastung	sampling
Admittanz	admittance
Anker	armature
Ankerrückwirkung	armature reaction
Anlaufdrehmoment	stall torque
Anschluss	terminal
Antrieb	drive
Arbeit	work
Asynchronmotor	induction motor, asynchronous motor
Bandbreite	bandwidth
Blindleistung	reactive power
Bodediagramm	Bode plot
Drehmoment	torque
Drehstrommotor	three-phase motor
Drehung	rotation
Drehzahl	rotational speed, speed
Dreieckschaltung	delta connection
Drossel	inductor
Durchflutung	magnetomotive force (MMF)
Effektivwert	root mean square (RMS) value
elektrische Feldstärke	electric field strength
elektromotorische Kraft	electromotive force (EMF)
Elektrotechnik	electrical engineering
Energie	energy
Entkopplung	decoupling controller
Erregung	excitation
Feld	field
Flussschwächung	flux weakening
Formfaktor	waveform factor
fremderregt	separately excited
Frequenz	frequency
Getriebe	gear
Gleichrichter	rectifier
Gleichspannung	direct voltage, DC voltage
Gleichstrom	direct current, DC
Gleichstrommotor	DC motor
Hauptinduktivität	mutual inductance
Hochsetzsteller	boost converter
Impedanz	impedance
Induktivität	inductance
induzierte Spannung	induced voltage
Istwert	actual value
Käfigläufer	squirrel cage rotor
Kapazität	capacity

Knoten	node
Kondensator	capacitor
Kapazität	capacity
Kraft	force
Kurzschluss	short circuit
Kurzschlussstrom	short-circuit current
Ladung	charge
Last	load
Leerlaufspannung	open-circuit voltage, off-load voltage
Leistung	power
Leistungsfaktor	power factor
Leitwert	conductance, conductivity
Losbrechdrehmoment	stall torque
Magnet	magnet
magnetische Feldstärke	magnetic force
magnetische Flussdichte	magnetic flux density
magnetische Spannung, Durchflutung	magnetomotive force (MMF)
magnetischer Fluss	magnetic flux
Magnetisierungsstrom	magnetizing current
Masche	mesh
Mittelwert	mean, average value
Mittelwertmodellierung	state-space averaging
Nennwert	rated value, rating
Netzwerk	network
Ortskurve	frequency response locus
Parallelschaltung	parallel connection
Permanentmagnet-Synchronmotor	permanent magnet synchronous motor
Polpaar	pole pair
Polteilung	pole pitch
Pulsweitenmodulation	pulse width modulation (PWM)
Quelle	source
Regelfehler	control error
Regelkreis	closed-loop control
Regler	controller
Reihenschaltung	series connection
Resonanzfrequenz	resonant frequency
Rotor, Läufer	rotor
Schalter	switch
Schaltkreis	circuit
Scheinleistung	apparent power
Scheitelfaktor	crest factor
Schlupf	slip
Sehnung	fractional pitch winding
Sollwert	set point, reference value
Spannung	voltage
Spannungsquelle	voltage source
Spule	coil
Stator, Ständer	stator

Stellbefehl	firing command
Stellgröße	actuating variable
Sternschaltung	star connection
Streuinduktivität	leakage inductance
Strom	current
Stromquelle	current source
Stromschwankung	current ripple
Tiefsetzsteller	buck converter
Totzeit	dead time
Transformator	transformer
Übertragungsfunktion	transfer function
Vektormodulation	vector modulatoin
Verlustleistung	losses
Vorsteuerung	feedforward control
Wechselrichter	inverter
Wechselspannung	alternating voltage, AC voltage
Wechselsperrzeit	interlocking time
Wechselstrom	alternating current, AC
Welle	shaft
Wicklung	winding
Wicklungsfaktor	winding factor
Widerstand	resistance, resistor
Windung	turn
Winkelgeschwindigkeit	angular velocity
Wirkleistung	active power
Wirkungsgrad	efficiency
Zeitkonstante	time constant

12 Bibliography

Dierk Schröder
Elektrische Antriebe – Grundlagen
Springer Verlag, 3. Aufl., 2007

> *Ein sehr umfangreiches reichhaltiges Buch (mehr als 700 Seiten), welches verschiedenste Systeme elektrischer Antriebe anspricht. Sehr gute Darstellung, sehr zu empfehlen.*

John Chiasson
Modeling and High-Performance Control of Electric Machines
Wiley, 2005

> *A very extensive & comprehensive book, which focuses on the modeling and control of electrical machines in detail.*

Werner Leonhard
Control of Electrical Drives
Springer, 3rd edition, 2001

> *Here, the basic principles of the flux-oriented control for synchronous and induction machines are elaborated.*

Duane Hanselman
Brushless Permanent Magnet Motor Design
The Writers' Collective, 2nd edition, 2003

> *A very interesting book, which puts focus on winding schemes and the resulting motor characteristics, a topic that is hardly dealt with in other books.*

Rudolf Richter
Elektrische Maschinen I
Birkhäuser Verlag, 3. Auflage, 1967

> *Ein klassisches Buch über elektromaschinenbauliche Aspekte und das Betriebsverhalten, welches zahlreiche Details liefert, die in modernen Darstellungen kaum noch zu finden sind.*

Germar Müller, Bernd Ponick
Grundlagen elektrischer Maschinen
Wiley-VHC, 9. Auflage, 2006

Germar Müller, Bernd Ponick
Theorie elektrischer Maschinen
Wiley-VHC, 4. Auflage

W. Nürnberg,
Die Asynchronmaschine
2. Auflage, Springer, 1962